


Spring 5-15-2019

Mechanics of Phenotypic Aging Trajectories in *C. elegans* and Humans

William Zhang

Washington University in St. Louis

Follow this and additional works at: https://openscholarship.wustl.edu/art_sci_etds

 Part of the [Biostatistics Commons](#), [Family, Life Course, and Society Commons](#), [Gerontology Commons](#), and the [Physiology Commons](#)

Recommended Citation

Zhang, William, "Mechanics of Phenotypic Aging Trajectories in *C. elegans* and Humans" (2019). *Arts & Sciences Electronic Theses and Dissertations*. 1821.

https://openscholarship.wustl.edu/art_sci_etds/1821

This Dissertation is brought to you for free and open access by the Arts & Sciences at Washington University Open Scholarship. It has been accepted for inclusion in Arts & Sciences Electronic Theses and Dissertations by an authorized administrator of Washington University Open Scholarship. For more information, please contact digital@wumail.wustl.edu.

WASHINGTON UNIVERSITY IN ST. LOUIS

Division of Biology & Biomedical Sciences
Computational and Systems Biology

Dissertation Examination Committee:

Zachary Pincus, Chair

Gautam Dantas

Todd Druley

Shin-ichiro Imai

Gary Stormo

Ting Wang

Mechanics of Phenotypic Aging Trajectories in *C. elegans* and Humans

by

William B. Zhang

A dissertation presented to
The Graduate School
of Washington University in
partial fulfillment of the
requirements for the degree of
Doctor of Philosophy

May 2019
St. Louis, Missouri

©2019, William B. Zhang

Table of Contents

List of Figures	v
List of Tables	vi
Acknowledgements	vii
Abstract	ix
1 Introduction	1
1.1 Evolutionary Theories of Aging	2
1.1.1 Programmed Aging	3
1.1.2 Mutation Accumulation	3
1.1.3 Antagonistic Pleiotropy	3
1.1.4 Disposable Soma	4
1.1.5 Discussion	4
1.2 Molecular Mechanisms and Genetics of Aging	4
1.2.1 Telomeres	5
1.2.2 Insulin/IGF-1 Signaling	5
1.2.3 Dietary Restriction	6
1.2.4 Discussion	8
1.3 Biodemography of Aging	8
1.3.1 Gompertz-Makeham Model of Mortality	9
1.3.2 Late-Life Mortality Deceleration	10
1.3.3 Postponement of Senescence	11
1.3.4 Biomarkers of Aging	12
1.3.5 Discussion	12
1.4 Mechanics of Phenotypic Aging Trajectories	13
2 The Physiological Basis of Variation in Longevity within an Isogenic Population	15
2.0 Introduction	16
2.1 Results	17
2.1.1 Longitudinal Measurements of Physiology in Individual <i>C. elegans</i>	17

2.1.2	Distinct Physiology of Long- vs. Short-Lived Individuals	18
2.1.3	Differences in Aging Rate and Health at Death in Long- vs. Short-Lived Individuals	22
2.1.4	Uneven Rates of Aging Produce Lower Quality of Life in Longer-Lived Individuals	24
2.1.5	Longer-Lived Individuals Have Disproportionately Extended Gerospans	27
2.2	Discussion	29
2.3	Methods and Resources	33
2.3.1	Key Resources Table	33
2.3.2	Contact for Reagent and Resource Sharing	34
2.3.3	Experimental Model and Subject Details	34
2.3.4	Method Details	34
2.3.5	Quantification and Statistical Analysis	40
2.3.6	Data and Software Availability	41
2.3.7	Additional Resources	41
2.4	Acknowledgements	42
2.5	Author Contributions	42
2.6	Supplementary Information	43
3	Predicting All-Cause Mortality from Basic Physiology in the Framingham Heart Study	75
3.0	Introduction	76
3.1	Results	78
3.1.1	Amount of Mortality Predictable from Physiology	79
3.1.2	Incorporating Physiological History into Mortality Prediction	83
3.2	Discussion	86
3.3	Experimental Procedures	90
3.3.1	Data Collection	90
3.3.2	Statistics	90
3.3.3	Construction of Clinical Risk Scores	91
3.3.4	Blood Pressure Treatment	91
3.3.5	Pulse Pressure	92
3.3.6	Exam Weighting in History Accumulation	92
3.4	Acknowledgements	92
3.5	Funding	92
3.6	Conflict of interest	93
3.7	Author contributions	93
3.8	Supplementary Information	93
	Bibliography	96

List of Figures

1.1	The longevity of <i>daf-2</i> mutants.	6
1.2	Regulation of <i>C. elegans</i> aging by an elaborate endocrine network.	6
1.3	Signaling network of caloric restriction in yeast.	7
1.4	Age trajectories of death rates for human females.	10
1.5	The postponement of mortality for females.	11
2.1	Experimental workflow for monitoring <i>C. elegans</i> physiological aging	19
2.2	Variation in lifespan and physiology within a homogeneous population	21
2.3	How does aging physiology differ between long- and short-lived individuals?	23
2.4	Systematic differences in the trajectories of physiological decline.	26
2.5	Healthspan and gerospan analysis	27
2.6	Summary of key <i>C. elegans</i> findings	29
2.7	Data Quality Controls	45
2.8	Sample images of worms in each of our adult lifespan cohorts	46
2.9	Subpopulation Analysis	48
2.10	Alternate Health Definitions	50
2.11	Thresholding Validation	52
2.12	Gallery of Measurements	54
2.13	Autofluorescence at day 7 of adulthood	60
2.14	Autofluorescence at day 8 of adulthood	61
2.15	Autofluorescence at day 9 of adulthood	62
2.16	Movement at day 2 of adulthood	63
2.17	Movement at day 5 of adulthood	64
2.18	Movement at day 8 of adulthood	65
2.19	Reproduction at day 1 of adulthood	66
2.20	Reproduction at day 2 of adulthood	67
2.21	Reproduction at day 3 of adulthood	68
2.22	Body size at day 2 of adulthood	69
2.23	Body size at day 5 of adulthood	70
2.24	Body size at day 8 of adulthood	71
2.25	Tissue integrity at day 2 of adulthood	72

2.26	Tissue integrity at day 5 of adulthood	73
2.27	Tissue integrity at day 8 of adulthood	74
3.1	Early-to-mid adulthood lifespan prediction	79
3.2	Predictable lifespan from composites generally decreases with age.	81
3.3	Individual variables' ability to predict survival changes over time	82
3.4	Hypotheses for the relationship between health and trends in physiology	84
3.5	The mortality-predictive ability of single variables changes as history is incorporated	86
3.6	Accumulation of predictivity using history, starting at different exams	87
3.7	Early-to-mid adulthood lifespan prediction, men	93
3.8	Early-to-mid adulthood lifespan prediction, women	94
3.9	Individual variables' ability to predict survival, stratified by gender	95

List of Tables

2.1	Correlations between aspects of physiology.	55
2.2	Contributions of different aspects of health	56
2.3	Contributions of different raw physiological measures	57
2.4	Summary of key analysis repetitions	58
2.5	Contributions of each raw measurement to the linear regression	59
3.1	Changing demographics of the surviving cohort over time	78
3.2	Comparison of the selected vs. excluded Framingham Heart Study (FHS) participants .	91

Acknowledgements

First, I am sincerely grateful to my extraordinary advisor, Professor Zachary Pincus. I have been constantly amazed by his deep knowledge, keen insights, dizzying array of skills, and perpetual optimism. He is a brilliant scientist, and beyond that is one of the kindest and most genuine people I know. I hope to someday be a leader as dedicated, capable and approachable as him, but I could probably never give a talk quite as good!

I would also like to thank Zach for an outstanding commitment to his students. Despite a swarm of other duties, he always found time to thoughtfully engage with each and every one of our ideas. From restlessly roaming the lab in search of a problem to solve, to personally contributing to the back-breaking labor of worm experimentation, Zach was always willing to help. He is unceasingly supportive and always ready with honest advice. I could not have asked for more from a mentor or a friend.

I also thank the members of my thesis committee, Professors Shin-ichiro Imai, Gary Stormo, Todd Druley, Gautam Dantas, and Ting Wang for helpful comments and suggestions. I would also like to thank my fellow graduate students, Drew Sinha, Will Pittman, Holly Kinser, and Nick Jacobs for their camaraderie in this shared journey. I am grateful for support from the National Institutes of Health, the Washington University Medical Scientist Training Program, and the Longer Life Foundation.

William Zhang

Washington University in St. Louis

May 2019

I dedicate this dissertation to my partner *Amy*.
Thank you for always being my steadfast companion.

ABSTRACT OF THE DISSERTATION

Mechanics of Phenotypic Aging Trajectories in *C. elegans* and Humans

by

William B. Zhang

Doctor of Philosophy in Biology and Biomedical Sciences

Computational and Systems Biology

Washington University in St. Louis, 2019

Assistant Professor Zachary Pincus, Chair

Overall, my dissertation integrates longitudinal measurements of physiology to investigate the aging process. In the first half, I examine the surprising and largely unexplained degree of variation in lifespan within even homogeneous populations. I sought to understand how physiological aging differs between long- and short-lived individuals within a population of genetically identical *C. elegans* reared in a homogeneous environment. Using a novel culture apparatus, I longitudinally monitored aspects of aging physiology across a large population of isolated individuals. Aggregating several measures into an overall estimate of senescence, I find that long- and short-lived individuals start adulthood on an equal physiological footing. However, longer-lived individuals then experience slower declines in function, but spend a disproportionately large portion of life in poor physiological health. Indeed, the period of early-life good health is much less variable than the period of late-life advanced senescence, which I conclude to be a more plastic phase of life. In the second half, I show that simple physiological measurements have broader lifespan-predictive value than previously believed and that incorporating information from multiple time points can significantly increase that predictive capacity. Using longitudinal data from a cohort of 1349 human participants in the Framingham Heart Study, I show that as early as 28–38 years of age, almost 10% of variation in future lifespan can be predicted from simple clinical parameters. Further, different clinical measurements are predictive of lifespan in different age regimes. Moreover, I find that several blood glucose and blood pressure are best considered as measures of a rate of “damage accrual”, such that total historical exposure, rather than current measurement values, is the most relevant risk factor (as with pack-years of cigarette smoking). Together, this work has established the physiological basis of variation in longevity within an isogenic population of *C. elegans* and extended our ability to predict mortality from basic clinical measurements in humans.

All the world's a stage,

And all the men and women merely players;
They have their exits and their entrances,
And one man in his time plays many parts,
His acts being seven ages. At first the infant,
Mewling and puking in the nurse's arms.
Then, the whining school-boy with his satchel
And shining morning face, creeping like snail
Unwillingly to school. And then the lover,
Sighing like furnace, with a woeful ballad
Made to his mistress' eyebrow. Then, a soldier,
Full of strange oaths, and bearded like the pard,
Jealous in honour, sudden, and quick in quarrel,
Seeking the bubble reputation
Even in the cannon's mouth. And then, the justice,
In fair round belly, with a good capon lined,
With eyes severe, and beard of formal cut,
Full of wise saws, and modern instances,
And so he plays his part. The sixth age shifts
Into the lean and slippered pantaloon,
With spectacles on nose and pouch on side,
His youthful hose, well saved, a world too wide
For his shrunk shank, and his big manly voice,
Turning again toward childish treble, pipes
And whistles in his sound. Last scene of all,
That ends this strange eventful history,
Is second childishness and mere oblivion,

Sans teeth, sans eyes, sans taste, sans everything.

—William Shakespeare, *As You Like It*, Act II, Scene VII

Chapter 1

Introduction

Aging is a fundamental and universal experience of the human condition. In some ways, aging can be considered to be development in reverse. Developmental processes start with a single-celled zygote and guide it through embryonic developmental, birth, childhood, adolescence, and finally, sexually mature adulthood. With each successive developmental stage, the individual grows stronger, more able, and more independent. In contrast, aging begins with an adult in peak condition, weakens the mind, dulls the senses, and saps the strength of the body. Gradually, an aging individual loses their vitality, their acuity, their independence (and eventually, life itself).

Given the effects of aging, it is no wonder that attempts to slow or reverse its progression are as old as civilization itself. Myths about substances with astonishing anti-aging properties have persisted for millennia. The “elixir of life” and “fountain of youth” have been the subject of fervent interest on the part of explorers, kings, and conquerors throughout recorded history. Alexander the Great, the first Chinese emperor Qin Shi Huang, and (perhaps most famously) the Spanish conquistador Ponce de León have all been connected to quests for these legendary substances [1]. As we know from history, none of these efforts were successful.

On the other hand, with the advent of the scientific method and modern medicine, giant strides have been made in the understanding and treatment of other disease processes. Joseph Lister applied germ theory to surgery in the form of antiseptic techniques [2], and patient outcomes have improved dramatically. With antibiotics, deaths from infectious disease in the United States have fallen from 797 (per 100,000 individuals) in 1900 to just 59 in 1996 [3]. Many forms of cancer, once only treatable when small and localized enough to be completely removed by surgery [4–10], are now eminently

curable using chemotherapy, targeted molecular therapies (such as imatinib for chronic myelogenous leukemia [11]), and other modern treatment methods.

By comparison, our understanding of the aging process remains relatively immature. We do not yet have a complete understanding of the root causes of aging or its evolutionary origins [12]. Until the late 20th century, it was widely thought that aging had little genetic basis and was an entirely stochastic process driven by entropy, by probabilistic damage accumulation (“wear and tear”) [13]. Furthermore, epidemiological studies on twins have shown that only 25% of variability in human lifespan can be possibly explained by heritable factors [14].

While it is clear that much remains to be discovered, aging research has progressed considerably since the days of Ponce de León. A number of promising hypotheses have been proposed to explain the core principles and evolutionary derivation of aging [12]. The discovery of the insulin/IGF-1 pathway’s ability to extend life in the nematode *Caenorhabditis elegans* has illustrated the plasticity and coordinated nature of the aging process [15, 16], and has spearheaded an explosion of recent advances in our understanding of the genetics of aging. In parallel, biodemographic approaches have characterized the epidemiology of aging, describing it as an actuarial increase of mortality risk over time [17] and chronicling historical changes in mortality rates [18].

In this preface, I review historical developments in three distinct but critically interdependent approaches to the study of aging: evolutionary theory, genetics and molecular biology, and biodemography, motivating and contextualizing my dissertation.

1.1 Evolutionary Theories of Aging

The fundamental challenge in understanding aging’s evolutionary origins lies in explaining its emergence despite its drawbacks. Aging progressively impairs an organism’s ability to function, to survive, to reproduce, to pass on its genes. Yet, aging is widely observed across the tree of life. Why? Here, I review several prominent theories of the evolution of aging, highlighting how they each explain the development of aging in spite of the reduction of reproductive fitness in aged individuals.

1.1.1 Programmed Aging

One prevalent idea about the nature of aging is that while it is harmful to the survival and reproductive opportunities of aged individuals, it can be beneficial to the species as a whole [19]. By reducing the fitness of individuals from older generations, aging can reduce competition for limited resources and accelerate the pace of evolution by increasing generational turnover. Therefore, a type of group selection causes species with aging phenotypes to outcompete those that do not age, or age less dramatically.

A major objection to this idea rests on the fact that many wild animal populations do not survive to ages at which senescence is a significant contributor to mortality [20]. As a result, it is unlikely for any substantial positive evolutionary pressure (or any evolutionary pressure) to act on aged organisms. Therefore, aging could not have arisen by being positively selected for, and must be the consequence of some other evolutionary process.

1.1.2 Mutation Accumulation

The theory of mutation accumulation incorporates the finding that selective pressures for senescent individuals in the wild are either non-existent or very weak [20]. It posits instead that the aging process is a result of genetic drift. Specifically, detrimental mutations in alleles that act late in life are subject to only extremely weak purifying selection, and can drift to fixation on an evolutionary time scale. As successive generations fix more of these detrimental late-life mutations, they accumulate in the genome, and the aging process emerges.

One issue with the mutation accumulation theory is that it assumes the existence of genes that act specifically in old age—that they are there (in the genome) to accumulate mutations in the first place! If wild animals rarely survive to ages at which significant senescence occurs, why would they have genes specific to old-age to begin with? The rather neat answer lies in the idea of “antagonistic pleiotropy”.

1.1.3 Antagonistic Pleiotropy

The idea of antagonistic pleiotropy solves the issue of the existence of old-age genes by not requiring them specifically. Instead, it postulates that certain pleiotropic genes may have a positive influence on fitness in youth, but the opposite effect in old age [21]. For example, a gene that promotes cell division and robust growth may be beneficial in an adolescent, but may promote the growth of cancerous ma-

lignancies in older individuals. Thus, antagonistic pleiotropy argues that although the aging process is detrimental to an organism's evolutionary fitness, its late-life harm is more than balanced by a higher level of early-life fitness. Although aging itself is somewhat harmful, it is merely the side-effect of a stronger beneficial process.

1.1.4 Disposable Soma

Another theory of aging, the disposable soma theory, refines the scope of the antagonistic pleiotropy theory by focusing on energy usage. It asserts that there is an inherent tradeoff between investing in somatic maintenance and reproduction [22]. In this theory, an individual who heavily invests energy in reproduction does so at the cost of somatic maintenance; by being fertile in youth, an organism sacrifices the energy required to sustain later-life health and function. True to its name, the disposable soma theory answers our initial question by arguing that the most essential part of an organism is actually the germline. The somatic cells are merely a temporary vehicle for the reproduction of more germ cells. Thus, aging is not truly detrimental, since it primarily harms the soma. In fact, aging actually benefits the germ cells (which, by old age, reside in youthful descendents) by investing additional energy in reproduction.

1.1.5 Discussion

Today, the question of the evolutionary origins of aging remains open. Though antagonistic pleiotropy is the most prevalent current theory, the search for specific illustrative genes has been inconclusive, and clear and explicit examples have not yet been found [23]. It is possible that more than one of the proposed theories has contributed to the evolution of aging, or that a yet-undiscovered mechanism is responsible.

1.2 Molecular Mechanisms and Genetics of Aging

While the ultimate cause¹ of aging remains uncertain, more proximate causes have been studied extensively. A large body of work [16, 25–34] indicates that aging is a complex biological process with multiple contributing genetic pathways and molecular mechanisms of action. Here, I attempt to catalog,

¹See [24] for a thorough discussion of this term.

roughly chronologically, historical developments in our understanding of the mechanistic processes underlying aging, and to briefly summarize the current state of the field.

1.2.1 Telomeres

Leonard Hayflick's discovery of a limit to human cells' *in vitro* replicative potential [35, 36] demonstrated that senescence is a phenomenon at the cellular level in addition to being a macroscopic phenomenon at the organismal level. Later, short telomere² length was consistently found to be correlated with age and reduced replicative potential in human cells [37]. This motivated the attractive hypothesis that telomere shortening is a mechanism for human cellular senescence *in vivo*, and that it plays a role in organismal aging.

However, studies on the relationship between telomere length and longevity have been mixed. In *C. elegans*, animals with longer telomeres have been shown to have extended lifespans [38]. One study in humans has found that individuals with shorter telomeres have higher mortality risk than similarly-aged peers [39]. On the other hand, mice with the telomerase gene knocked out seem to have normal aging phenotypes and lifespans [40], and additional human studies have found no correlation between telomere length and mortality when the results are controlled for age [41, 42].

1.2.2 Insulin/IGF-1 Signaling

Mutations in a number of signaling pathways can result in an extended lifespan phenotype in model animals. The most well-characterized of these signaling pathways is the insulin/IGF-1 pathway, which is known to modulate lifespan in nematodes, flies, and rodents [43]. The ability of this pathway to influence lifespan was a landmark discovery, effecting a paradigm shift in our understanding of aging. As the first signaling pathway known to extend lifespan in a model animal when perturbed [15, 16] (also see figure 1.1³), the insulin/IGF-1 pathway demonstrated that aging is a coordinated process that it is not simple an accumulation of stochastic degradation.

Subsequent studies have elucidated a complex signaling network downstream of the insulin/IGF-1 receptor involving mediators such as DAF-16 and AKT-2, as illustrated in figure 1.2a. Further, the insulin/IGF-1 receptor cascade is subject to modulation by several hormones and environmental cues,

²Telomeres are protective repetitive DNA sequences at the ends of chromosomes.

³This is perhaps the single most famous figure in all of aging research.

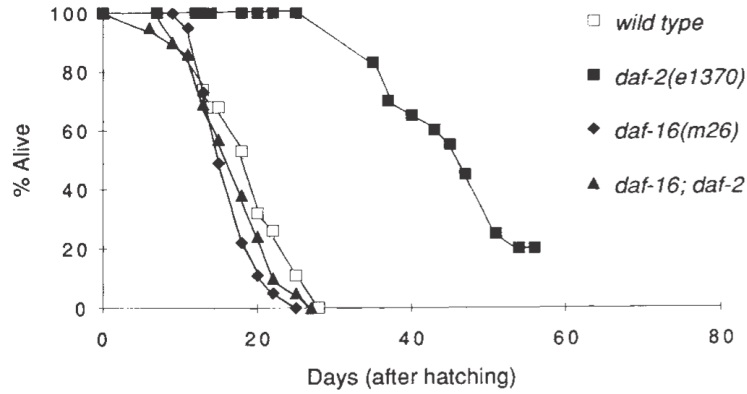


Figure 1.1: The longevity of *daf-2* mutants. We can see that *daf-2* single mutants have an extended lifespan phenotype, while *daf-16* single mutants and *daf-16; daf-2* double mutants have normal lifespans. This indicates that *daf-16* is required for the lifespan-modulating effects of *daf-2*, and that *daf-16* is downstream of *daf-2* in the signaling cascade. Adapted from figure 4 in [16].

which can also act in parallel to regulate lifespan (figure 1.2b-c).

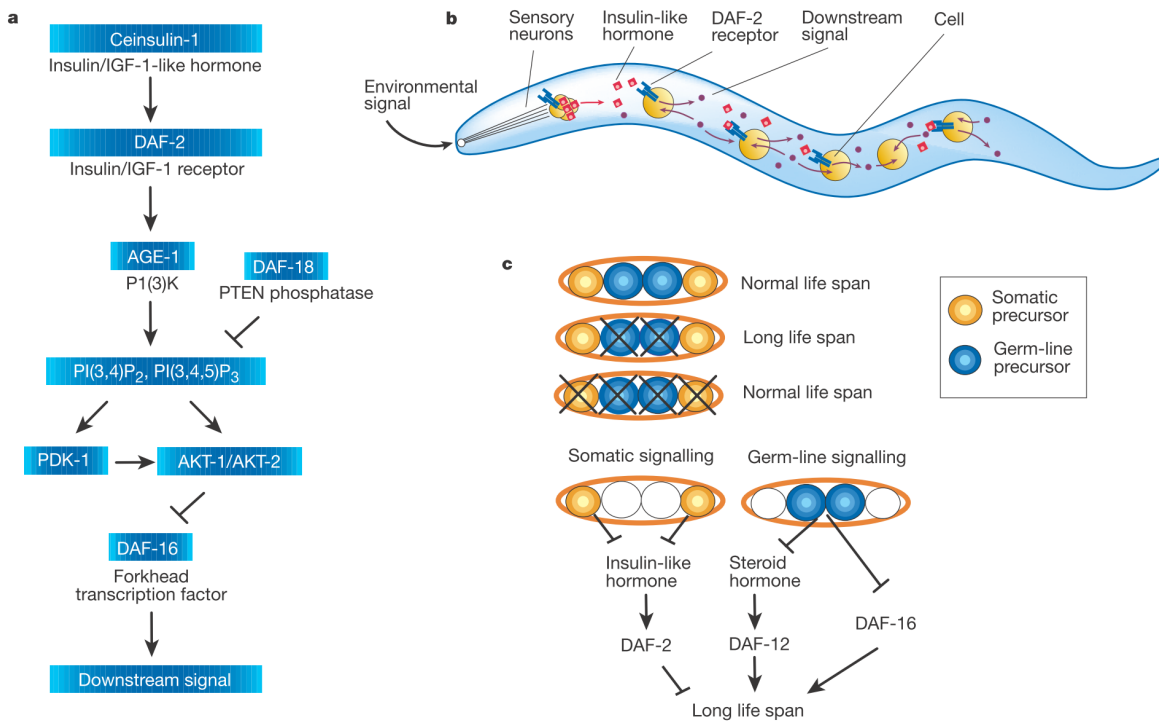


Figure 1.2: Regulation of *C. elegans* aging by an elaborate endocrine network. Adapted from figure 3 in [44].

1.2.3 Dietary Restriction

While the insulin/IGF-1 pathway is the most well-characterized prolongevity genetic pathway, dietary restriction (also known as caloric restriction), in which calories are limited to 60–70% of *ad libitum* in-

take, is the most well-understood intervention. It was first observed in 1935, when McCay and Crowell published their finding that by severely restricting nutrient intake, the lifespans of laboratory mice could be dramatically extended [45]. Since then, the lifespan-prolonging effects of dietary restriction have been observed in a variety of model animals, including other rodents, worms, and yeast [44]. Somewhat mixed but generally positive outcomes have also been reported in primates [46–48].

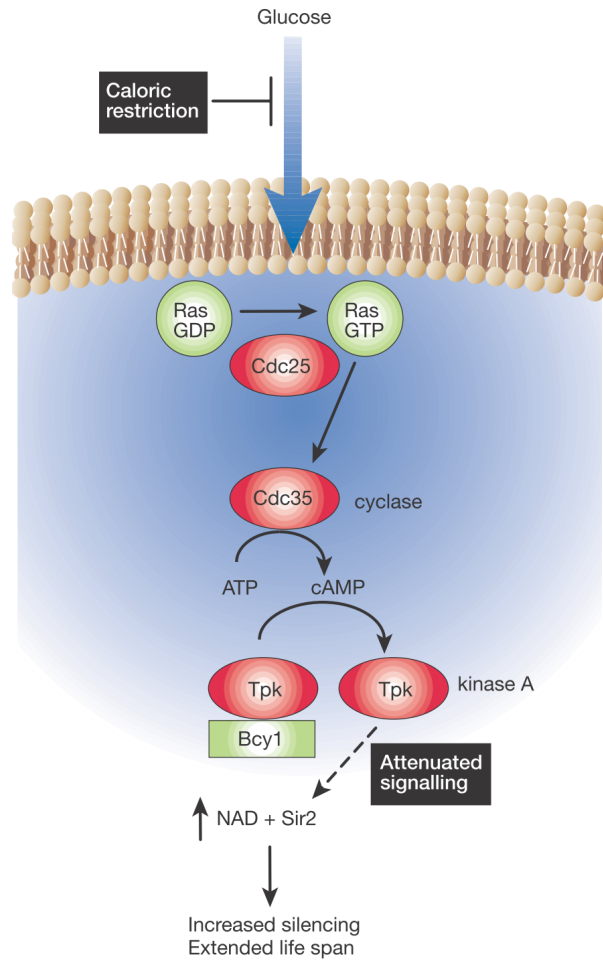


Figure 1.3: Signaling network of caloric restriction in yeast. Adapted from figure 2 in [44].

While the lifespan-prolonging effects of dietary restriction are well-documented, the general mechanism by which caloric restriction works remains unclear. One idea is that caloric restriction reduces an organism’s metabolic activity, therefore lowering the amount of reactive oxygen species produced and reducing the oxidative damage caused by those reactive oxygen species. This, according to the free-radical theory of aging [49], will slow the aging process and result in extended life.

While the general mechanism through which caloric restriction acts remains unclear, its down-

stream targets in budding yeast have been identified. Figure 1.3 outlines the pathway through which dietary restriction acts in yeast, acting through a Ras-GTPase-mediated pathway before activating NAD and Sir2. Interestingly, dietary restriction in yeast acts by silencing gene expression through chromatin remodeling [44]. However, it is not yet clear how the silenced genes go on to produce a phenotype and ultimately extend yeast lifespan.

1.2.4 Discussion

In general, genetics research on aging has been very successful at discovering the pathways and networks through which lifespan-associated genes act. In addition to the two pathways highlighted here, several others are known to modulate the aging process independently [26, 29]. Many efforts have been made to understand these pathways in a wide variety of model organisms, and a cohesive picture of the upstream portion of aging regulation has been built.

In sharp contrast, however, the mechanisms through which aging phenotypes are mitigated or exacerbated by these pathways remains unclear. The majority of studies consist of making genetic modifications and then observing lifespans. Through a series of careful and insightful mutants using tools such as double mutants, tissue-specific knock-outs, and knock-downs, scientists have been able to build models of the complex webs of interactions depicted in figures 1.2 and 1.3. This has served to move us a few steps closer to the ultimate phenotype down the signaling cascade. Conceptually, however, we have not made substantial advances in understanding the underlying mechanisms of aging.

1.3 Biodemography of Aging

In contrast with more deductive studies on the mechanisms of aging, inductive studies by biodemographers have provided rich epidemiological descriptions of aging. Despite its biological complexity and uncertain evolutionary origin, the defining empirical feature of aging is simple: At its core, aging is simply the statistical phenomenon of an increased probability of death over time. Alternatively, as an analogy, while evolutionary theory and molecular biology attempt to answer the questions of “why?” and “how?” we age, respectively, biodemography tackles the question of “when?” [50].

1.3.1 Gompertz-Makeham Model of Mortality

The field of biodemography has its roots in an observation made by Benjamin Gompertz, an actuary, in 1825. While seeking to increase efficiency of policy pricing for a life insurance company, Gompertz found that human mortality increases roughly exponentially with age [17, 51]. In other words, the hazard function has the form

$$\mu(x) = \alpha e^{\beta x}, \quad (1.1)$$

where $\mu(x)$ represents the probability of death for an individual at age x , and α and β are constants (and e is the base of the natural logarithm). This means that at a given age, the increase in mortality rate (i.e. aging) is proportional to the current mortality rate. While the mechanistic basis for this property of human mortality is still unclear, it suggests certain features for the underlying biological process.

In general, the Gompertz model from equation 1.1 is a good fit to real mortality data [52]. However, Gompertz himself noted two important exceptions: The first is that the Gompertz model does not appear to describe mortality trends at especially advanced ages (above age 92)⁴. The second issue is that the equation fails to model extrinsic mortality (such as accidents, etc.), which does not increase with age. A later modification, generally attributed to Makeham, to equation 1.1 addresses the second issue [53, 54]. The modified Gompertz-Makeham equation,

$$\mu(x) = \alpha e^{\beta x} + \lambda, \quad (1.2)$$

includes a λ term for extrinsic mortality. Note that the overall hazard function $\mu(x)$ is composed of an age-dependent term $\alpha e^{\beta x}$ and an age-independent term λ . In addition to founding the field of biodemography itself, Gompertz's insight continues to be relevant today, providing insights into the biology of aging [55].

⁴This is discussed more fully in a later section.

1.3.2 Late-Life Mortality Deceleration

One of the most striking features of empirically observed mortality curves is a deceleration of mortality at the oldest ages [18]. As mentioned earlier, this was noted by Gompertz himself, and is a subject of ongoing discussion among biodemographers. The phenomenon is illustrated in figure 1.4, which presents the actual data in red with a non-decelerated Gompertz function in dark blue for comparison. Further, models derived from logistic and quadratic fits are displayed in cyan and green, respectively.

The actual data dramatically deviates from the dark blue Gompertz curve and subsequently plateaus. This indicates that in some sense, the oldest individuals have stopped or slowed aging. Their mortality risk is no higher (or just barely higher) than that of their (slightly) younger counterparts. One proposed explanation is grounded in reliability theory have arisen, and argues that the aging process can be understood as a series of discrete steps, with individuals at the final steps of the progression all experiencing similar mortality risk [55]. While a number of interesting ideas have been proposed, there is currently no consensus on the mechanism underlying late-life mortality deceleration.

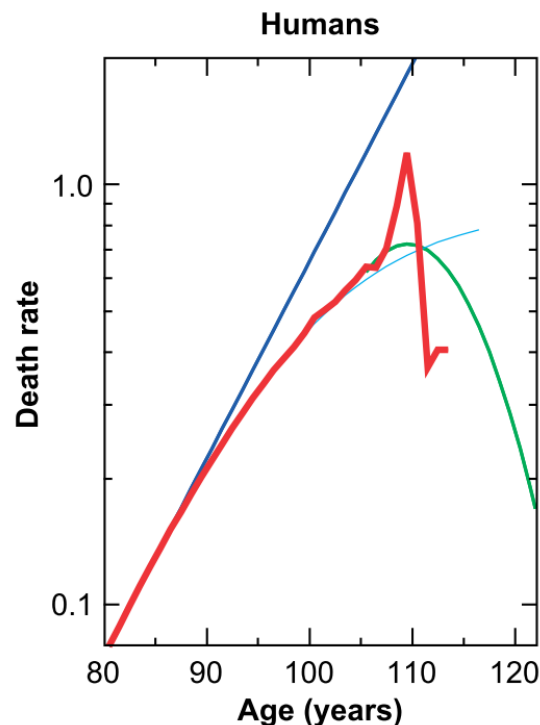


Figure 1.4: Age trajectories of death rates for human females. The red line represents an aggregation of data from Japan and 13 Western European countries. The cyan, and green lines represent best fit curves for the full data derived from logistic and quadratic functions, respectively. The darker blue line (note the logarithmic scale on the y-axis) represents a Gompertz-Makeham curve fit to the data between ages 80 and 84. Adapted from figure 3 in [18].

1.3.3 Postponement of Senescence

One relatively recent development in the biodemography of aging is the finding that mortality at old ages is being postponed [56]. The key piece of evidence for this assertion lies in the roughly constant gap between the X_5 and X_{10} curves in figure 1.5, which indicate the ages at which female life expectancy is 5 and 10 years, respectively. This implies that the X_{10} age represents a consistent “aged” state for women, since all women at age X_{10} can expect to reach age X_5 in a similar span of time⁵.

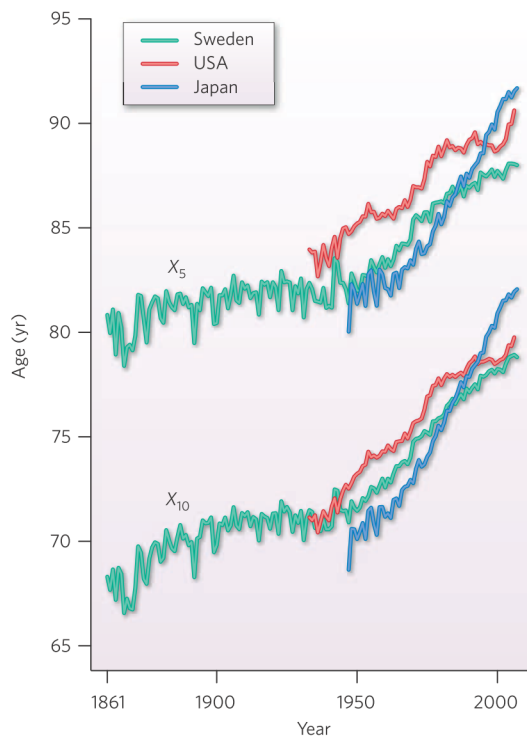


Figure 1.5: The postponement of mortality for females. Adapted from figure 1 in [56].

In some sense, this finding can be interpreted to mean that a Japanese 80-year-old woman in 2000 is equivalent in health to a Japanese 70-year-old women in 1950. If true, this would be very interesting indeed. However, the usual caveat about historical trends applies: two individuals from two different eras are in different environments. Improved medical care, for instance, can increase the life expectancy of sicker individuals. On the other hand, the impressive consistency of the X_{10} – X_5 gap

⁵To make an explicit analogy, if aging is a stereotyped journey consisting of discrete states, or “towns”, and stretches of road (periods of time) traveling between them, we can consider X_{10} and X_5 to be two towns along the way, and the period of time between them to be the road leading from one town to the other. In figure 1.5, we see that the length of road between these two states has not changed, while the corresponding chronological ages have increased. In the physical road analogy, this suggests that the road ahead has not been compressed or stretched, and that the distance landmarks beyond X_5 have also remained constant. Thus, the character of the journey ahead is constant for a woman at age X_{10} , regardless of her chronological age and historical time period.

argues for mortality postponement being genuine.

1.3.4 Biomarkers of Aging

While survival statistics can predict much of the mortality of a large population in aggregate, they are less accurate when applied to individuals. Since aging can vary significantly for different individuals at the same age, an individual's chronological age is a limited predictor of their actual mortality risk [18].

In order to develop improved prognostic capability for mortality, demographers have sought to identify biomarkers of aging, functionally defined as a biological parameter of an organism that either can better predict functional capability or mortality risk than chronological age [57]. This is motivated by an array of valuable applications, including improved actuarial modeling, biological investigations of the mechanisms of aging and therapeutics to slow its progress, and the clinical ability to better target interventions to at-risk patients.

Driven by these goals, researchers in the 1970s and 1980s proposed a large number of candidate biomarkers of aging [58–60]. Though these studies identified several putative biomarkers, many of the published multivariable composite scores were overfit—that is, overly tuned to a very specific dataset. For example, Consequently, these composite scores did not have broad applicability, and later studies failed to validate the original findings [57, 61–64].

Subsequently, much recent work has had a narrower scope, focusing on predicting specific disease processes instead of all-cause mortality [65–67]. Many physiological parameters, such as blood pressure [68] and body mass index (BMI) [69], have been well-characterized as risk factors for cardiovascular disease and other specific morbidities. In general, these studies have focused on middle-aged individuals and have emphasized risk over a limited term, often just 5- or 10-year periods (e.g. [70]). In addition, most of the work on both general biomarkers of aging and specific risk factors has been limited to the analysis of data from single time points (with a few exceptions, e.g. [71]).

1.3.5 Discussion

Overall, recent studies in biodemography have been the source of a number of interesting insights into the aging process. The plateauing of mortality at very old ages suggests that there is no inherent limit to maximum human lifespan. The postponement of mortality illustrated by figure 1.5 means that individuals today can look forward to significantly longer, healthier lives than our ancestors.

By focusing on only mortality, however, biodemographers are limited to a relatively sparse description of aging, and often have difficulty drawing mechanistic conclusions from their results. Further, aggregate results describing population-level trends in the aging process do not address individual differences in the aging process. I believe that a renewed focus on biomarkers and individual variation could provide a richer description and deeper understanding of aging. For example, attempting to detect and measure individuals who are more or less “aged” than their chronological age peers could lead to actionable insights into modulators of the aging process. It could help a generation to age well and to maintain good health and function longer.

1.4 Mechanics of Phenotypic Aging Trajectories

The results described in the body of the dissertation lie at the intersection of biodemography and mechanistic aging research. In particular, they serve to bridge some of the gaps between known molecular regulators of aging, which are upstream factors that modulate the aging process, and biodemography, which uses longitudinal tracking to understand downstream trends in aging and mortality in a population. Here, we focus on the characteristic patterns of physiological changes that accompany the aging process and exert their effects between molecules responsible for the initial portions of the cascade and the final organismal endpoint of increased mortality and death. In both the tractable model worm *C. elegans* and in more limited data in humans, this work uncovers fundamental insights into the nature of aging process and its associated physiological changes.

In the first chapter, we begin by developing a novel culture system to longitudinally and systematically monitor the physiological changes that occur in aging *C. elegans*. By following a genetically homogeneous population of 734 individuals reared in identical environments, we develop novel insights into how initial small-scale stochastic fluctuations are amplified through organismal physiology into dramatic differences in lifespan. This work, which is the first systematic study of the biology of individuality in metazoans, found that while long- and short-lived individuals start adulthood in similar levels of physiological health, longer-lived individuals then experience slower declines in function, but spend a disproportionately large portion of life in poor physiological health. We further find that the period of early-life good health is much less variable than the period of late-life advanced senescence, which we therefore conclude to be a more plastic phase of life.

In the second chapter, we extend a similar approach to existing human data from the Framingham Heart Study (FHS), the largest and most comprehensive longitudinal study of human physiology to date. In that study, we show that simple physiological measurements have broader lifespan-predictive value than previously believed and that incorporating information from multiple time points can significantly increase that predictive capacity. Using longitudinal data from a cohort of 1349 human participants in the Framingham Heart Study, we show that even in early-to-mid adulthood, almost 10% of variation in future lifespan can be predicted from simple physiological parameters. Further, different clinical measurements are predictive of lifespan in different age regimes, indicating a diversity of mechanisms of physiological aging. Finally, we find that blood glucose and blood pressure are best considered as measures of a rate of “damage accrual”, such that total historical exposure, rather than current measurement values, is the most relevant risk factor (as with pack-years of cigarette smoking). This insight is broadly applicable, indicating that future recovery does not necessarily fully compensate for present poor health.

Chapter 2

The Physiological Basis of Variation in Longevity within an Isogenic Population

The authors of the following publication [72] are: William B. Zhang, Drew B. Sinha, William E. Pittman, Erik Hvatum, Nicholas Stroustrup, and Zachary Pincus.

Abstract

The surprising degree of variation in lifespan within even homogeneous populations remains largely unexplained. We sought to understand how physiological aging differs between long- and short-lived individuals within a population of genetically identical *C. elegans* reared in a homogeneous environment. Using a novel culture apparatus, we longitudinally monitored aspects of aging physiology across a large population of isolated individuals. Aggregating several measures into an overall estimate of senescence, we find that long- and short-lived individuals start adulthood on an equal physiological footing. However, shorter-lived individuals then experience more rapid declines in function. Unexpectedly, we find that longer-lived individuals, despite a slower rate of decline, spend a disproportionately large portion of life in poor physiological health. Overall, the period of early-life good health is much less variable than the period of late-life advanced senescence, which we conclude to be a more plastic phase of life.

2.0 Introduction

Pioneering work over the last quarter century has identified many molecular pathways involved in determining lifespan, illustrating that aging is a plastic process [13, 44, 73]. To date, many genes, small molecules, and environmental interventions have now been found that alter a population's mean lifespan. However, even in very homogeneous conditions, there is a large degree of variability in lifespan around that mean [18]. Comparatively little is known, however, about the origins and consequences of inter-individual differences in the aging process.

Often, the bulk of variability in lifespan is of neither genetic nor environmental origin. Studies estimate that only 15–25% of variation in human lifespan is attributable to genetic variation [14, 74–76]. Moreover, even genetically identical populations of model organisms, reared in tightly-controlled laboratory conditions have a similar degree of variability in lifespan as outbred humans (relative to the population mean) [18, 77]. Even conditions and mutations that dramatically extend or shorten lifespan do not generally change the degree of inter-individual variation in longevity [78].

This raises a fundamental question: what distinguishes long-lived from short-lived individuals, when they are genetically identical and reared in the same cage, vial, or culture dish? We and others have identified inter-individual differences in gene expression that are predictive of future lifespan in *C. elegans*, either early [79, 80] or late [80, 81] in adulthood. However, chronological lifespan merely measures the end of a complex process of aging and senescence. Pioneering studies of individual animals have therefore sought correlates of early and mid-life physiological health as well [80, 82–84]. But due to technical limitations and the use of invasive measurements, most previous efforts were unable to follow individuals longitudinally. Therefore, the relationship between the complex progression of aging and ultimate lifespan has been relatively unstudied. In this work, we focus on the physiological changes that characterize senescent decline in *C. elegans* [85–88].

In particular, we aimed to determine how the physiological process of aging differs between long- and short-lived wild-type *C. elegans*. Do individuals with different lifespans senesce in a qualitatively different manner? Or does an identical aging process simply play out at a different rate for short- and long-lived individuals? In order to address these questions, we developed a novel experimental technique to isolate and image many individual *C. elegans* over each animal's entire lifespan. This is not possible with existing automated vermiculture methods, which generally focus on enumeration

of lifespans for screening purposes [89–91], and are not designed for making detailed measurements of physiology. Here, using custom microscopy hardware and image-analysis software, we performed a battery of non-invasive physiological measurements of each individual, every three hours over their approximately two-week lifespans. This rich dataset of longitudinal measures of 734 animals, based on over 400,000 images obtained at subcellular resolution, allowed us to retrospectively understand how and when the aging process diverges between long- and short-lived individuals.

Overall, we find two chief differences between longer- and shorter-lived individuals. First, though long- and short-lived individuals start out on an equal physiological footing, longer-lived individuals experience a lower rate of physiological decline. In effect, individuals with long lifespans *age more slowly* than their short-lived siblings. Second, counterintuitively, long-lived individuals experience an overall *lower* average quality of life compared to shorter-lived individuals, due to a disproportionately extended “twilight” period of low physiological function. Indeed, inter-individual differences in the length of this low-function period account for the bulk of all variability in lifespan. These findings lead us to conclude that within a homogeneous population subject to stochastic perturbation, the most plastic period in the aging process is end-of-life senescence.

2.1 Results

2.1.1 Longitudinal Measurements of Physiology in Individual *C. elegans*

In order to measure physiological changes throughout aging, we developed a specialized culture system to allow for observation of many freely moving, isolated individuals throughout their entire lives. This new system dramatically improves on our previous culture techniques [79], allowing for denser culture (~100 animals per standard microscope slide) and fully-automated image acquisition and processing. In brief, we produce a smooth hydrogel surface atop standard microscope slides by polymerizing polyethylene glycol (PEG) monomers *in situ* (see Materials and Methods). We then dispense a grid of ~2 mm diameter droplets of concentrated bacteria onto the gel, to provide a food source. After allowing each droplet to adsorb to the surface, we transfer one egg from the temperature-sensitive sterile strain *spe-9(hc88)* to each food pad. Finally, we pour a thin layer of polydimethylsiloxane (PDMS) over the gel. While polymerizing overnight at room temperature, the PDMS also cross-links with unreacted acrylate moieties in the PEG gel. This cross-linking proceeds everywhere except where the

PEG is separated from the PDMS by the bacterial food pads. Thus while each individual *C. elegans* is free to move about the 2-dimensional surface of its food pad, it is constrained at all borders by strong covalent bonds within and between the PEG and PDMS polymers (Figure 2.1A).

We placed slides constructed in this fashion on the stage of a computer-controlled microscope, housed in a temperature- and humidity-controlled enclosure. Every three hours, timepoint data for each individual was acquired autonomously, driven by custom microscope-control scripts (Figure 2.1B). We designed a comprehensive panel of phenotypic measurements encompassing five diverse aspects of aging physiology. For this, we drew from previously validated “biomarkers of aging” [57,92]. These biomarkers measure aspects of physiology that differ prospectively between long- and short-lived individuals, and can thus be used to predict an individual’s future lifespan. First, we examined *C. elegans* neuromuscular function, as measured by locomotory ability. Second, we assessed age-associated tissue deterioration through quantitative measurements of textural order and disorder in brightfield images [79,93]. Third, we measured age-related declines in homeostatic ability, as manifested in the accumulation of fluorescent non-hydrolyzable materials in intestinal endosomes [85,94–97]. Fourth, we evaluated nutritional history and somatic investment through cross-sectional body size [79,98]. Fifth, we quantified reproductive output and investment through the number of oocytes laid [88,99]. These measurements were all performed via custom, fully automated image segmentation and analysis software (Figure 2.1C and D; see Materials and Methods). Taken together, this panel comprises a diverse set of individual measurements, allowing us to characterize longitudinal changes in distinct aspects of aging physiology.

2.1.2 Distinct Physiology of Long- vs. Short-Lived Individuals

In total, we observed 734 individuals from hatching to death, through the stages of larval development, reproductive maturity, and senescence. The population, maintained throughout life at 25°C, had a mean lifespan of 12.1 days with a standard deviation of 2.3 days from hatch, within the range of lifespans previously observed at this temperature [79,100,101]. In order to rule out potential systematic biases in our data, we confirmed that overall lifespan distributions are consistent across experimental runs spanning roughly three months of time (Figure 2.7A), and are not influenced by the specific culture slide used within an experimental run, or by the spatial position of an individual’s food pad within the slide (Figure 2.7B–G).

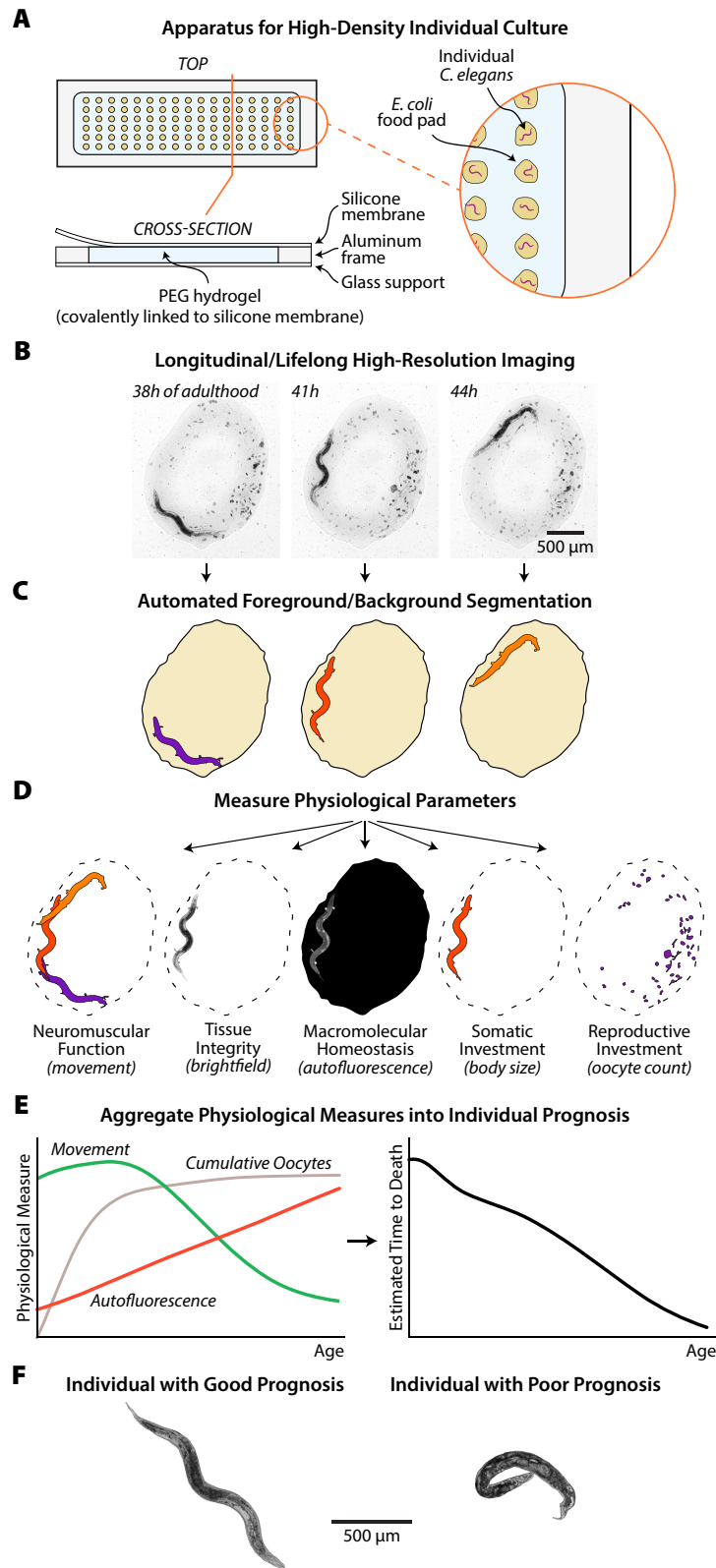


Figure 2.1: Experimental workflow. (A) A novel culture device allows for lifelong, longitudinal observation of a high-density array of isolated individual *C. elegans*. Individuals are free to move about on pads of bacterial food, but cannot depart the pads. (B) Images of each individual *C. elegans* are acquired every three hours throughout life, at 2.2 μm resolution. The *spe-9(hc88)* temperature-sensitive sterile strain is used to prevent reproduction. Unfertilized oocytes are visible as dark clumps on the bacterial food pad. (C) Custom software automatically annotates the region of the food pad and the position of the animal. (D) These annotations are used to make several physiological measurements (left to right): Movement between and within timepoints is scored as a measure of neuromuscular function. The brightfield image of the animal is used to automatically score tissue integrity. Red autofluorescence is used as a measure of macromolecular homeostasis. To characterize somatic maintenance, body size is measured as cross-sectional area. Last, the number of oocytes laid is counted as a measure of reproductive investment. (E) This battery of five longitudinal physiological measurements is aggregated together to produce an estimate of remaining lifespan at each timepoint. We use this “prognosis” as an operational definition of an individual’s overall degree of senescence. (F) Examples of prognosis scores. Left: a healthy, young adult with 10.3 estimated days of life remaining. Right: an unhealthy, late-life animal with 0.5 estimated days remaining.

We find that virtually all variation in lifespan is due to differences in the period between reproductive maturity and death, rather than in the length of larval development (Figure 2.7H–J). Though larval development takes 2.1 days on average (17.3% of an average animal’s lifespan), the variability of time in development accounts for less than 0.1% of the variability in total lifespan. Therefore, we limited our analysis to the animals’ lifespans after reproductive maturity.

The mean adult lifespan in our population is 10.0 days, ranging from 2.2–15.5 days. For illustration, we grouped the animals into seven cohorts by lifespan, with the first cohort containing individuals with adult lifespans of 2–4 days, the second containing individuals with adult lifespans of 4–6 days, and so forth (Figures 2.2A and B, 2.8), and plotted cohort averages of each of our physiological measurements over time (Figure 2.2C). For our measures of autofluorescence, body texture, and long-term movement, we observed a graded difference between shorter-lived and longer-lived cohorts (Figure 2.2D–F). At any given age, the shorter-lived cohorts had higher levels of autofluorescence, worse tissue maintenance, and were less mobile than their longer-lived peers. In contrast, for our measures of body size and reproductive output, we noticed a nonlinear trend among our lifespan cohorts (Figure 2.2G and H). For animals with adult lifespans from 2 to 8 days, larger body size and greater reproductive output were correlated with longer life, as in the existing literature [79, 88, 98]. Among the longest-lived cohorts, however, this trend reverses itself: of individuals with lifespans between 10 and 16 days, longer-lived individuals tend to be smaller and produce fewer oocytes.

We therefore examined this nonlinear relationship between longevity and certain aspects of physiology more closely. Overall, this effect is largely driven by a small subpopulation (13.7% of the total) of small, sickly-looking individuals which appear unhealthy throughout their lives but have very long lifespans (Figure 2.9A–G). We have also found evidence of this population in standard *C. elegans* culture conditions (Figure 2.9D). Overall, however, the existence of this sub-population suggests that there may be a component of functional health that can be de-coupled from lifespan. In particular, it appears that some longer-lived individuals may be qualitatively less healthy over the course of their lives compared to shorter-lived peers. Regardless, excluding this population does not substantially alter the results described below (Figure 2.10A–H).

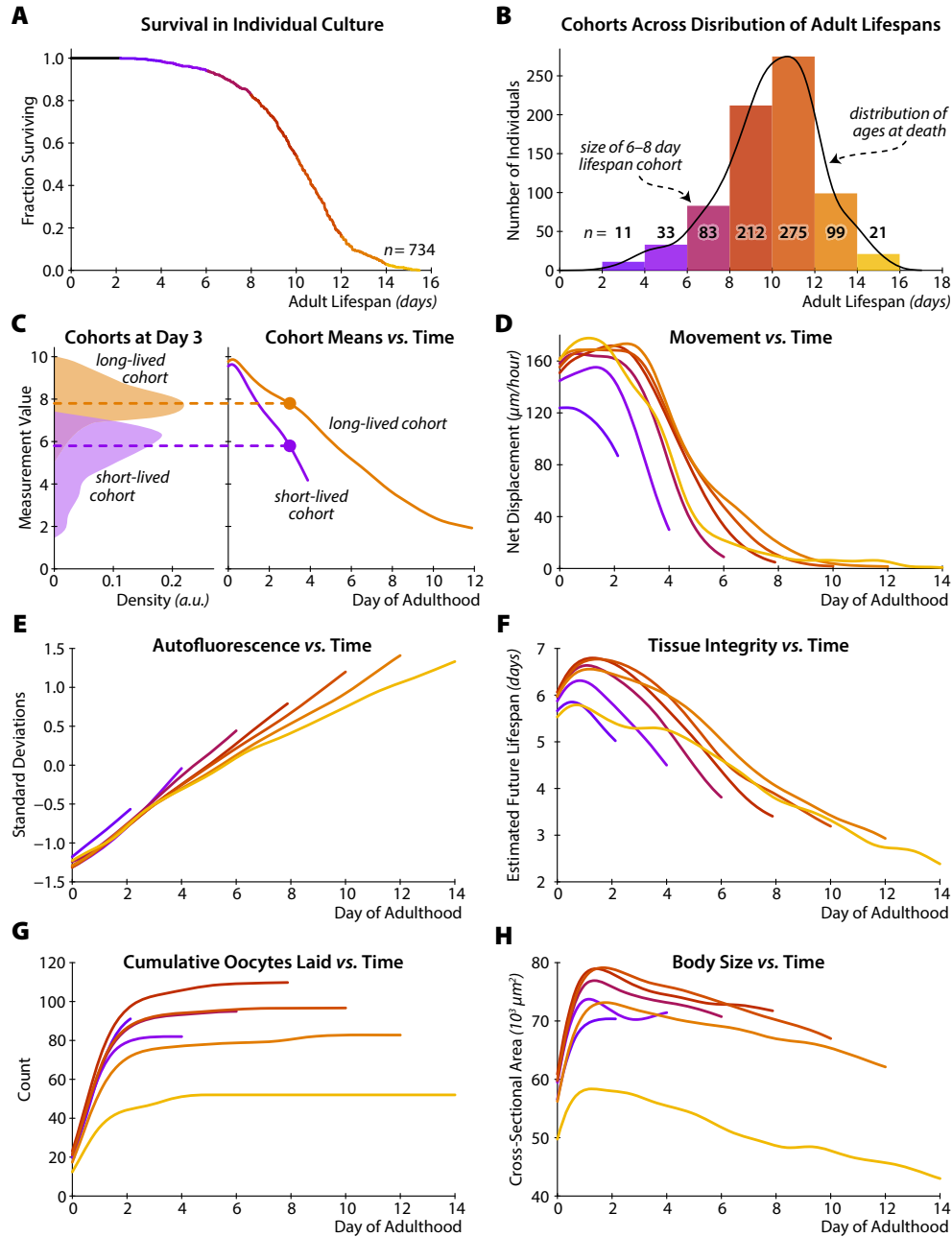


Figure 2.2: Variation in lifespan and physiology within a homogeneous population. (A) The survival curve for all 734 individuals in our study population, as a function of age after reproductive maturity. (B) Histogram of the number of individuals in each of seven cohorts, grouped by lifespan into 2-day-wide bins. A kernel density estimate of the underlying distribution of ages at death is shown in black. (C) An illustration of how we calculate trends of a given measurement over time. At left, the distributions of values for some lifespan-predictive measurement are shown for a long- and short-lived cohort, at day three of adulthood. Dashed lines show the mean of each distribution. At right, the trend in these means over time is plotted for each cohort. (D) Trends of bulk movement between three-hour timepoints over time, for each lifespan cohort. Due to the limited size of the food pad, this measurement saturates around $160 \mu\text{m}/\text{hour}$. (E) Trends in autofluorescence over time, measured as the 80th-percentile of whole-body red-channel autofluorescence. (F) Trends in tissue integrity score over time. This score is produced via support vector regression that maps brightfield image texture into an estimate of remaining days of life. (G) Trends in cumulative oocytes laid. (H) Trends in body size.

2.1.3 Differences in Aging Rate and Health at Death in Long- vs. Short-Lived Individuals

To understand how aging differs in long- and short-lived individuals, we developed a physiological measure of overall senescence. Since the main hallmark of aging is increased mortality over time, older and less healthy individuals will have a shorter expected future lifespan. As each of the diverse physiological parameters we measured is a known biomarker of aging—that is, a predictor of future lifespan—we therefore aggregated these measures into a single, maximally informative estimate of future lifespan. We use this estimate, which we term prognosis, as a measure of an individual’s degree of senescence, or, equivalently, its state of health.

To construct this prognosis, we first verified that in our dataset, each of our measures is a *bona fide* biomarker of aging and of mortality (Table 2.3). The trends over time of the raw measurements also indicate that the relationship between each parameter and future lifespan is generally nonlinear (Figure 2.2D–H). Therefore, we used support vector regression to define a nonlinear mapping from an individual’s measured physiological parameters at any given timepoint to an estimate of its future lifespan at that time. The overall r^2 for this regression is 0.695 (10-fold cross-validated $r^2 = 0.669$), suggesting that throughout life, these measures are able to explain the bulk of the total variability in future lifespan. While some of the measurements correlate with one another and thus redundantly measure certain aspects of physiology (Table 2.1), each contributes a measurable amount of independent, nonredundant information about future lifespan (Tables 2.2 and 2.3). This indicates the physiological parameters as a set, and thus our prognosis score, report on multiple distinct aspects of the aging process. We then performed extensive controls, described in the Methods and Resources section, to verify that this prognosis score is neither driven by our choice of regression methodology, nor by any particular physiological measurement.

We next use this prognosis of future lifespan to distinguish among several possibilities for how long- and short-lived individuals differ in physiological aging. First, it could be that short-lived individuals simply start their adulthoods in worse health (the “starting point hypothesis”; Figure 2.3A). Second, it is possible that senescence proceeds more rapidly in short-lived individuals (the “rate of aging hypothesis”; Figure 2.3B). Finally, it may be the case there is no difference in the trajectory of senescent decline between long- and short-lived individuals, and all individuals start out with similar prognoses

and decline at the same rate. Here, shorter-lived animals will be those that die “prematurely”, in more healthy-appearing states, before the full process of senescence has played out (the “premature death hypothesis”; Figure 2.3C). In this latter case, all individuals would be, by our measurements, indistinguishable over the course of aging, and death would be stochastic and unpredictable. Short-lived individuals would differ from long-lived ones by simply happening to be the ones that died early.

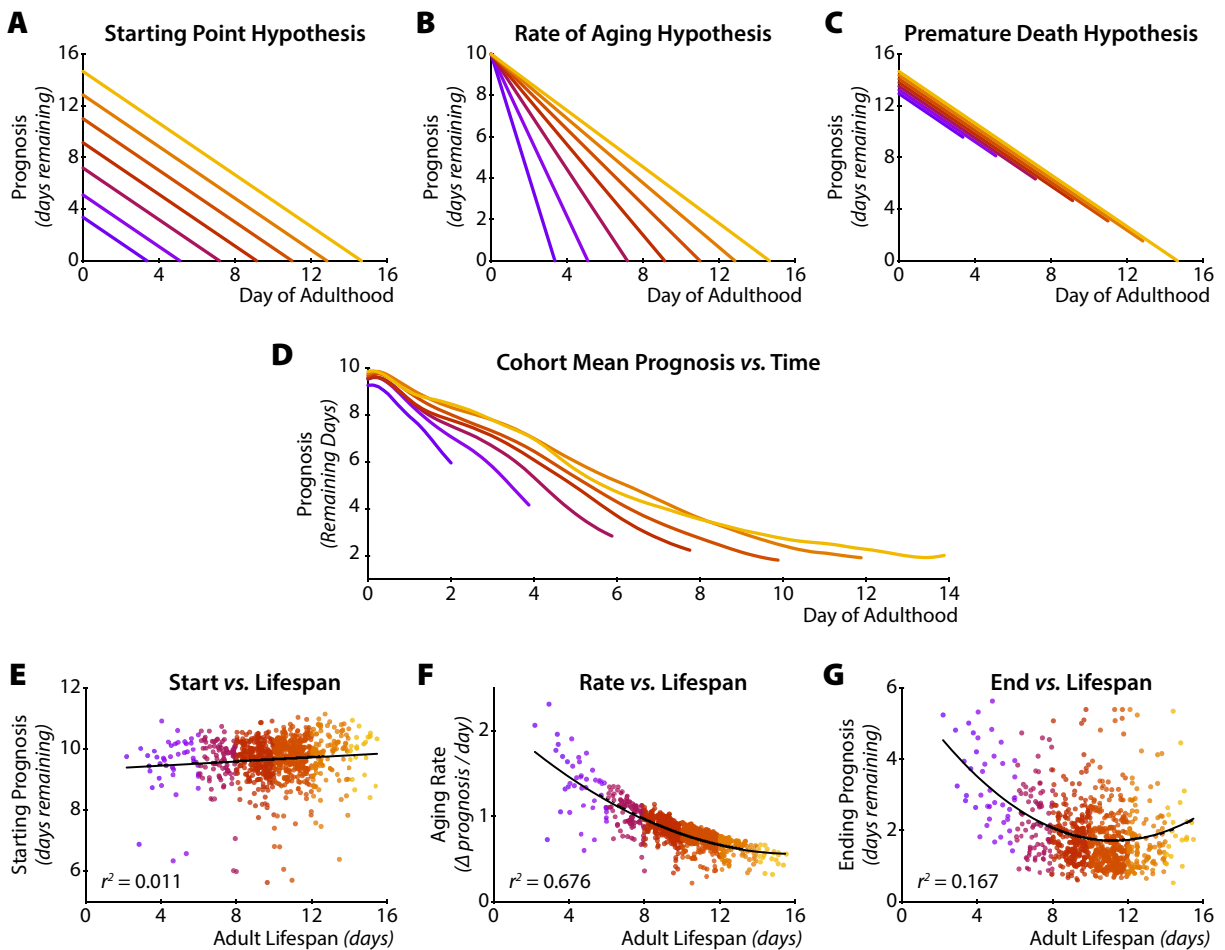


Figure 2.3: How does aging physiology differ between long- and short-lived individuals? (A) “Starting Point” hypothesis: long-lived individuals start their adulthood healthier than short-lived individuals. (B) “Rate of Aging” hypothesis: long-lived individuals age more slowly than do short-lived individuals. (C) “Premature Death” hypothesis: short- and long-lived individuals are indistinguishable over the course of their lives. In this case, differences in lifespan arise from stochastic, inherently unpredictable causes of death or from factors outside our prognostic criteria. (D) Trends in the decline of prognosis over time, for each of the seven lifespan cohorts in Figure 2.2. These qualitatively match the “rate of aging” and “premature death” hypotheses from panels b and c. (E) We observe little quantitative relationship between lifespan and starting health (measured by an individual’s prognosis score at reproductive maturity). (F) In contrast, there is a strong negative correlation between lifespan and the rate of decline of physiological health. (G) Last, there is a moderate negative correlation between health at death and lifespan, suggesting stochasticity in death or unmeasured differences in functional health.

Strikingly, the trajectories of our health score look very similar to those predicted by the “rate of aging” and “premature death” hypotheses, even from a cursory visual inspection of Figure 2.3D. To

test this more rigorously, we examined the relationships between lifespan and an individual’s prognosis at the first day of adulthood (i.e. its starting health), its rate of decline in prognosis (its rate of aging, or senescence), and its prognosis at the time of death (how “premature” its demise appears to have been). As shown in Figure 2.3E and F, there is no substantial relationship between starting health and lifespan, but a strong correlation between the rate of decline (as measured by simply subtracting an individual’s ending health from its starting health and dividing by its lifespan) and lifespan (Pearson $r^2 = 0.676$; $p < 10^{-180}$, F-test; Spearman $r^2 = 0.615$; $p < 10^{-153}$, F-test) and a modest one between prematurity of death and lifespan (Pearson $r^2 = 0.096$; $p < 10^{-30}$, F-test; Spearman $r^2 = 0.123$; $p < 10^{-16}$, F-test). (Quadratic fits were used to estimate r^2 values due to the clear nonlinearity of these two relationships.) This latter trend indicates a modest but significant contribution either from stochastic death, or from differences in health not captured by our measurements. Overall, we conclude that long-lived individuals are not physiologically different from short-lived individuals at the start of reproductive maturity, but age more slowly throughout adulthood and experience the full scope of senescent decline.

2.1.4 Uneven Rates of Aging Produce Lower Quality of Life in Longer-Lived Individuals

Next, we asked whether long and short-lived individuals exhibit qualitatively different aging processes, in addition to having quantitatively different rates of aging. The black line in Figure 2.4A presents a “neutral rate of aging” for both long- and short-lived individuals: the level of health decreases uniformly throughout life. However, an individual might have a positive deviation (green line) from the neutral, straight-line decline, such that the individual appears to maintain a high level of function until a precipitous decline at the very end of its life—a phenomenon known as “morbidity compression” [102]. Alternately, an individual may have a negative deviation (red line) from the neutral decline, and will thus senesce relatively early in its life, and persist in an extended “twilight” period of low physiological function for a larger fraction of its life.

To visualize these qualitatively different classes of functional declines independently of their quantitative rate, we represent physiological change not as a function of chronological time, but as a function of the relative fraction of lifespan elapsed. If the process of aging is identical between long- and short-lived individuals except for differences in rate, then the trajectory of physiological decline of co-

horts with different lifespans should fully overlap when rescaled to “relative time” (Figure 2.4C, left). Alternately, long-lived individuals may have systematically more positive deviations, and thus will remain healthy for a greater proportion of their lives (Figure 2.4C, center). This would lead long-lived animals to experience a higher average quality of life, as measured by the area under the health vs. relative-lifespan curve for long-lived vs. short-lived individuals. Finally, the opposite may be true: long-lived individuals may exhibit declines in health relatively earlier in life, leading to a greater proportion of life spent in poor health (Figure 2.4C, right). In this scenario, due to an extended period of poor physiological function, longer-lived individuals would have an overall lower average quality of life than shorter-lived individuals.

Figure 2.4D shows that this latter hypothesis is most accurate, and that long-lived individuals experience a lower average quality of life compared to their short-lived counterparts. This is visible not only in the cohort averages of Figure 2.4D but in the clear negative relationship between each individual’s lifespan and the deviation from a neutral, straight-line decline from the population mean starting prognosis to the mean prognosis at death (Figure 2.4E; Pearson $r^2 = 0.207$; $p < 10^{-37}$, F-test; Spearman $r^2 = 0.183$; $p < 10^{-33}$, F-test). Longer-lived animals typically have negative deviations (i.e. they decline in health relatively early in life), while shorter-lived animals have more positive deviations and decline in health relatively late in life.

To control for shorter-lived individuals dying in healthier states, we repeated the analysis with each animal’s health set to 1 at the onset of reproductive maturity and to 0 at the time of death (Figure 2.4F and G). Even when adjusted for each individual animal’s starting and ending health, the association between long lifespan and negative deviation remains (Pearson $r^2 = 0.123$; $p < 10^{-21}$, F-test; Spearman $r^2 = 0.106$; $p < 10^{-18}$, F-test).

Taken together, these results demonstrate that longer-lived individuals have systematically worse qualitative physiological declines, despite the fact that longer-lived individuals typically have a better health prognosis on any chronological day of life (Figure 2.3D). The extended end-of-life period of low function in long-lived animals simply drags the overall average quality of life below that of short-lived animals.

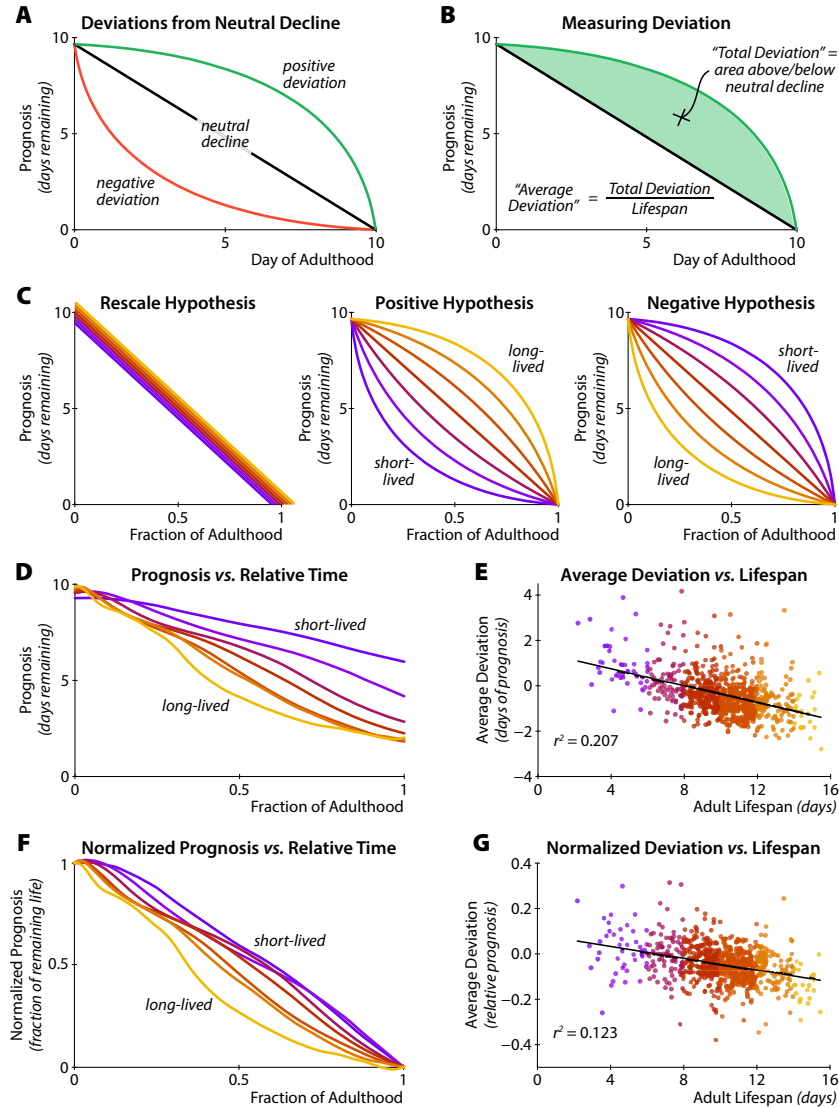


Figure 2.4: Systematic differences in the trajectories of physiological decline. (A) The pattern of decline can differ even among individuals with identical lifespans, starting prognoses, and ending prognoses. Individuals may experience senescence evenly throughout life (black; “neutral decline”). Alternately, senescence can accelerate early (red; a “negative deviation”), which produces a relatively extended period of low function. Finally, senescence can be delayed (green; “positive deviation”), leading to a compressed period of low function. (B) We quantify an individual’s trajectory deviation as the area between the actual trajectory (green) and a linear decline (black). This value is positive for trajectories above neutral decline, and negative for those below. To compare individuals with different lifespans, we divide this total area by each individual’s lifespan to produce the “average deviation” throughout life. (C) How trajectories of senescent decline may differ between long- and short-lived individuals. Left: Senescence is identical between long- and short-lived individuals and is merely stretched in time, causing the trajectories to align when plotted in terms of the relative fraction of life elapsed. Middle: Longer-lived individuals might have more positive deviations from neutral declines. Right: Shorter-lived individuals may have more negative deviations. (D) Trajectories of senescence for different lifespan cohorts in relative time. As in the “negative hypothesis”, shorter-lived individuals are systematically healthier at any given fraction of adult lifespan. (E) Lifespan is plotted against “average deviation”, where neutral decline is defined as the straight line between the population mean prognoses at reproductive maturity and death. Longer-lived individuals have negative deviation, while short-lived individuals experience positive deviation. (F) After controlling for differences in starting and ending prognosis, the “negative hypothesis” still applies qualitatively and (G) quantitatively.

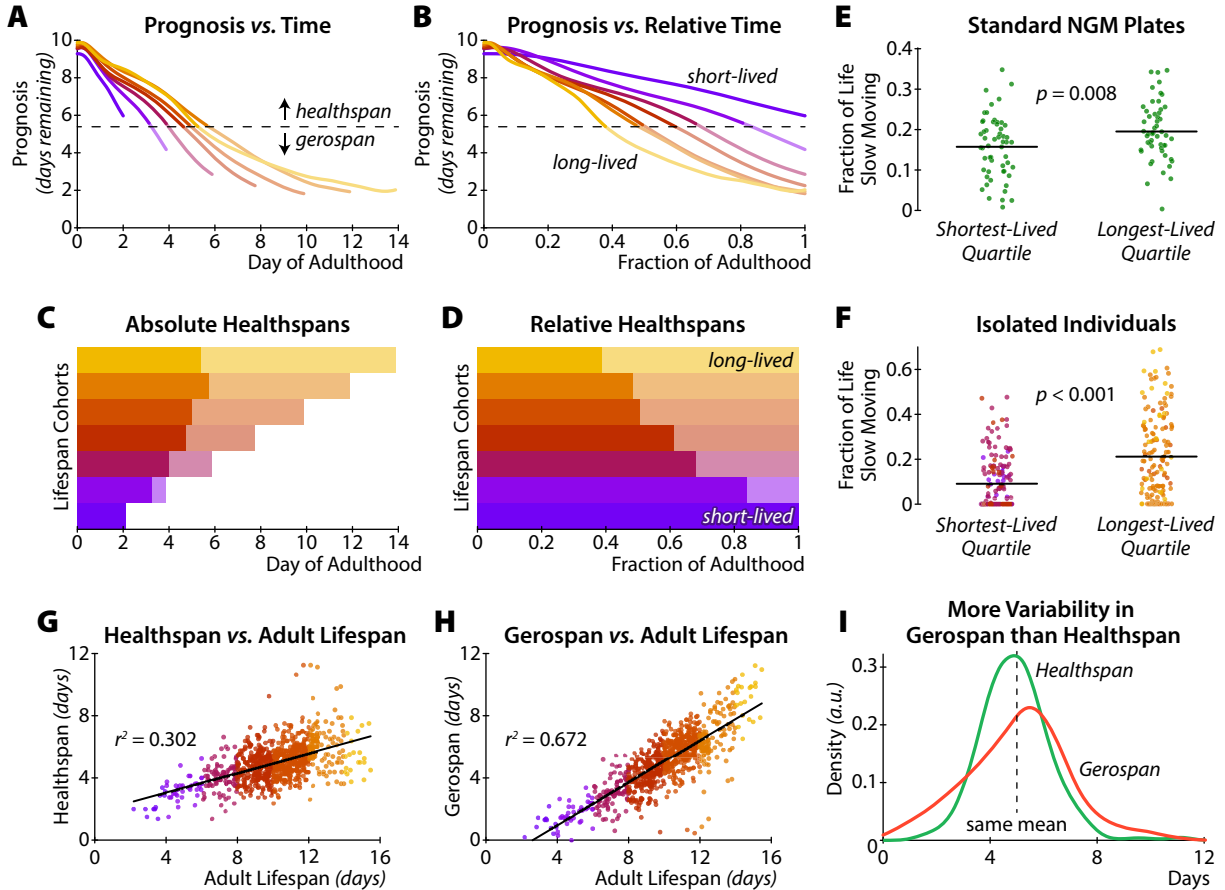


Figure 2.5: In both chronological (A) and relative (B) time, the trajectory of physiological aging can be thresholded into a span of high physiological function (“healthspan”; time spent above dotted line) and a span of low function (“gerospan”; time below dotted line). (C) In chronological time, longer-lived cohorts generally have longer period of good prognosis. However the differences in healthspan between these cohorts are small compared to the differences in gerospan. (D) In relative time, it is clear that longer-lived individuals are healthy for a smaller fraction of their total lifespan than shorter-lived individuals. (E) Data from a previous experiment using *spe-9(hc88); fer-15(b26)* individuals on standard *C. elegans* culture conditions [91] confirm that individuals with longer lifespans spend a larger fraction of their life in poor physiological function, as measured by fraction of life spent moving very poorly or not at all ($n = 55$ in each group). (F) An equivalent analysis of movement data from our culture apparatus produces similar results ($n = 146$ in each group). Across our population, lifespan positively correlates with both (G) healthspan (as calculated in panel A), and (H) gerospan. Compared to healthspan, variability in gerospan explains almost twice as much of the variability in lifespan (r^2 of 0.302 vs. 0.672). (I) This is because, despite having the same mean duration by construction, gerospan (red curve) is more variable across our study population than healthspan (green curve). The mean of both distributions is 5.0 days, with standard deviations of 1.3 and 1.9 days for healthspan and gerospan respectively.

2.1.5 Longer-Lived Individuals Have Disproportionately Extended Gerospans

The qualitatively worse senescent declines of long-lived individuals can be observed more starkly by partitioning each individual’s life into two segments: “healthspan”, the period of high physiological function, and “gerospan”, the period of low physiological function. Given a threshold prognosis score, we define healthspan as the period of time from the beginning of adulthood until an individual’s prog-

nosis dips below that threshold for the first time. Gerospan is then the remainder of life thereafter (Figure 2.5A and B). In order to make a neutral comparison, we selected a threshold value that yields identical average healthspans and gerospans across the population: 5.0 days each. (Similar analysis with different thresholds yields essentially identical results to the below; see Figure 2.11A–P.) Figure 2.5A and C show that, unsurprisingly, longer-lived individuals enjoy longer healthspans in absolute chronological time. However, the differences in healthspans among long- and short-lived cohorts are small compared to the differences in gerospans.

In contrast, we observe that despite this long chronological healthspan, longer-lived individuals nevertheless experience a systematically larger fraction of their total lives in senescent gerospan (Figure 2.5B and D). This is analogous to the results of our analysis of the full trajectories of senescence, above: long-lived individuals enjoy a better prognosis at any point in absolute chronological time, but experience declines in health relatively early in their lives.

In order to validate this key result and ensure it is not an artifact of our culture system or analysis methods, we turned to data from the “Lifespan Machine”, which measures the movement individual *C. elegans* on standard culture plates in order to tally lifespans in an automated fashion [91]. The Lifespan Machine tracks individual animals once they are no longer able to move more than a few hundred microns in any direction; therefore this system inherently measures a “fast moving span” and a “slow moving” span for each individual. We manually validated these span annotations from an extant dataset with a similar genetic background and culture conditions, and computed the “slow moving span” (i.e. gerospan) as a fraction of total lifespan for each individual. As shown in Figure 2.5E, longer-lived individuals in these conditions experience a larger portion of life in senescent, slow-moving states. If we define the slow-moving and fast-moving spans similarly in our present dataset, we observe a very similar trend in (Figure 2.5F).

This analysis provides an intuitive understanding of why longer-lived individuals spend more of their lives in gerospan. Figure 2.5G and H plot the relationship between total lifespan and healthspan or gerospan, respectively. Longer-lived individuals are both likelier to have longer healthspans and longer gerospans. However, while inter-individual differences in healthspan account for about 30% of the total variability in lifespan, differences in gerospan account for about 67% of variability in lifespan. As shown in Figure 2.5I, though we selected a threshold that yields equal mean healthspan and gerospan, there is simply more inter-individual variability in gerospan than healthspan. Indeed, this

relationship holds for several choices of threshold (Figure 2.11Q and R) and our full deviation analysis, which is not subject to any arbitrary threshold. In sum, variability in lifespan is in large part driven by differences in individual gerospans, and much less so by differences in healthspans. Taken together, this indicates that gerospan may be inherently more flexible than healthspan.

2.2 Discussion

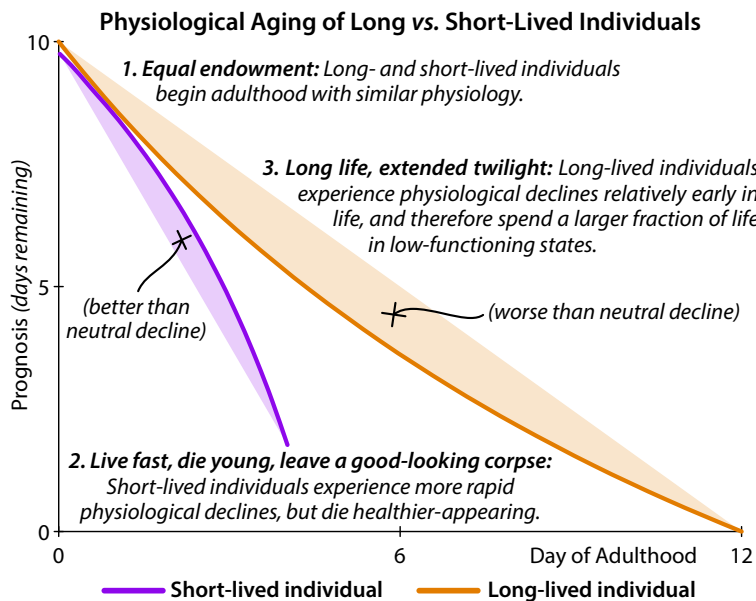


Figure 2.6: Summary of key findings. We evaluated the process of senescence in long- vs. short-lived individual, based on a “prognosis” score that aggregates multiple measures of aging physiology. First, based on our physiological measurements, long- and short-lived individuals are indistinguishable at the beginning of adulthood. Second, soon after the onset of reproductive maturity, short- and long-lived individuals diverge rapidly. Overall, short-lived individuals experience faster physiological aging than long-lived individuals. In addition, short-lived individuals often die “prematurely”, while still healthy-appearing. Third, we discovered that long-lived individuals spend a disproportionate fraction of their lives in highly senescent, ill-appearing states. This extended “twilight period” of low physiological function has the paradoxical effect of reducing the overall average physiological health of long-lived individuals to below that of short-lived individuals.

In this work, we examined the substantial variation in lifespan and aging physiology that exists even in isogenic individuals reared in identical environments. We developed a novel culture method that, for the first time, allows high-resolution imaging of a large number of individual *C. elegans* throughout life. This enabled us to analyze many different aspects of each individual animal’s physiology in longitudinal fashion, from hatching until death. Motivated by similar efforts to define and characterize a “biological age” [57, 103] or “frailty score” [104, 105] in humans, we aggregated these measurements into a prognostic estimate of days of life remaining. Using this prognosis, we were able to determine

how the progress of senescence differs between longer- and shorter-lived individuals.

As one might expect for a genetically identical population reared in homogenous conditions, long-lived *C. elegans* do not begin adulthood with healthier physiology according to any of our measures. This is consistent with our previous work, which found that while physiological measurements made on the third and fourth day of adulthood can readily distinguish long- from short-lived individuals, physiological measures earlier in life cannot [79]. However, several fluorescent gene-expression reporters can be used to predict future lifespan even at the onset of adulthood: the level of the microRNA *mir-71*, which regulates insulin signaling [79], and the expression, after a heat shock, of the heat-shock response protein *hsp-16.2* [106]. Thus, while long- and short-lived animals are not physiologically distinguishable at the start of adulthood, gene-regulatory and biochemical differences between individuals with different future fates are already established, and only later manifest themselves as phenotypic differences.

Indeed, we find that the population does not remain physiologically identical for long. Systematic differences between the longest- and shortest-lived individuals are detectable less than one day after reproductive maturity. Overall, shorter-lived animals age more rapidly throughout adulthood. That is, short-lived individuals are generally in worse physiological health than their long-lived counterparts at any particular chronological age. In addition, short-lived individuals typically die before experiencing the most advanced stages of senescence. However, senescence typically occurs relatively late in life in shorter-lived individuals, which thus remain healthy-appearing for a large fraction of their lives. In contrast, longer-lived animals undergo the full range of senescent decline, from good to ill health. These declines typically begin relatively earlier in life, leading long-lived animals to die after an extended twilight period of low physiological function (Figure 2.6). While the mechanisms underlying this expansion in fractional gerospan in long-lived individuals are unclear, it is possible that they may result from diminished homeostatic capacity in older animals. One possibility is that phenotypically similar individuals entering gerospan may nevertheless have different degrees of homeostatic capacity (also known as “organ reserve” [107, 108] or “resilience” [78, 109]). Such latent, unobservable variability could allow some individuals to persist longer than others in highly senescent states. Alternately, a uniformly diminished homeostatic reserve in gerospan might leave individuals susceptible to stochastic insults (e.g. free-radical damage or protein translation errors) that would be survivable by a healthier individual. In this scenario, the variability in gerospan would be driven by the rate at which these in-

sults occur. Therefore, determining the mechanistic underpinnings of these systematic trends in aging physiology is an important direction for future study. Finally, we identified a previously uncharacterized subpopulation of individuals that demonstrate these trends in the extreme. Small in size, with very poor oocyte production, and qualitatively and quantitatively ill appearing, these individuals are, however, extremely long-lived. Nevertheless, our overall findings are neither driven by this population nor by any specific physiological measurement. Instead, we have identified graded trends across physiological systems, from the shortest-lived to the longest-lived of individuals within a population.

Our examination of physiological variability throughout aging provides an interesting contrast with a recently discovered invariant property of survival statistics in *C. elegans*. Stroustrup and colleagues rigorously demonstrated that a number of diverse interventions—including oxidative stress, different ambient temperatures, and lifespan-extending mutations—do not change the overall shape of the survival curve, but merely scale it uniformly in time [78]. The authors argue that these interventions must therefore all act, directly or indirectly, on a single emergent parameter (termed “resilience” by the authors) that determines lifespan. In contrast, our data show that within a single population, the processes that drive variation in physiological aging do not scale uniformly between long-lived and short-lived individuals. Further, by visual inspection we find that different individuals segregate into very different “terminal phenotypes” in old age, such as gonadal hypertrophy, large collections of clear fluid, “wrinkling” of the cuticle due to loss of body size, and distended intestines due to packing of bacteria (Figure 2.9H–K). Overall, it is clear that there exists a diversity of qualitatively different ways in which individuals can be unhealthy prior to death, suggesting that the drivers of inter-individual variability in health within a population may be different from those that modulate lifespan distributions between populations. Perhaps surprisingly, we did not observe any significant differences in lifespan among individuals with different terminal phenotypes (Figure 2.9L and M). Thus, consistent with the findings of Stroustrup *et al.*, distinct physiological processes of aging can nevertheless converge, perhaps through a shared mechanism of “resilience”, on very similar mortality statistics.

Our data also offer a new perspective on recent studies of functional declines in health in long-lived mutants. Bansal *et al.* measured the population average of several tests of stress resistance and physiological function in wild-type and long-lived mutant *C. elegans*, defining “healthspan” for any particular test as the period of time with greater than 50% of the maximal wild-type functional capacity [110]. These investigators found that while some long-lived mutants had longer healthspans in absolute

time on certain functional tests, the relative fraction of life spent in good health was diminished in many long-lived mutant strains. (A notable exception is the insulin-signaling deficient mutant *daf-2*; see also [111].) This overall result has been taken by some to suggest that these long-lived mutants are not good models for wild-type aging, and that the observed extension of relative time spent in poor life may have been a pleiotropic effect of the lifespan-extending genetic mutations. However, we show here that this is not necessarily the case. Our study, which incorporates comprehensive, lifelong measurements and an integrated definition of overall health (suggested to be critical factors for such an analysis [112]) shows similar results in a genetically identical, wild-type population. Specifically, we observe a continuum in which the fraction of lifespan spent in good health systematically diminishes from short- to long-lived individuals. The results of Bansal *et al.* can thus be seen as placing many longevity mutants along this same continuum. As such, a relative expansion in gerospan may not be a “bug” specific to certain long-lived mutants, but rather a general property of the aging process itself.

Together, these results demonstrate that extended lifespan, whether induced by stochastic events (in the case of inter-individual variability) or mutations (in the case of inter-strain differences), is often due to a disproportionate extension of a highly senescent “twilight period” of low physiological function. Put simply, it appears that an individual’s gerospan is inherently more plastic than its healthspan.

Determining whether these results hold in more complex organisms is an important task. First, it is certainly true that in humans and other mammals, longer-lived individuals typically enjoy more total days of healthy life. Likewise, it is well established that individuals with higher physiological function and better physical fitness generally live longer. In particular, several remarkable studies in humans have shown that heritable factors that favor exceptional longevity also increase healthspan [113, 114]. Further, longevity is more generally associated with a longer chronological span of healthy life, both within a relatively homogeneous Ashkenazi Jewish population [115], and among the ethnically diverse general Chinese population [116]. Our results in *C. elegans* are identical: longer-lived *C. elegans* enjoy longer absolute healthspans (Figure 2.4C), and better health at any point in time is correlated with extended future lifespan (Figure 2.4A).

It is an open question, however, whether longer-lived individuals within mammalian populations spend a smaller *fraction* of their lives in good health, as we observe in *C. elegans* (Figure 2.4D). As above, several studies in humans have demonstrated in different contexts that extended lifespan is associated with extended chronological healthspan. Nevertheless, it remains a matter of some debate

whether longer life brings with it a *proportionate* extension in healthspan [114, 117]. As most of the current studies do not include data on ultimate lifespan, either due to cross-sectional study design or ongoing follow-up in a longitudinal study, these analyses cannot yet shed light on the proportion of life spent in good health in short- vs. long-lived individuals. Some recent work has been able to address this question by asking whether modern advances in medicine have been more successful in extending disability-free life (healthspan) or activity-limited life (gerospan). There is evidence that, especially for females, medical advances have prolonged longevity primarily by expanding the late-life period of morbidity, without much effect on the span of disability-free life [118]. Fundamentally, however, whether it is worthwhile to extend lifespan in this fashion is a value judgment that may vary between individuals, and is thus more in the realm of clinical decision analysis [119–121] than experimental biology. (The simple analysis in Figure 2.11S–U shows how the desirability of such extensions can depend on the threshold for acceptable quality of life.)

It is, however, an experimental question whether there are conditions or mutations that can extend fractional healthspan as easily as fractional gerospan. In mammals, exercise [122] and caloric restriction [47] may extend the ratio of healthspan to gerospan. In *C. elegans*, the data from Bansal *et al.* and Hahm *et al.* both show that the long-lived *daf-2* mutant enjoys a proportionate extension of both healthspan and gerospan in relevant physiological assays. Thus the *daf-2* mutant likely departs from the relationship between long life and extended fractional gerospan that we have characterized. Our longitudinal approach now allows for a more detailed understanding of how health integrates across physiological systems and evolves over time in different genetic backgrounds, filling a previously unmet experimental need [112]. Future studies with these approaches promise to unravel the complex relationship between the plasticity of different phases of senescence and lifespan extension in general.

2.3 Methods and Resources

2.3.1 Key Resources Table

Resources and Reagents

	Source	Identifier
PDMS	Dow Corning	Sylgard 184 Silicone Elastomer Kit
PEG-DA	Jenkem Technology	8ARM(TP)-SH-10K
PEG-85H	Sigma-Aldrich	455008 Aldrich
<i>spe-9(hc88)</i> <i>C. elegans</i>	Caenorhabditis Genetics Center	BA671
Image Acquisition Software	GitHub	https://github.com/zplab/pc-scope
Analysis Software	GitHub	https://github.com/zplab/wormPhysiology
Data	Supplemental Data	Supplemental_Data.zip

2.3.2 Contact for Reagent and Resource Sharing

Zachary Pincus is the Lead Contact and may be contacted at 660 South Euclid Avenue; Department of Genetics, CB 8232; St. Louis, MO 63110-1031 and at zpincus@wustl.edu.

2.3.3 Experimental Model and Subject Details

Strains

The *C. elegans* strain *spe-9(hc88)*, a temperature-sensitive fertilization-defective mutant, was provided by the Caenorhabditis Genetics Center (CGC). The strain was maintained at 15°C and assays were conducted at a restrictive temperature of 25°C. *spe-9(hc88)* strains are widely used as an alternative to 5-fluoro-2'-deoxyuridine (FUDR) sterilization, and have been validated to have wild-type lifespans at the restrictive temperature of 25.5°C [101] and wild-type brood sizes at the permissive temperatures of 16°C and 20°C [123]. We used *spe-9(hc88)* to avoid the known confounding effects of FUDR [124] and to eliminate issues due to the timing of administration (such as being administered at different phases of life for fast- and slow-developing individuals on the same slide).

2.3.4 Method Details

Single-Animal Vermiculture

Standard 25 mm × 75 mm (1.2 mm thick) glass microscopy slides (obtained from VWR International, LLC; Radnor, PA, USA) were used as the base support for our culture device. Before use, the glass slides were bonded to custom-machined aluminum frames (outer dimensions 25 mm × 75 mm; inner dimensions 20 mm × 70 mm; thickness 2.36 mm) using 120 µL of polydimethylsiloxane (PDMS; Sylgard

184 Silicone Elastomer Kit obtained from Dow Corning Corporation; Midland, MI, USA). The PDMS was then cured in an oven at 100°C for 3 hours. The device was then cleaned with distilled water and ethanol, sealed in aluminum foil, and dry heat sterilized at 160°C for 2 hours.

Next, a modified version of standard nematode growth media (NGM) [125] was made by mixing 97.5 mL of distilled water with 0.3 g of sodium chloride, 0.25 g of peptone, 0.1 mL of 1M magnesium sulfate, and 2.5 mL of 1M potassium phosphate buffer (pH 6.3, titrated with sodium hydroxide and hydrochloric acid). We omit the calcium chloride used in standard NGM, and modify the pH of the potassium phosphate buffer from 6.0 to 6.3 to allow for polymerization of the polyethylene glycol (PEG) gel. Instead of autoclaving, which can darken sugar-containing solutions, we filter-sterilized the modified NGM to maximize optical clarity.

Then, 8 μ L/mL of cholesterol stock (5 mg/mL in 95% ethanol) was added to the NGM, which was then used to separately dissolve an 8-armed PEG-thiol (Jenkem Technology; Beijing, P. R. China; Item Number: 8ARM(TP)-SH-10K) and PEG-diacrylate (Sigma-Aldrich; St. Louis, MO, USA; Catalog Number: 455008 Aldrich) at 140 mg/mL and 40 mg/mL, respectively. The NGM-PEG-thiol and NGM-PEG-diacrylate solutions were then mixed in a 1:1 ratio and vortexed vigorously. 1.7 mL of the mixture was then added to the center of the aluminum frame on the culture device. The device was tilted to break the surface tension of the PEG mixture and to achieve an even layer of fluid. The device was then placed in a standard 100 mm \times 15 mm petri dish. A delicate task wipe was cut in half and added to the petri dish, and 700 μ L of distilled water was pipetted onto each half wipe in order to maintain the humidity of the petri dish and prevent excessive evaporation of water from the PEG gel. Finally, an additional 25 mm \times 75 mm glass slide was sterilized with ethanol, dried, and placed on top of the aluminum frame to further isolate the gel during polymerization. The petri dish containing the device is then left at room temperature for 90 minutes, during which the 8-armed PEG-thiol crosslinks to the PEG-diacrylate via Michael addition.

Next, an array of 0.2 μ L droplets of an OP50 *E. coli* (50% by mass) food source was deposited onto the gel. Single, individual pretzel-stage eggs were picked into each droplet using an eyelash pick. Approximately 100 eggs can be picked onto each slide in 20 rows of 5 eggs each. After the *E. coli* droplets were dried, 1.2 mL of PDMS was deposited over the PEG gel using a syringe. The PDMS polymerizes overnight; moreover where the gel is in contact with the PDMS (i.e. all locations other than the bacterial food pad), hydrosilylation addition of unreacted moieties in the PDMS cure agent

with unreacted acrylate groups in the PEG-diacrylate cause a the PDMS and gel to bond covalently, trapping each animal on its individual food pad. Immediately after deposition of the PDMS, the glass slide was placed on the stage of our computer-controlled microscope, and automated image acquisition was initiated.

Image Acquisition

All images were acquired at $5\times$ magnification using custom-built hardware and software. The microscope itself was housed in a climate-controlled enclosure to provide consistent temperature and humidity for the animals studied. A thermoelectric cooler with continuous temperature monitoring (Torrey Pines Scientific, La Jolla, CA) was used to maintain the temperature of the enclosure at $25.0 \pm 0.1^\circ\text{C}$. Humidity was maintained at $85 \pm 10\%$ relative humidity by including a tub of distilled water in the enclosure and using two aquarium air diffusion stones along with an air pump to aerate the water. Consistent air circulation was achieved with the use of several 80 mm DC fans attached to the thermoelectric cooler and the walls of the enclosure.

Custom in-house control software was developed and used to move to and automatically focus [126, 127] on each animal every three hours. At each time point, a series of six brightfield and one fluorescence image was acquired, taking approximately 17 seconds per animal. The fluorescence image and one bright-field image were taken first, taking less than 60 ms combined time to acquire. The fluorescence image taken with a 50 ms exposure using a TRITC filter (Semrock part DA/FI/TR-3X-A-000), with light from a Lumencor Spectra X. The center wavelengths of the excitation and emission bands were 556 nm and 613 nm, respectively. Next, a series of 5 bright-field images to assess short-term movement were taken over 4.5 seconds, with 0.5 seconds between the first and second images, 1.0 seconds between the second and third images, during which time the animals were stimulated with a 0.5 second pulse of cyan light [128], 1.5 seconds between the third and fourth images, and 1.5 seconds between the fourth and fifth images. For the first 10 timepoints, the 0.5 second pulse of cyan light and the fluorescence image were omitted to avoid excessive stimulation of the animals during early larval development.

The microscope was automatically re-calibrated at every three-hour timepoint for spatial and temporal variation in light-source intensity for both the bright-field lamp and the fluorescence light source. In addition, images were corrected for variation in sensitivity of the camera image sensor. Finally,

bright-field exposure times and lamp intensities were adjusted at every time point to optimize the dynamic range of the acquired images. Overall, all images were corrected for background camera noise (dark current), spatial illumination inhomogeneity (flat field) and temporal variation in illumination. After correction, image intensity values were divided by the exposure time to render all images comparable.

Image Segmentation

The acquired image series were then manually annotated for time of hatching, reproductive maturity as indicated by first oocyte laid, and death as indicated by total cessation of coordinated movement. Eight developmentally defective animals that never reached reproductive maturity were censored from our analysis, while 734 were included in the final analysis. All animals were observed for an additional 30 hours post-mortem to confirm death.

A suite of custom image analysis software was written to automatically identify the location of the animal in the over 400,000 bright-field images. First, the rough location of the animal was determined using background subtraction [129], which takes advantage of the fact that the animal moves around in the image, while other objects such as the bacterial lawn are stationary. The current image was combined with the previous nine images taken for the same individual by computing a pixel-wise median, which produces a model of the background. This background image was then subtracted from the current image, and thresholded for only pixels above the 97.5th percentile of brightness. The largest contiguous object in the thresholded image was then identified as the animal, and all internal holes in the object were filled. This location was then masked out of future background contexts to improve the robustness of the background model. Finally, the algorithm was run backwards in time to identify the position of the animal during the first nine time points.

Next, the location of the individual was refined using the Canny edge detector [130]. While the background subtraction segmentation is sensitive to changes in the bacterial lawn surrounding the animal due to illumination changes or physical churning by the animal's movement, edge-detection defines sharper borders based on local spatial intensity gradients. The largest object in the field of view (excluding the edge of illumination from vignetting and the border of the bacterial lawn itself) was identified as the worm, and all internal holes in the object were filled. However, edge detection can occasionally locate the wrong object due to a large pattern of churned bacteria or the introduction

of a piece of dust or air bubble into the field of view. Therefore, the background subtraction-derived location was used as a fallback for cases in which the location of the animal as defined by edge detection was more than 50 pixels from the location as identified by the more reliable background subtraction.

Finally, a support vector classifier [131] with a radial basis function kernel ($\gamma = 4.88 \times 10^{-4}$, $\nu = 8.99 \times 10^{-4}$) was trained on the intensities from 10,000 5×5 pixel patches from 1,617 manually drawn outlines of worms to distinguish between the animals and their surrounding bacteria. This classifier was then applied to patches centered on each individual pixel within the animal's location as computed by the previous two methods. Using the SVC allowed us to improve our image segmentation significantly in cases in which the animal was in a curled posture and looped back on itself. While the simple hole-filling would naïvely identify patches of bacteria surround by the animal as part of the animal itself, the SVC is generally able to distinguish between the two. Overall, the automated segmentation agreed strongly with manual segmentation, with Pearson correlation coefficients between automated size and manual size of $r^2 = 0.81$ and between automated position and manual position of $r^2 > 0.95$ (Figure 2.7K–O).

Physiological Panel Design

Several “biomarkers of aging” [57,92] – properties that can predict an individual's future lifespan better than age alone – have previously been identified in *C. elegans*. As each biomarker represents an aspect of physiology that differs between long- and short-lived individuals at some point in life, we selected a number of these markers to follow longitudinally across our population. First, we examined *C. elegans* neuromuscular function, as measured by locomotory ability. Previous work has shown that locomotion in age-matched animals diminishes over time, correlates with remaining lifespan [79,86–88,98,132] and with the degree of sarcopenia [87]. Second, we assay the accumulation of non-hydrolyzable autofluorescent material in intestinal endosomes [85,94–97]. This is a marker for declining macromolecular homeostatic capacity over time, as individuals fail to clear the fluorescent material at a pace that balances its production. We chose to follow red-wavelength autofluorescence, which is most predictive of future lifespan [97], instead of blue or green autofluorescence, which largely report only incipient death [97,133]. Third, we also measure declining tissue organization through quantitative measurements of textural order and disorder in brightfield images, which has been shown to correlate with lifespan [79,87,93,134]. Fourth, *C. elegans* reproductive output has also been identified as a biomarker

of aging and has been shown to decrease with age [99]. While Huang *et al.* found no correlation between reproduction and lifespan was found in unmated, and hence sperm-limited, hermaphrodite *C. elegans* [88], we here examine the temperature-sensitive sterile strain *spe-9*, which lays unfertilized oocytes, and may thus not be sperm-limited in the same way. Finally, we and others have shown that overall body size, and rate growth and/or shrinkage correlate with future lifespan [79, 98]. Taken together, this panel comprises a diverse set of individual measurements, allowing us to characterize longitudinal changes in distinct aspects of aging physiology (Figure 2.1C–E).

Image Measurements

Autofluorescence measurements (in red wavelengths; excitation 556 nm, emission 613 nm [97]) were made using pixel values within the defined animal location from automated image segmentation of the paired bright field image. Intensity values were extracted and summary statistics such as 80th percentile of intensity and integrated total body fluorescence were computed. Using a percentile score provides robustness against brightly autofluorescent clumps of debris or oocytes overlapping the individual (see Figures 2.12A for example illustrative images).

Four measures of motion were made at each time point. Long-term movement over a three-hour time scale was assessed by measuring the displacement between the centroid of the animal's current position and that of its previous position. Unstimulated movement and stimulated movement immediately before and after blue-light stimulus were assessed by measuring distances between centroids of animal positions from the sequence of five bright-field images (see Figures 2.12B for example illustrative images).

An estimate of the number of oocytes laid was used as a proxy for reproductive investment. This measure was made by measuring the total area of objects detected within the bacterial lawn, excluding the animal itself and thresholding by size to remove small debris. This total area was then divided by the area of an average oocyte to obtain an estimate of the total number laid (see Figure 2.12C for example illustrative images).

Cross-sectional size of the animal was measured by simply counting the number of pixels within the segmented animal region. The raw measured size was adjusted for a slight systematic bias towards overestimating the animal's size by a linear regression between automatically measured size and size from 1,617 human-drawn outlines of the animal (see Figure 2.12D for example illustrative images).

Finally, a quantitative measure of tissue degeneration similar to the score used in [79] was made by analyzing pixel patches within animals' outlines. First, representative texture patches ("textons") for different stages of decrepitude were obtained by grouping images by the number of days remaining in the animal's life at that point in time (bins of 0–3, 3–6, 6–9, etc. days left to live), sampling 200,000 17×17 pixel patches from images in each bin, and using k-means classification to obtain 60 representative patches for bin (300 total). Then, the texture pattern of an image was defined as the 300-element histogram containing the count of closest-matching 17×17 pixel patches for each texton, normalized by the total number of patches in that image. These histograms were then used to train a support vector regression procedure to produce a tissue degeneration score in terms of predicted days of remaining life (see Figure 2.12E for example illustrative images).

2.3.5 Quantification and Statistical Analysis

Smoothing

Individual animals' time traces for each measurement were smoothed using 3 iterations of the one-dimensional Savitzky-Golay filter [135] with a 1-degree polynomial and a window length of 9. Smoothing parameters were optimized for signal-to-noise ratio by checking the physiological measurements' cross-validated partial Pearson r^2 with remaining lifespan, controlled for age.

Pearson Correlations

p-values for Pearson correlations were computed using an F-test for linear regression. The F-statistic was computed in the usual way as $F = r^2(df)/(1 - r^2)$, where $df = n - 2$, n is the sample size, and r is the Pearson coefficient of correlation. The test was performed under the assumption of normality, so for computational efficiency an appropriately renormalized chi-squared distribution was used as an approximation for the exact Fisher-Snedecor distribution.

Non-parametric Spearman Correlations

To validate our results without the assumption of normality made in computing Pearson correlations and their associated p-values, we also performed non-parametric Spearman correlations on the ranks

of the data for each statistical test. These were performed identically to the Pearson correlation p-values.

Overfitting and Multiple Hypothesis Testing

To guard against overfitting, we analyzed the cross-validated Pearson r^2 for defining our prognosis measurement, finding that it was not substantially lower than the non-cross-validated version.

All p-values are significant even after applying the conservative Bonferroni correction for 6 tests.

Alternate Health Regression Approaches

To ensure that our results were not artifacts of our particular methodology for computing a prognosis and measuring health, we examined several alternate approaches, none of which altered our key findings. Table 2.4 demonstrates our key results are visible from each of the individual aspects of aging physiology we measured, without combining them to form the prognosis score. Figure 2.10I–P shows that these results also hold when using linear regression to create the prognosis, which also allows the relative contributions of each raw measurement used to be compared (Table 2.5). This indicates that no specific measurement, nor the regression methodology, drives the central findings of this study.

Next, we used multivariate support vector regression to create alternates to our “prognosis” score. By regressing against age rather than remaining lifespan we created a “youthfulness” or “biological age” score [57, 103]. Similarly, regressing against predicted three-day survival created a “frailty” score [104, 105] (Figure 2.10Y, inset). Both frailty and youthfulness scores produced similar findings to our approach above (Figure 2.10Q–X and Y–FF).

2.3.6 Data and Software Availability

All physiological data used in this study is included with this manuscript in Supplemental_Data.zip.

The image acquisition software is freely available at <https://github.com/zplab/rpc-scope>, and the image processing and statistical analysis software is freely available at <https://github.com/zplab/wormPhysiology>.

2.3.7 Additional Resources

None.

2.4 Acknowledgements

We would like to thank Shin-ichiro Imai, Heidi Tissenbaum, Brian Kim, Amy Xu, and Seth Pincus for helpful discussions and thoughtful feedback. ZP began this work in the lab of Frank J. Slack, supported by NIH R01 AG033921. WZ, DS, WP, EH and ZP are supported by NIH R00 AG042487. WZ and ZP are supported by Longer Life Foundation grant 2015-008. WZ is additionally supported by NIH T32 GM07200. Some strains were provided by the CGC, which is funded by the NIH Office of Research Infrastructure Programs (P40 OD010440).

2.5 Author Contributions

WZ and ZP designed the experiments. WZ designed and implemented the image segmentation and analysis software and analyzed the data. WZ, DS, and WP conducted the experiments. WP, WZ, DS, and ZP developed the single-worm culture system. ZP designed and built the custom microscope control and incubation hardware, and ZP and EH wrote the custom microscope control software. NS provided data and analysis for validation of key results in standard culture conditions. WZ and ZP wrote the manuscript with feedback from DS and NS.

2.6 Supplementary Information

Data Quality Controls

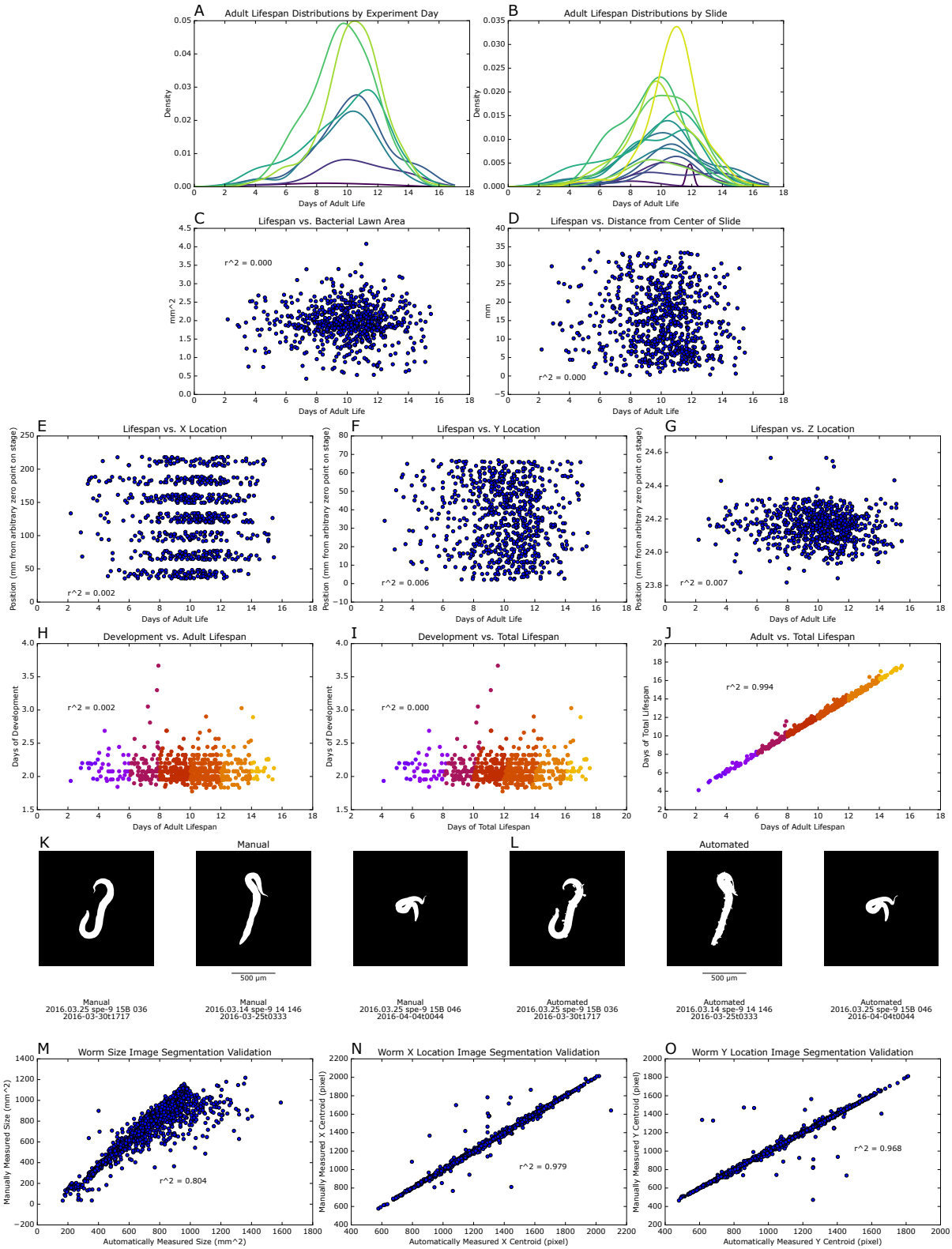


Figure 2.7: Related to Figure 2.1. Data Quality Controls.

(A) Variation in the lifespan distributions on a trial-by-trial basis. Each trial consists of multiple physical slides run simultaneously.

(B) There is some variation in the lifespan distributions on a slide-by-slide basis, but the results across all slides were comparable. We re-analyzed our data excluding the two slides with fat tails on the left side, and found no substantial changes to our results (data not shown).

(C–G) We also checked for lifespan effects from area of bacterial food source (C), distance from the center of the slide (edge effects) (D), and x (E), y (F), and z-position (G) in the microscope enclosure, finding no substantial biases.

(H–J) Scatterplots of the relationships between total lifespan, adult lifespan, and duration of larval development.

(K–L) Gallery of worm segmentations. Randomly selected sample images of manually (K) and automatically (L) detected worm positions.

(M–O) Summary of worm segmentation accuracy. Correlations between summary statistics of manually- and automatically-detected worm positions: cross-sectional size (M), position in the field of view along the x-axis (N), and position in the field of view along the y-axis (O).

Lifespan Cohorts at Day 2.0

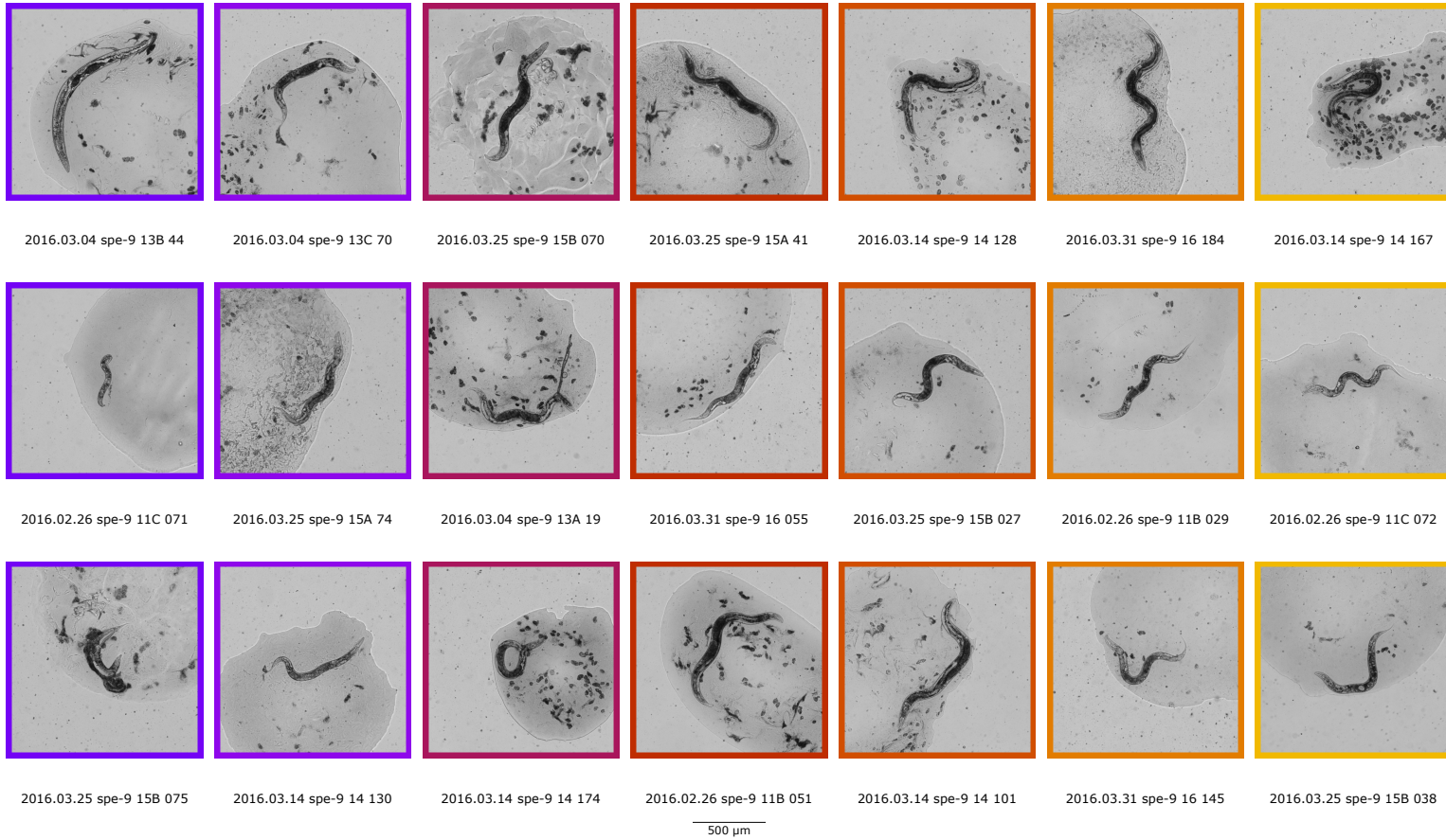


Figure 2.8: Related to Figure 2.2. Randomly selected sample images of worms in each of our adult lifespan cohorts at day 2 of adulthood.

Subpopulation Analysis

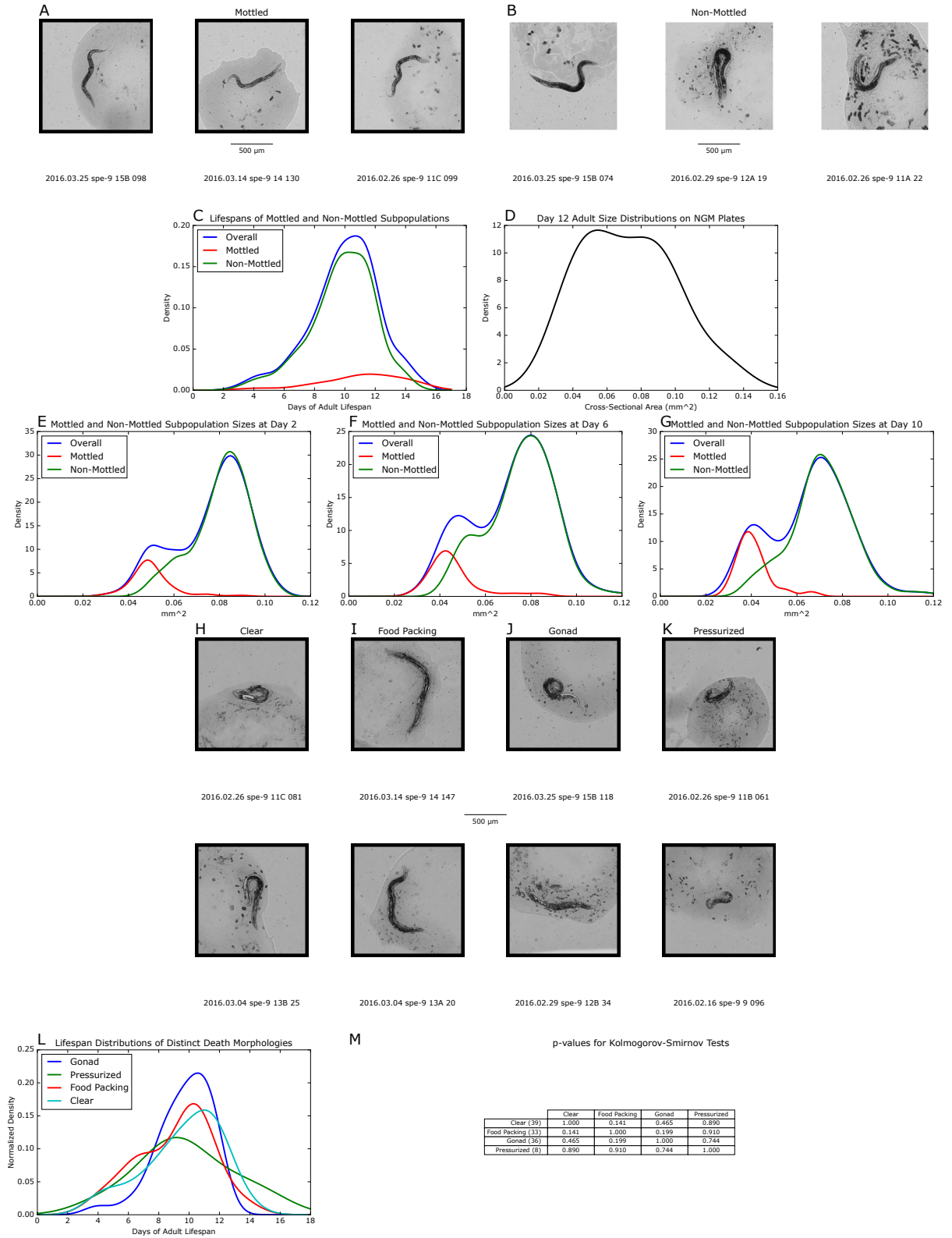


Figure 2.9: Related to Figure 2.2. Subpopulation Analysis.

(A–B) Mottled subpopulation sample images. The “mottled” subpopulation is a small subpopulation (13.7% of the total) of small, sickly-looking individuals which appear unhealthy throughout their lives but have very long lifespans. Randomly selected sample images of worms in the “mottled” subpopulation (A), and the non-mottled population (B) at day 2 of adulthood.

(C) Longevity of the “mottled” subpopulation.

(D) A bimodal size distribution in standard conditions. The kernel density estimate shown was generated from 22 surviving individuals at day 12 post-hatch. They were raised at 25°C on a standard NGM plate with minor modifications to match the conditions of our PEG gels: calcium chloride was excluded from the formulation, 4× the usual concentration of cholesterol was used, a more concentrated OP50 food source (50% by mass) was used, and the pH of the NGM was titrated to 6.3 rather than the usual 6.0.

(E–G) Size distributions of subpopulations over time, at days 2 (E), 6 (F), and 10 (G) of adulthood.

(H–K) Gallery of images illustrating four distinctive morphological “fates” one day before mortality. Randomly selected images for worms exhibiting a clear morphology (H), packing of bacteria within the digestive tract (I), gonadal hypertrophy (J), and a wrinkled-appearing “compressed” or “pressurized” phenotype (K).

(L) Lifespan distributions for subpopulations exhibiting the four distinctive morphological “fates”.

(M) p-values from 2-sample Kolmogorov-Smirnov tests among the four “fates” subpopulations.

Alternate Healths

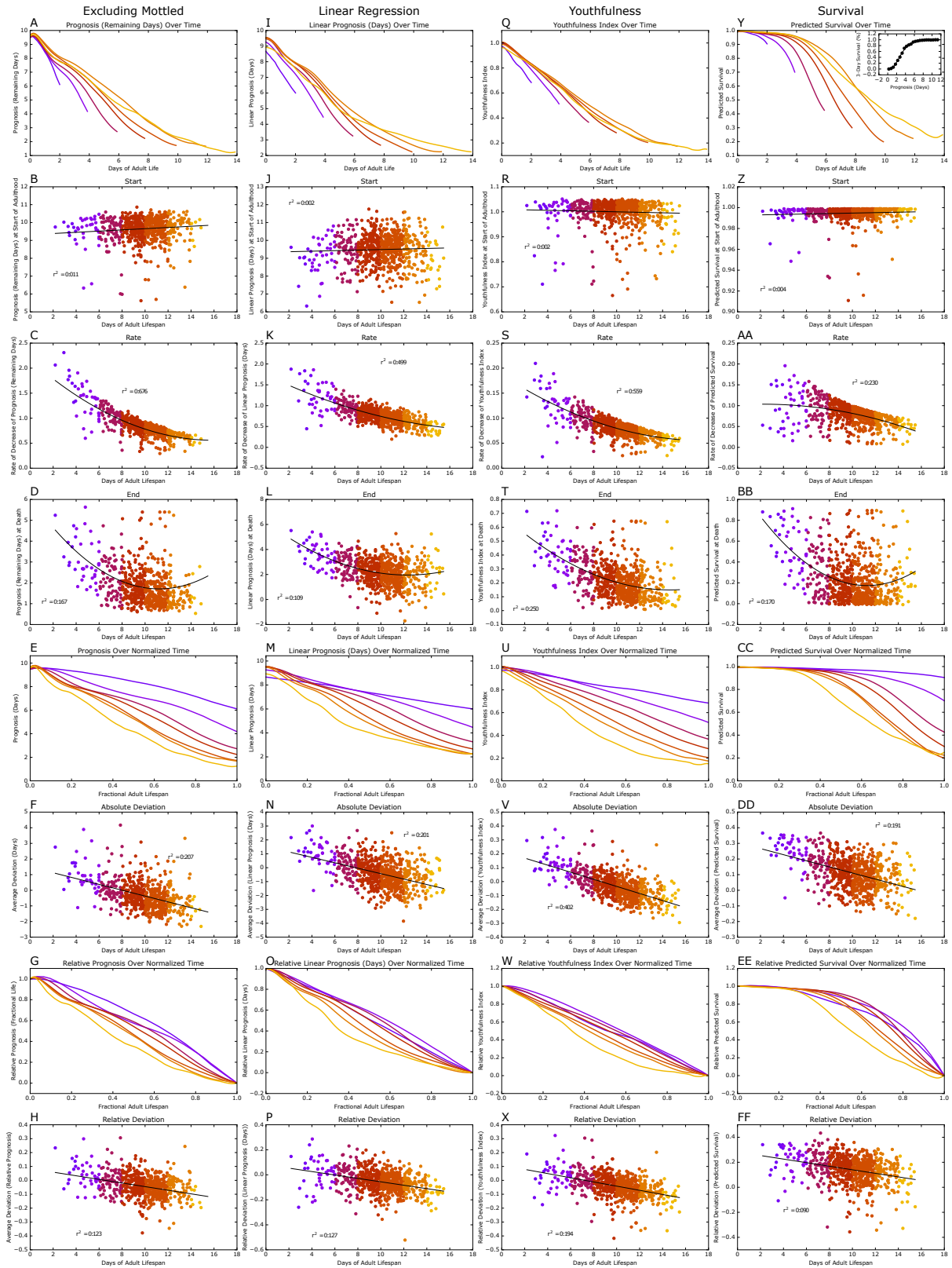


Figure 2.10: Related to Figure 2.3 and Figure 2.4. Alternate Health Definitions.

(A–H) Key analysis excluding mottled subpopulation. Our key analysis is repeated, excluding the mottled subpopulation.

(I–P) Key analysis using linear regression. Our key analysis is repeated using a linear regression in place of a support vector regression to generate the “prognosis” variable.

(Q–X) Key analysis using youthfulness. We repeat our key analysis by regressing our measured parameters against age to create a “youthfulness” score, instead of regressing against remaining lifespan to create a “prognosis” score. Biomarkers of aging have often been used to estimate an individual’s “biological age” in this fashion [57]. Biological age, or “youthfulness”, is closely related to our original measure of prognosis: if a chronologically old individual is nevertheless physiologically youthful appearing (a young “biological age”), it is likely to live for relatively more days (a good “prognosis” score) [103]. As shown, using this “youthfulness” score (scaled such that young individuals have a high “youthfulness”) as an alternative measure of senescence does not alter the results of our analyses.

(Y, inset) Converting from prognosis to 3-day survival. Individual data points were binned into groups of individuals within a 0.5 day range of predicted remaining lifespan, and then the fraction remaining alive after 3 days was calculated to be the survival rate. A polynomial is then fit to convert from prognosis (predicted days of remaining life) to predicted survival rate.

(Y–FF) Key analysis using survival rate. Our key analysis is repeated using “3-day survival” in place of “prognosis”.

Thresholding Validation

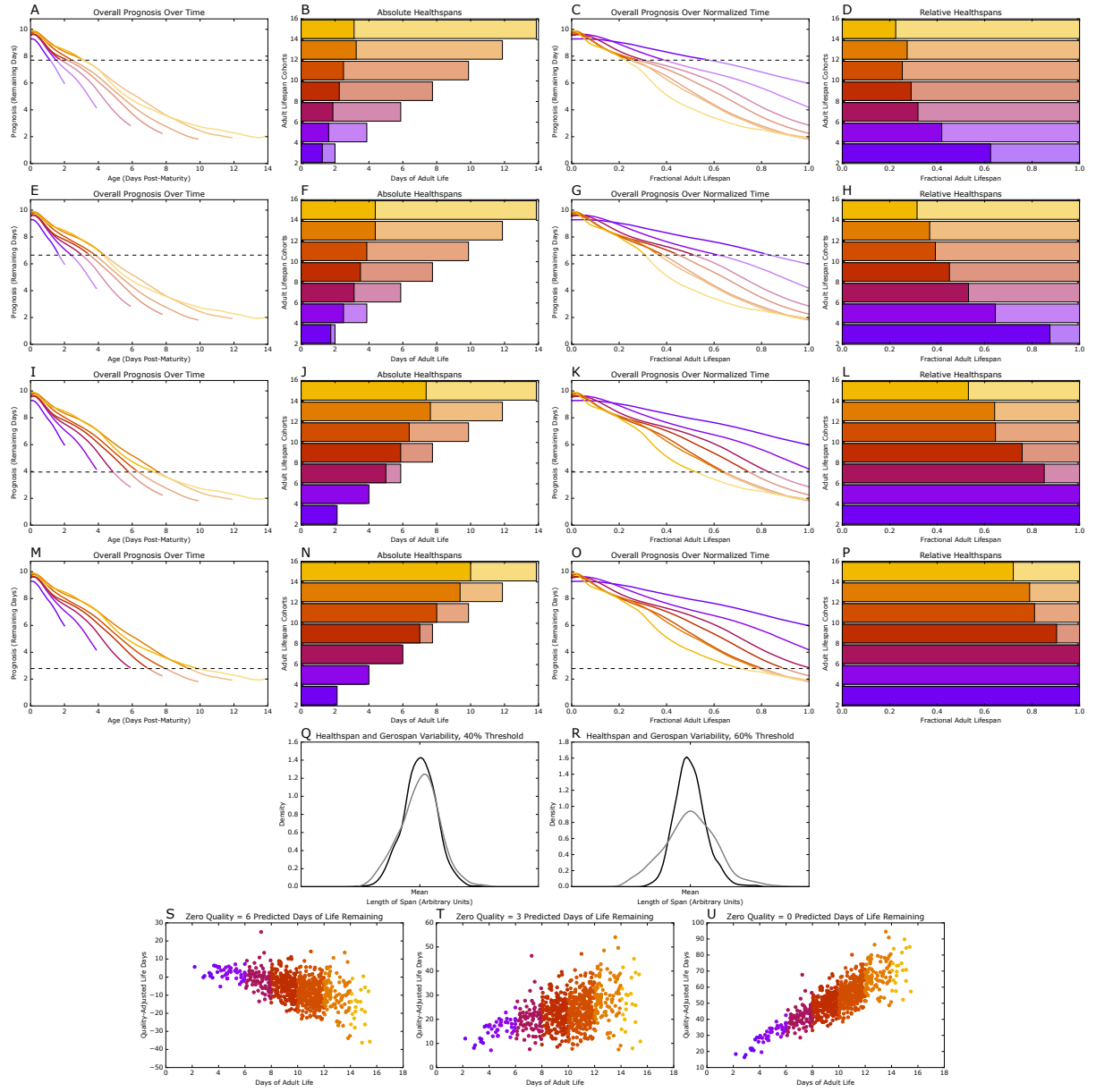


Figure 2.11: Related to Figure 2.5. Thresholding Validation.

(A–D) Spans analysis is repeated using 25% threshold. Our spans analysis is repeated—dividing life into “healthspan” and “gerospan”—using an alternate threshold so that 25% of life is spent in “healthspan”.

(E–H) Spans analysis is repeated using 37.5% threshold. Our spans analysis is repeated—dividing life into “healthspan” and “gerospan”—using an alternate threshold so that 37.5% of life is spent in “healthspan”.

(I–L) Spans analysis is repeated using 62.5% threshold. Our spans analysis is repeated—dividing life into “healthspan” and “gerospan”—using an alternate threshold so that 62.5% of life is spent in “healthspan”.

(M–P) Spans analysis is repeated using 75% threshold. Our spans analysis is repeated—dividing life into “healthspan” and “gerospan”—using an alternate threshold so that 75% of life is spent in “healthspan”.

(Q) Plasticity analysis is repeated using 40% threshold. The analysis in Figure 2.5I is repeated for a threshold which partitions 40% of the population’s total lifetime into healthspan (black) and the remainder into gerospan (gray). After re-scaling to account for differences in means of the distributions, gerospan remains more variable.

(R) Plasticity analysis is repeated using 60% threshold. The analysis in Figure 2.5I is repeated for a threshold which partitions 60% of the population’s total lifetime into healthspan (black) and the remainder into gerospan (gray). After re-scaling to account for differences in means of the distributions, gerospan remains more variable.

(S–U) Quality of life analysis. Overall length of life compared to quality of life depends on definition of quality. We defined a parameter analogous to “Quality-Adjusted Life Years” [120]. For simplicity, we assumed that the “quality” of a *C. elegans* life at any point in time is proportional to its prognosis of remaining lifespan as measured by our parameters. We then calculated the total “Quality-Adjusted Life Days” for each animal and analyzed that variable’s relationship with lifespan (U). Unsurprisingly, longer-lived worms experience a higher total number of “Quality-Adjusted Life Days”. To reflect the fact that it is possible to be in such poor health that an individual may actually experience a negative quality of life, we adjusted our scaling so that having a positive health score of “3 predicted days of life remaining” (T) or “6 predicted days of life remaining” (S) corresponded to zero utility/quality of life. In those cases, the overall “Quality-Adjusted Life Days” were reduced more drastically for long-lived animals, to the point that in the “6 predicted days of life remaining” case, they experienced substantially worse lives overall than their short-lived counterparts.

Measurements Gallery

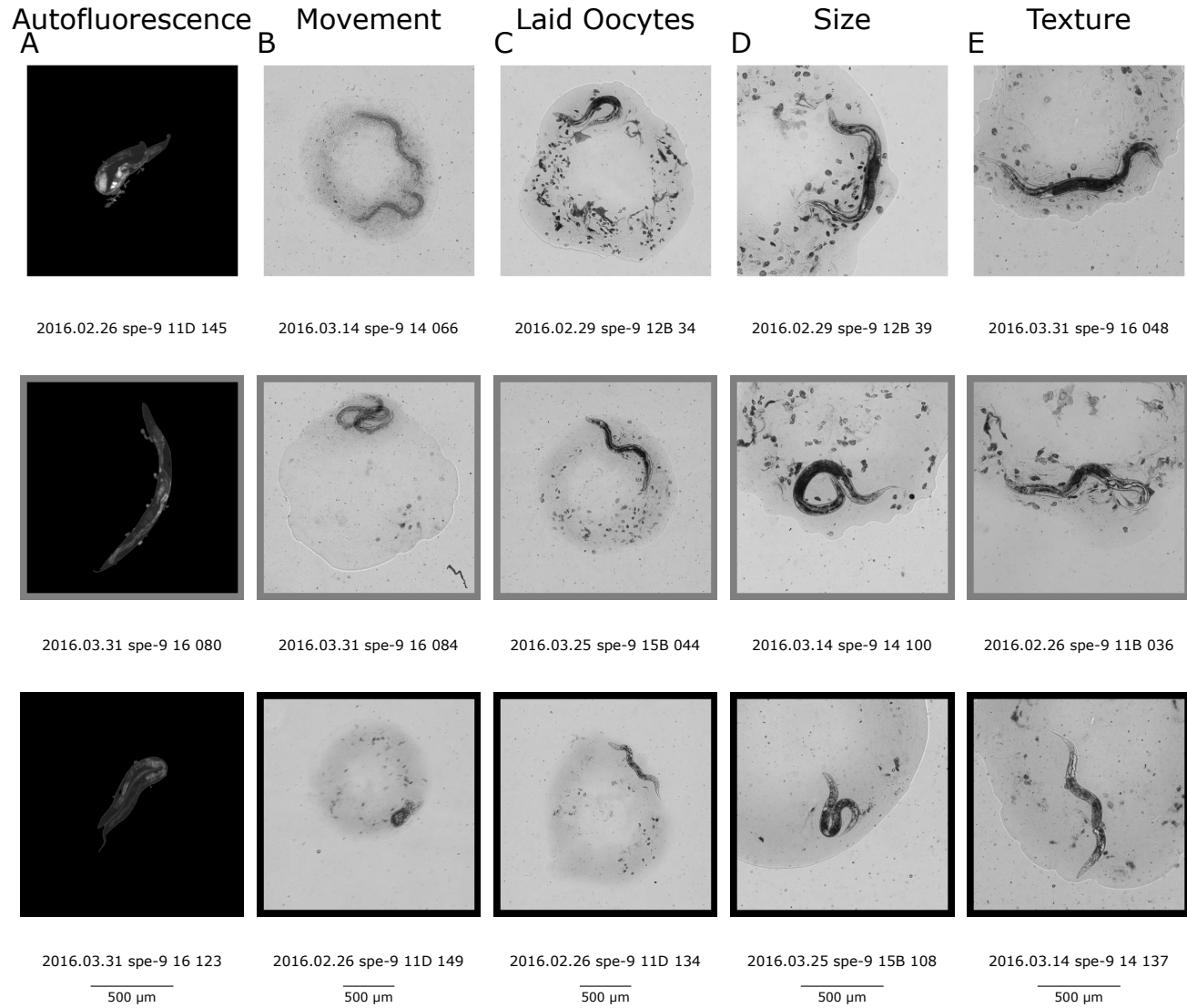


Figure 2.12: Related to Figure 2.1. Measurements Gallery.

(A) Autofluorescence at day 9 of adulthood. Representative randomly selected sample images of worms in the lower (bottom), middle (middle) and upper (top) quintiles of autofluorescence at day 9 of adulthood. For illustration, non-worm regions are masked out in black.

(B) Movement at day 5 of adulthood. Randomly selected sample images of worms in the lower (bottom), middle (middle) and upper (top) quintiles of movement at day 5 of adulthood. For illustration, two consecutive time points (separated by three hours) are superimposed here.

(C) Reproduction (Laid Oocytes) at day 3 of adulthood. Randomly selected sample images of worms in the lower (bottom), middle (middle) and upper (top) quintiles of reproductive output at day 8 of adulthood.

(D) Body size at day 2 of adulthood. Randomly selected sample images of worms in the lower (bottom), middle (middle) and upper (top) quintiles of cross-sectional size at day 2 of adulthood.

(E) Tissue integrity at day 2 of adulthood. Randomly selected sample images of worms in the lower (bottom), middle (middle) and upper (top) quintiles of textural integrity at day 2 of adulthood.

	Autofluorescence Prognosis	Body Size Prognosis	Reproductive Prognosis	Texture Prognosis	Movement Prognosis	Overall Prognosis
Autofluorescence Prognosis	1.0	0.198	0.421	0.298	0.566	0.732
Body Size Prognosis	0.198	1.0	0.328	0.179	0.248	0.297
Reproductive Prognosis	0.421	0.328	1.0	0.164	0.297	0.434
Texture Prognosis	0.298	0.179	0.164	1.0	0.587	0.607
Movement Prognosis	0.566	0.248	0.297	0.587	1.0	0.847
Overall Prognosis	0.732	0.297	0.434	0.607	0.847	1.0

Table 2.1: Related to Figure 2.2.
Correlations between aspects of physiology and longevity.

	Total Lifespan Variance Explained	Unique Lifespan Variance Explained
Movement Prognosis	0.588	0.030
Body Size Prognosis	0.213	0.014
Texture Prognosis	0.418	0.017
Overall Prognosis	0.519	0.024
Autofluorescence Prognosis	0.316	0.005
Reproductive Prognosis	0.695	N/A

Table 2.2: Related to Figure 2.2.

Contributions of different aspects of health to our overall prognosis in terms of their ability to predict remaining lifespan. “Total” variance explained is computed as the r^2 value between a prognosis made from only measurements in that physiological category and remaining lifespan, while “unique” variance explained is computed as the difference between the r^2 value between the overall prognosis and lifespan and r^2 value between the overall prognosis excluding that category of physiology and lifespan.

	Total Lifespan Variance Explained	Unique Lifespan Variance Explained
Movement	0.570	0.018
Movement (Stimulated A)	0.416	-0.00
Movement (Stimulated B)	0.425	-0.00
Movement Rate (Unstimulated)	0.290	-0.00
Cross-Sectional Size	0.046	0.012
Size Rate of Change	0.147	0.002
Textural Degradation	0.418	0.017
Autofluorescence 80th Percentile Intensity	0.519	0.024
Cumulative Oocytes Laid	0.041	0.006
Oocyte Laying Rate	0.284	0.000

Table 2.3: Related to Figure 2.2.

Contributions of different raw physiological measures to our overall prognosis in terms of their ability to predict remaining lifespan. “Movement (Stimulated A)” is the movement rate of an individual 0.5–2.0 seconds after stimulation with cyan light, and “Movement (Stimulated B)” is the movement rate of an individual 2.0–3.5 seconds after stimulation.

Correlations (Pearson r , r^2) with Adult Lifespan

	Start	Rate	End	Average Deviation	Relative Deviation
Autofluorescence Prognosis	0.031, 0.001	0.685, 0.470	0.487, 0.237	-0.445, 0.198	-0.362, 0.131
Reproductive Prognosis	-0.129, 0.017	0.810, 0.656	0.266, 0.071	-0.144, 0.021	-0.526, 0.277
Movement Prognosis	0.038, 0.001	0.825, 0.681	0.183, 0.034	-0.389, 0.152	-0.452, 0.204
Body Size Prognosis	0.055, 0.003	0.704, 0.496	0.248, 0.062	-0.271, 0.073	-0.105, 0.011
Texture Prognosis	-0.017, 0.000	0.347, 0.120	0.216, 0.047	-0.209, 0.044	-0.166, 0.027
Overall Prognosis	0.105, 0.011	0.822, 0.676	0.408, 0.167	-0.455, 0.207	-0.351, 0.123
Youthfulness Index	-0.043, 0.002	0.747, 0.559	0.500, 0.250	-0.634, 0.402	-0.441, 0.194
Predicted Survival	0.065, 0.004	0.479, 0.230	0.412, 0.170	-0.437, 0.191	-0.300, 0.090
Linear Prognosis	0.041, 0.002	0.706, 0.499	0.330, 0.109	-0.448, 0.201	-0.356, 0.127
Non-Mottled Prognosis	0.041, 0.002	0.706, 0.499	0.330, 0.109	-0.448, 0.201	-0.356, 0.127

Table 2.4: Related to Figure 2.3 and Figure 2.4.

Correlations between geometric characteristics of trajectories and lifespan for individual aspects of physiology and for alternate definitions of health.

Linear Regression Weights

	Weight	Units	Category
Autofluorescence 80th Percentile Intensity	-0.75	Days per Standard Deviation	Autofluorescence
Cross-Sectional Size	-0.21	Days per Standard Deviation	Body Size
Size Rate of Change	0.25	Days per Standard Deviation	Body Size
Textural Degradation	-0.86	Days per Standard Deviation	Texture
Cumulative Oocytes Laid	-0.31	Days per Standard Deviation	Reproductive
Oocyte Laying Rate	0.18	Days per Standard Deviation	Reproductive
Movement	0.99	Days per Standard Deviation	Movement
Movement (Stimulated A)	0.05	Days per Standard Deviation	Movement
Movement (Stimulated B)	0.27	Days per Standard Deviation	Movement
Movement Rate (Unstimulated)	-0.03	Days per Standard Deviation	Movement

Table 2.5: Related to Figure 2.2.
Contributions of each raw measurement to the linear regression prognosis.

Autofluorescence 80th Percentile Intensity at Day 7.0



Figure 2.13: Randomly selected sample images of worms in the lower (bottom), middle (middle) and upper (top) quintiles of autofluorescence at day 7 of adulthood. For illustration, non-worm regions are masked out in black.

Autofluorescence 80th Percentile Intensity at Day 8.0

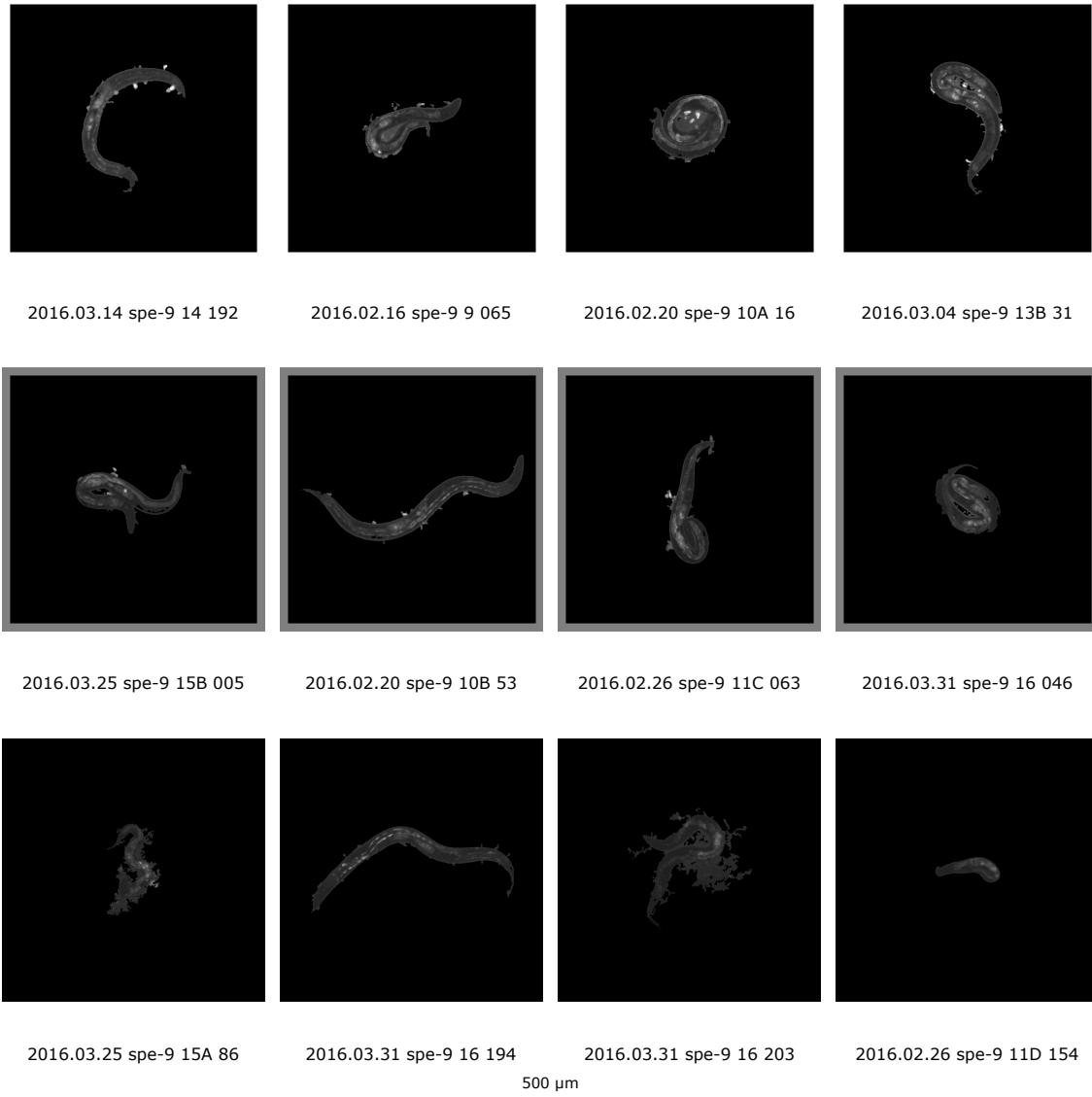


Figure 2.14: Randomly selected sample images of worms in the lower (bottom), middle (middle) and upper (top) quintiles of autofluorescence at day 8 of adulthood. For illustration, non-worm regions are masked out in black.

Autofluorescence 80th Percentile Intensity at Day 9.0

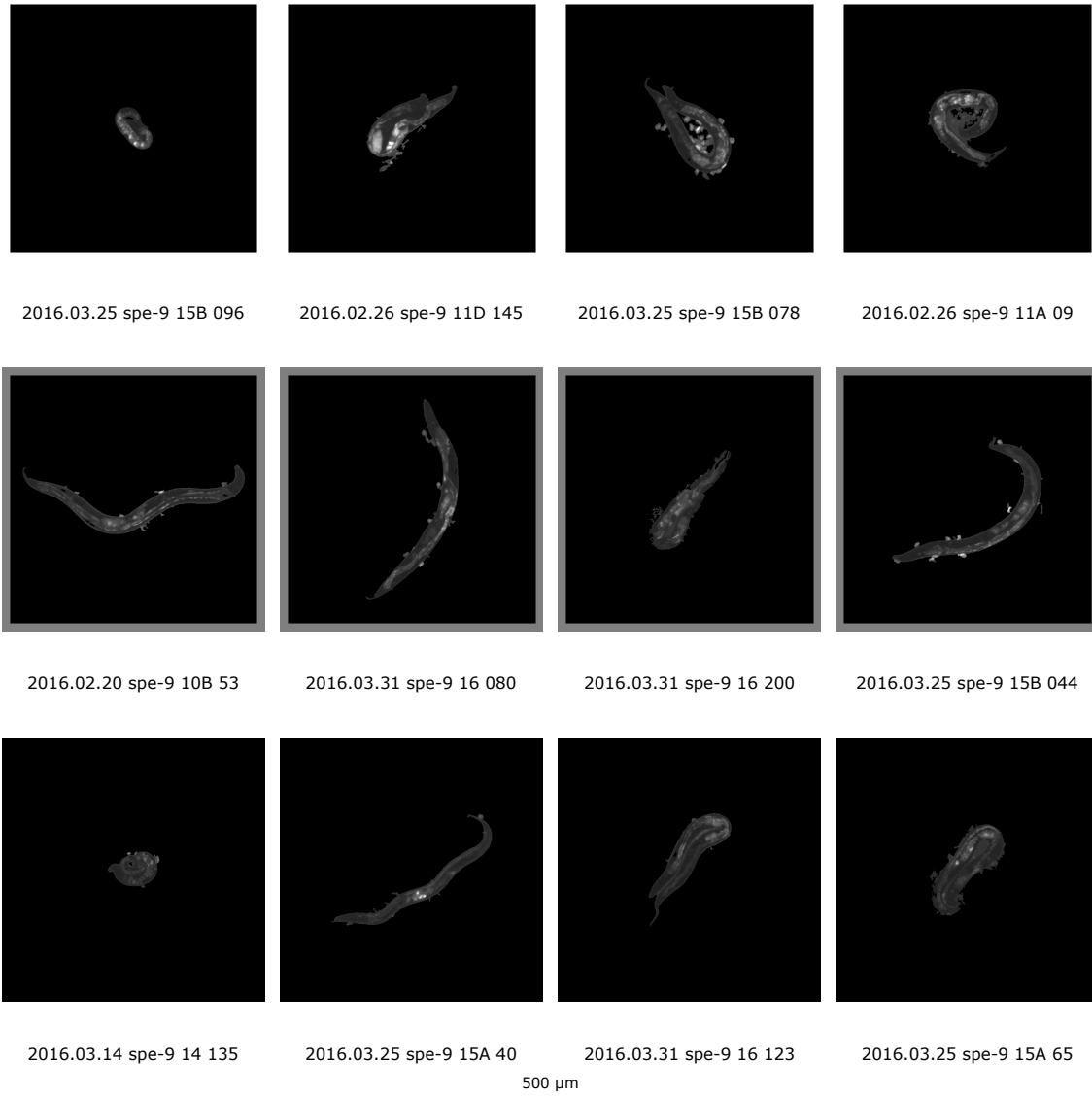


Figure 2.15: Randomly selected sample images of worms in the lower (bottom), middle (middle) and upper (top) quintiles of autofluorescence at day 9 of adulthood. For illustration, non-worm regions are masked out in black.

Movement at Day 2.0

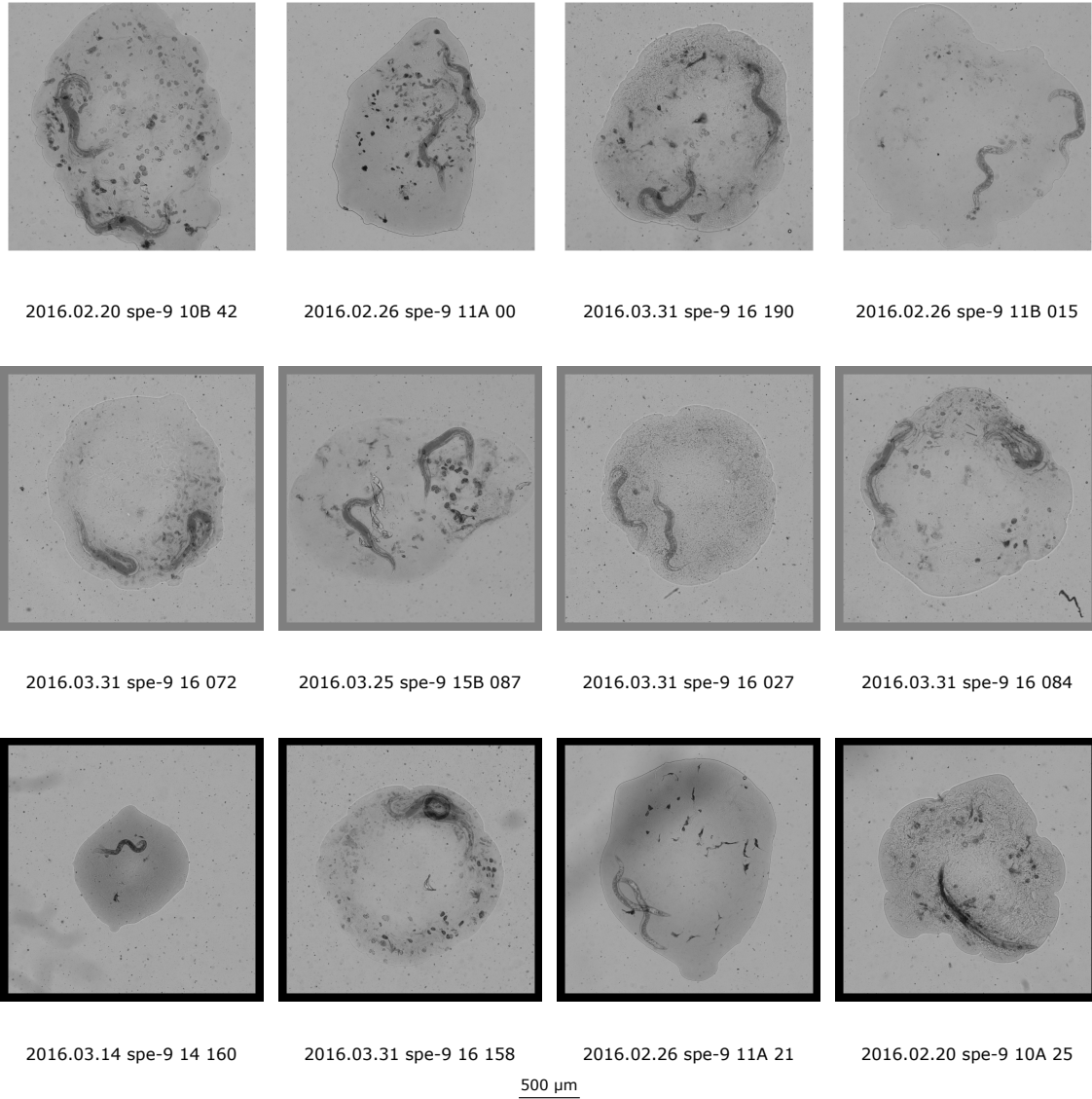


Figure 2.16: Randomly selected sample images of worms in the lower (bottom), middle (middle) and upper (top) quintiles of movement at day 2 of adulthood. For illustration, two consecutive time points (separated by three hours) are superimposed here.

Movement at Day 5.0

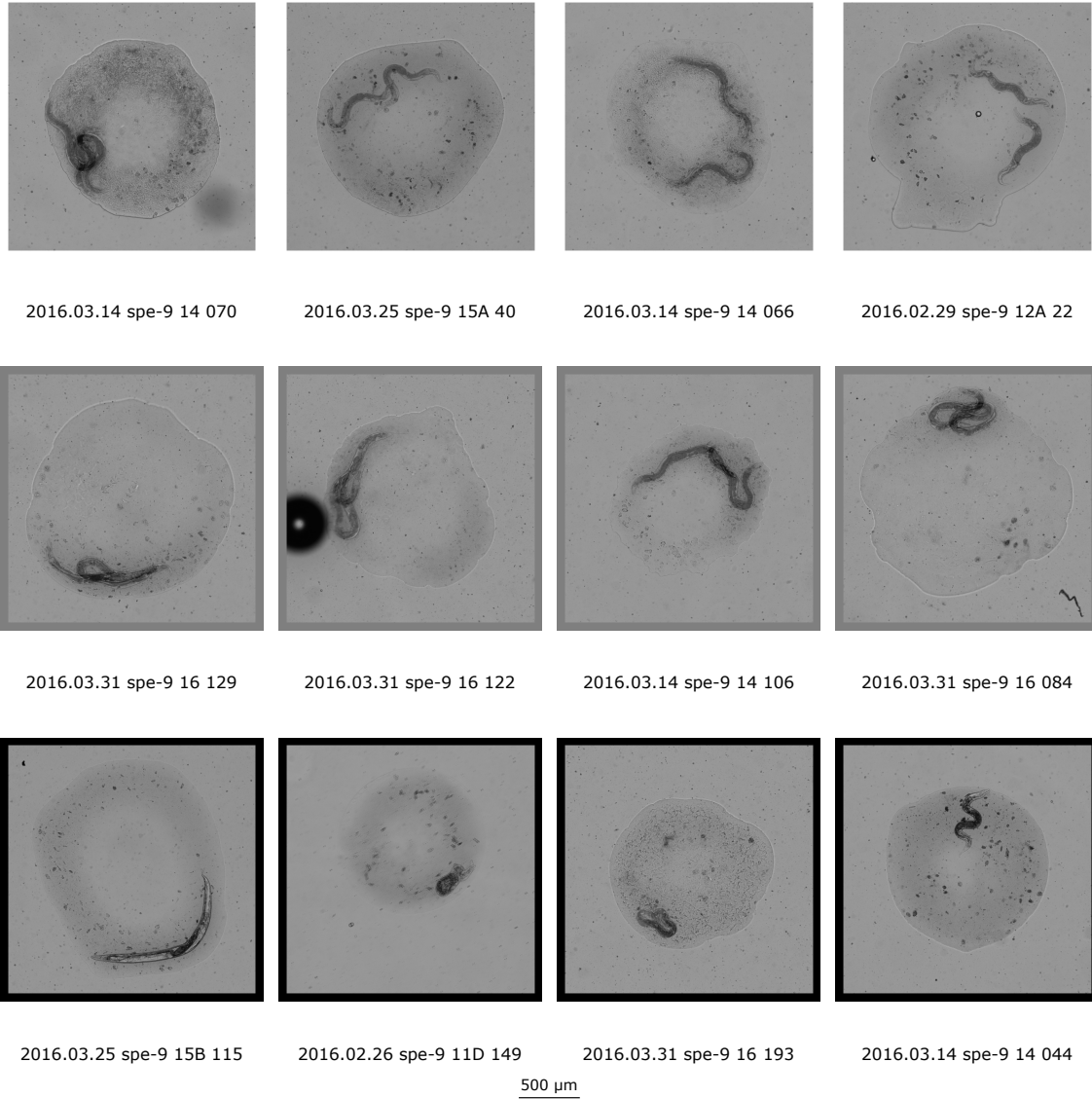
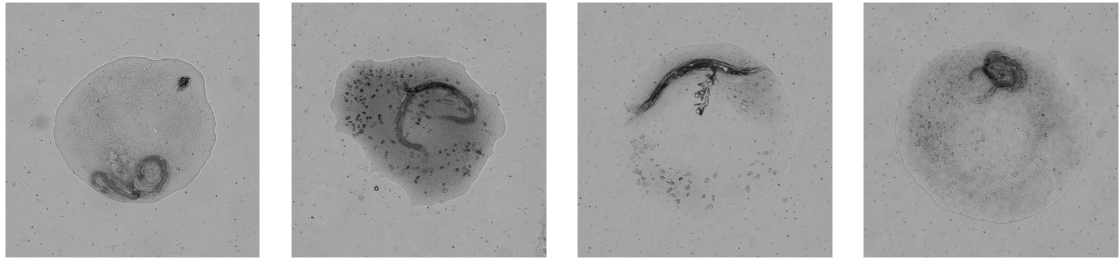


Figure 2.17: Randomly selected sample images of worms in the lower (bottom), middle (middle) and upper (top) quintiles of movement at day 5 of adulthood. For illustration, two consecutive time points (separated by three hours) are superimposed here.

Movement at Day 8.0

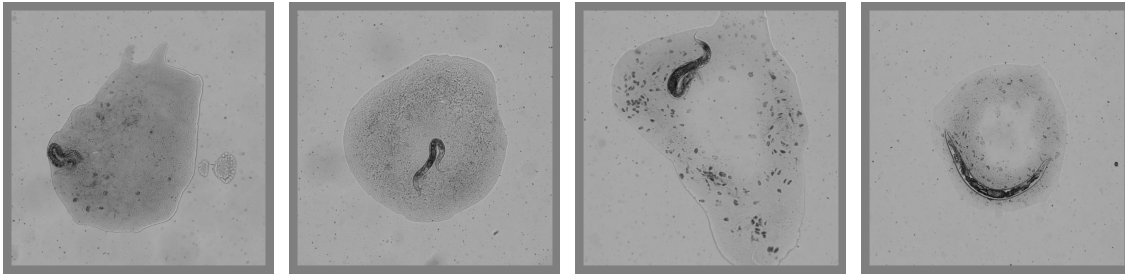


2016.03.14 spe-9 14 092

2016.03.14 spe-9 14 192

2016.03.25 spe-9 15B 037

2016.03.14 spe-9 14 071

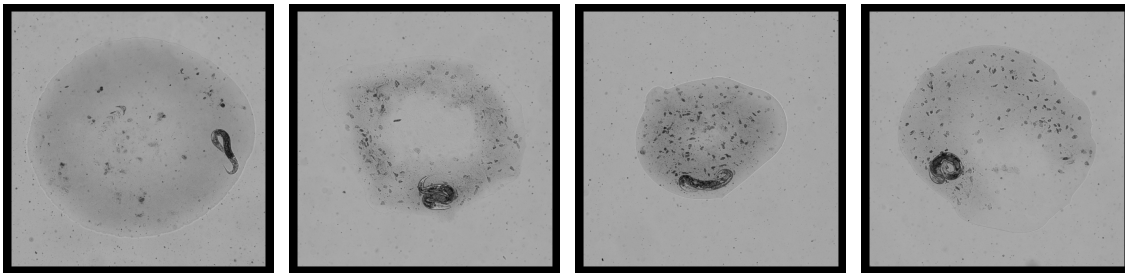


2016.03.14 spe-9 14 098

2016.03.14 spe-9 14 081

2016.03.04 spe-9 13C 69

2016.02.26 spe-9 11B 017



2016.03.25 spe-9 15B 083

2016.02.26 spe-9 11C 093

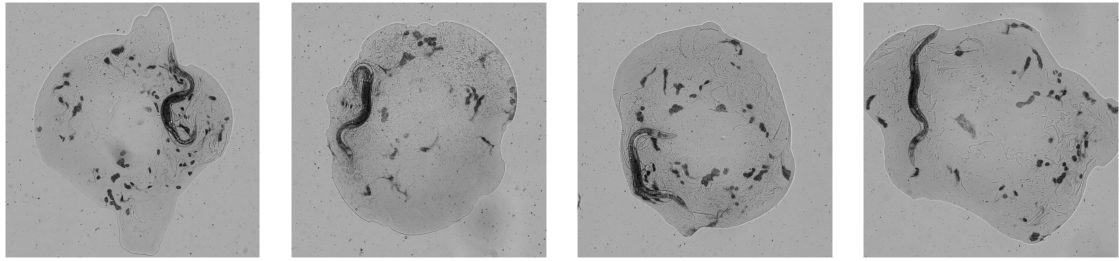
2016.02.26 spe-9 11B 052

2016.02.29 spe-9 12A 18

500 μ m

Figure 2.18: Randomly selected sample images of worms in the lower (bottom), middle (middle) and upper (top) quintiles of movement at day 8 of adulthood. For illustration, two consecutive time points (separated by three hours) are superimposed here.

Visible Laid Oocytes at Day 1.0

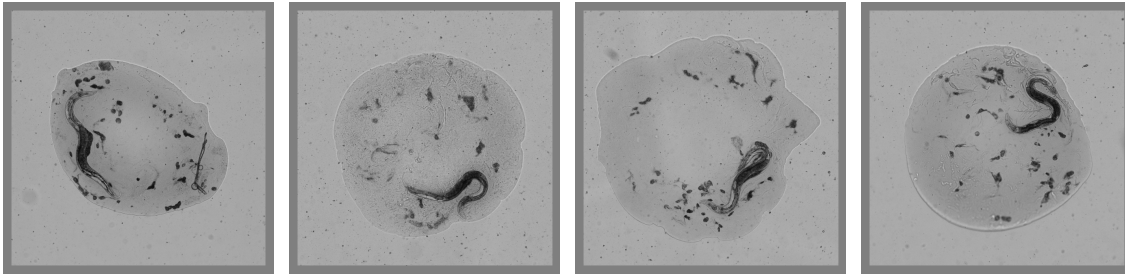


2016.03.04 spe-9 13C 59

2016.03.31 spe-9 16 020

2016.02.26 spe-9 11A 16

2016.02.26 spe-9 11A 04

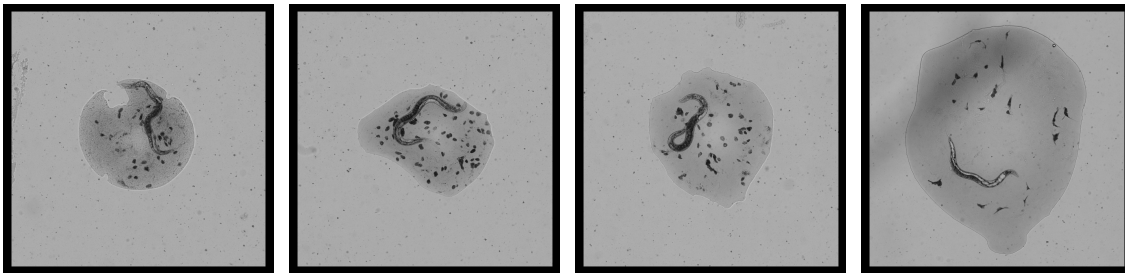


2016.03.04 spe-9 13A 19

2016.03.31 spe-9 16 178

2016.03.31 spe-9 16 049

2016.03.14 spe-9 14 049



2016.03.14 spe-9 14 188

2016.03.14 spe-9 14 163

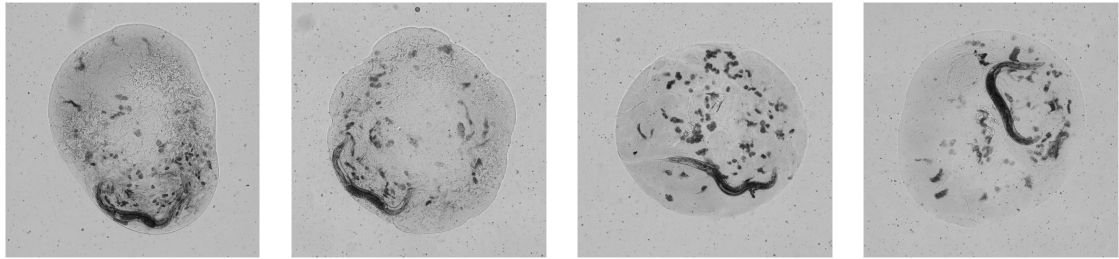
2016.03.14 spe-9 14 119

2016.02.26 spe-9 11A 21

500 μm

Figure 2.19: Randomly selected sample images of worms in the lower (bottom), middle (middle) and upper (top) quintiles of reproductive output at day 2 of adulthood.

Visible Laid Oocytes at Day 2.0

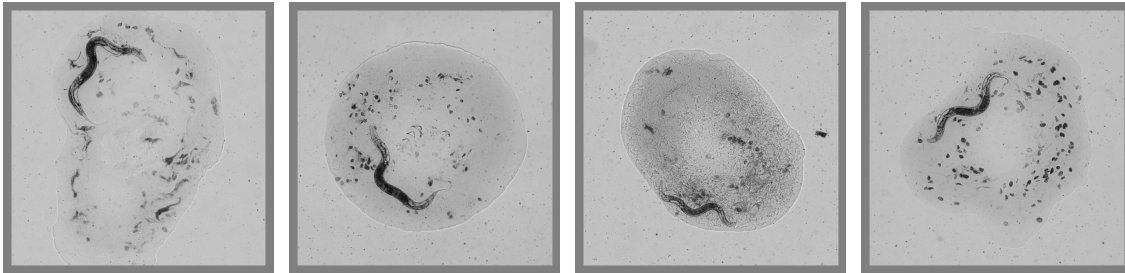


2016.03.25 spe-9 15A 60

2016.03.31 spe-9 16 029

2016.03.25 spe-9 15B 077

2016.03.25 spe-9 15B 051

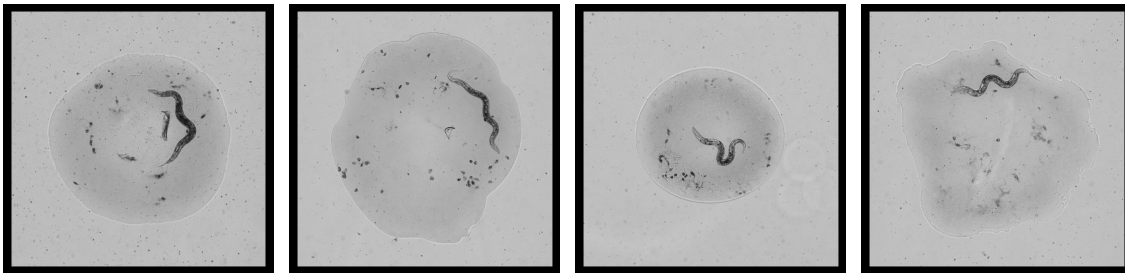


2016.02.26 spe-9 11C 096

2016.03.25 spe-9 15B 092

2016.03.14 spe-9 14 072

2016.03.04 spe-9 13C 57



2016.03.25 spe-9 15B 046

2016.02.29 spe-9 12B 43

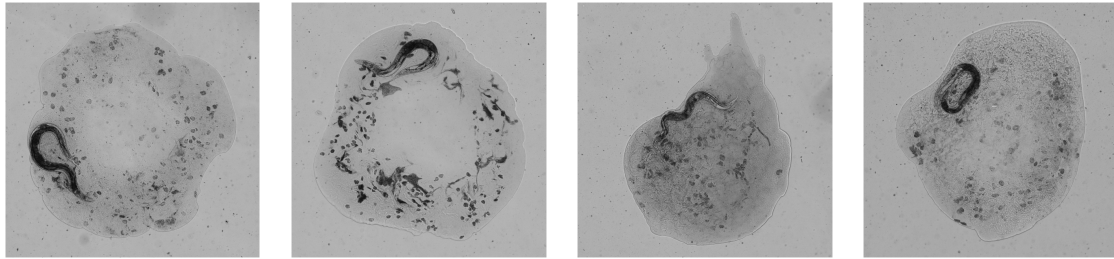
2016.02.26 spe-9 11D 143

2016.02.26 spe-9 11C 072

500 μ m

Figure 2.20: Randomly selected sample images of worms in the lower (bottom), middle (middle) and upper (top) quintiles of reproductive output at day 5 of adulthood.

Visible Laid Oocytes at Day 3.0

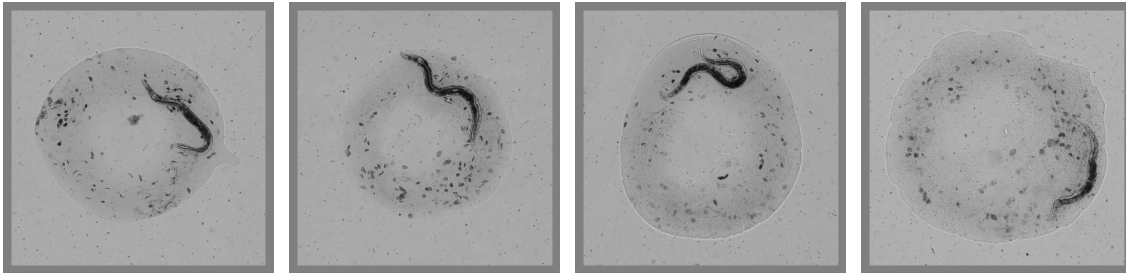


2016.02.20 spe-9 10A 16

2016.02.29 spe-9 12B 34

2016.03.14 spe-9 14 097

2016.03.25 spe-9 15A 69

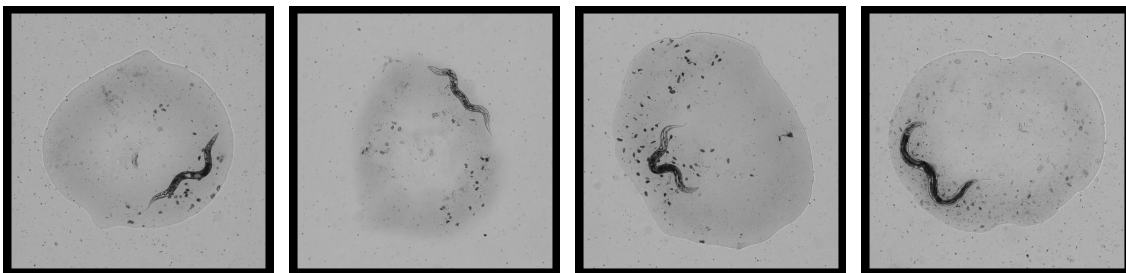


2016.03.25 spe-9 15B 008

2016.03.25 spe-9 15B 044

2016.03.25 spe-9 15B 023

2016.03.31 spe-9 16 036



2016.03.25 spe-9 15B 027

2016.02.26 spe-9 11D 134

2016.03.04 spe-9 13C 74

2016.03.31 spe-9 16 107

500 μ m

Figure 2.21: Randomly selected sample images of worms in the lower (bottom), middle (middle) and upper (top) quintiles of reproductive output at day 8 of adulthood.

Cross-Sectional Size at Day 2.0

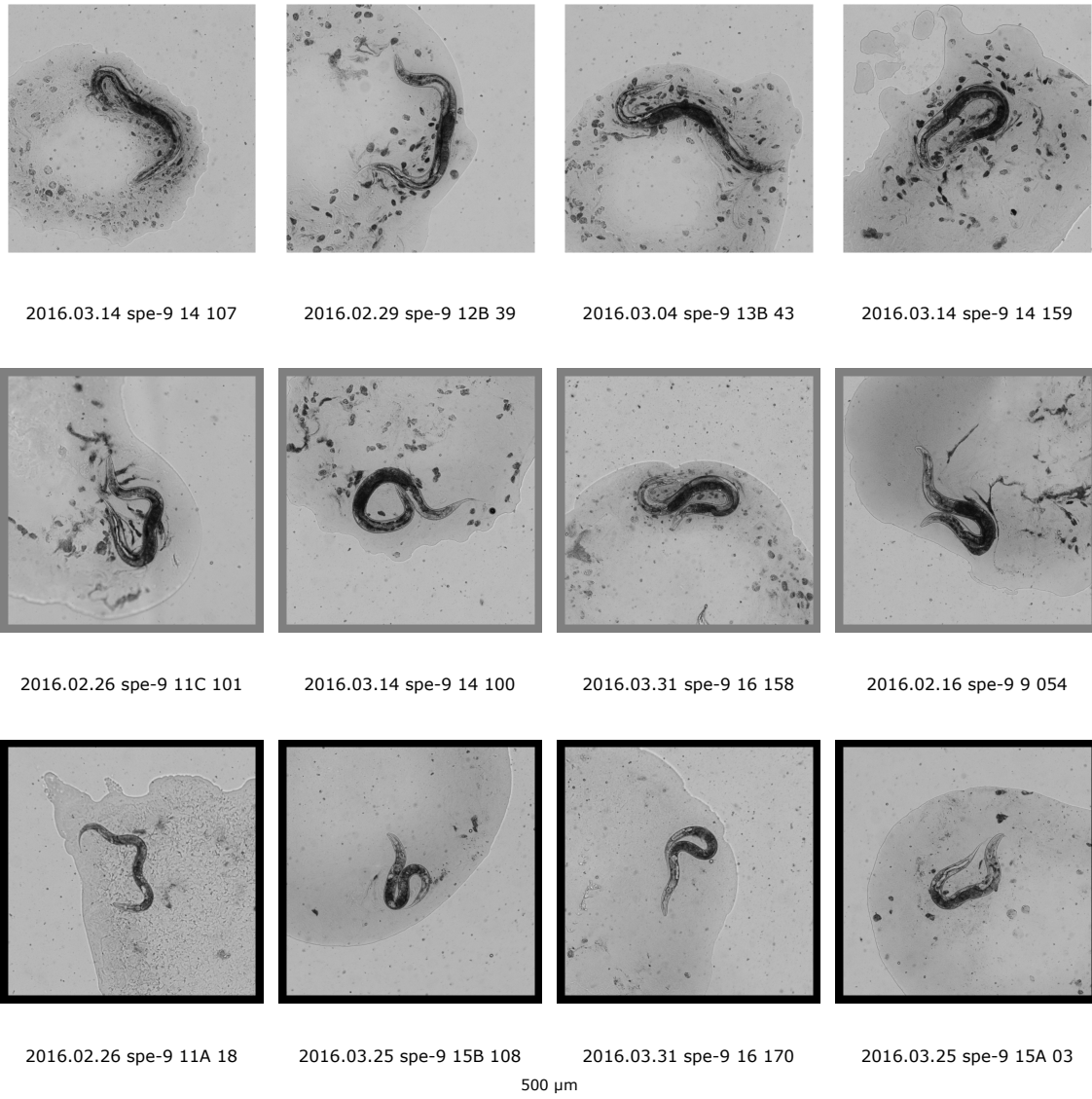


Figure 2.22: Randomly selected sample images of worms in the lower (bottom), middle (middle) and upper (top) quintiles of cross-sectional size at day 2 of adulthood.

Cross-Sectional Size at Day 5.0

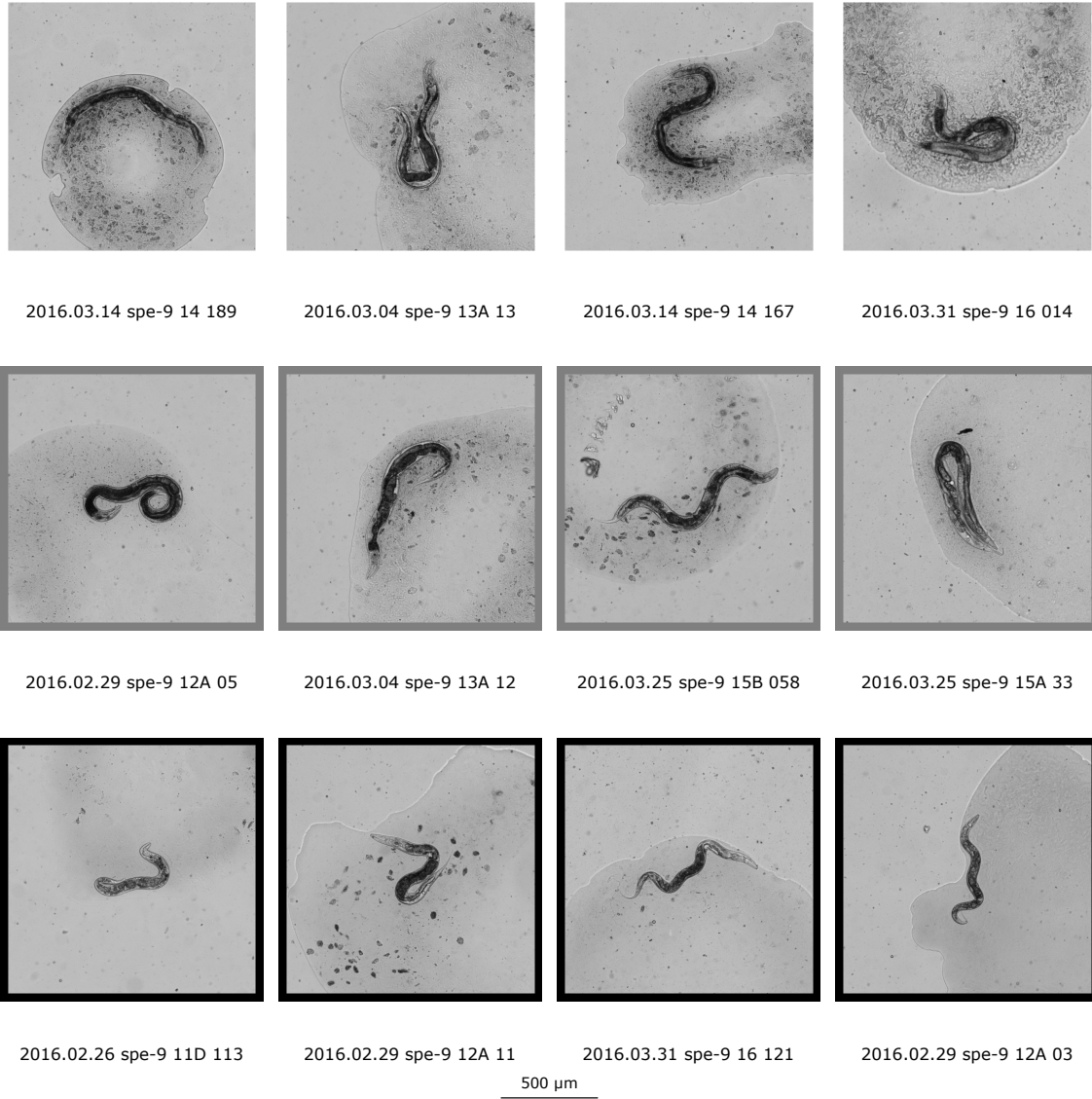


Figure 2.23: Randomly selected sample images of worms in the lower (bottom), middle (middle) and upper (top) quintiles of cross-sectional size at day 5 of adulthood.

Cross-Sectional Size at Day 8.0

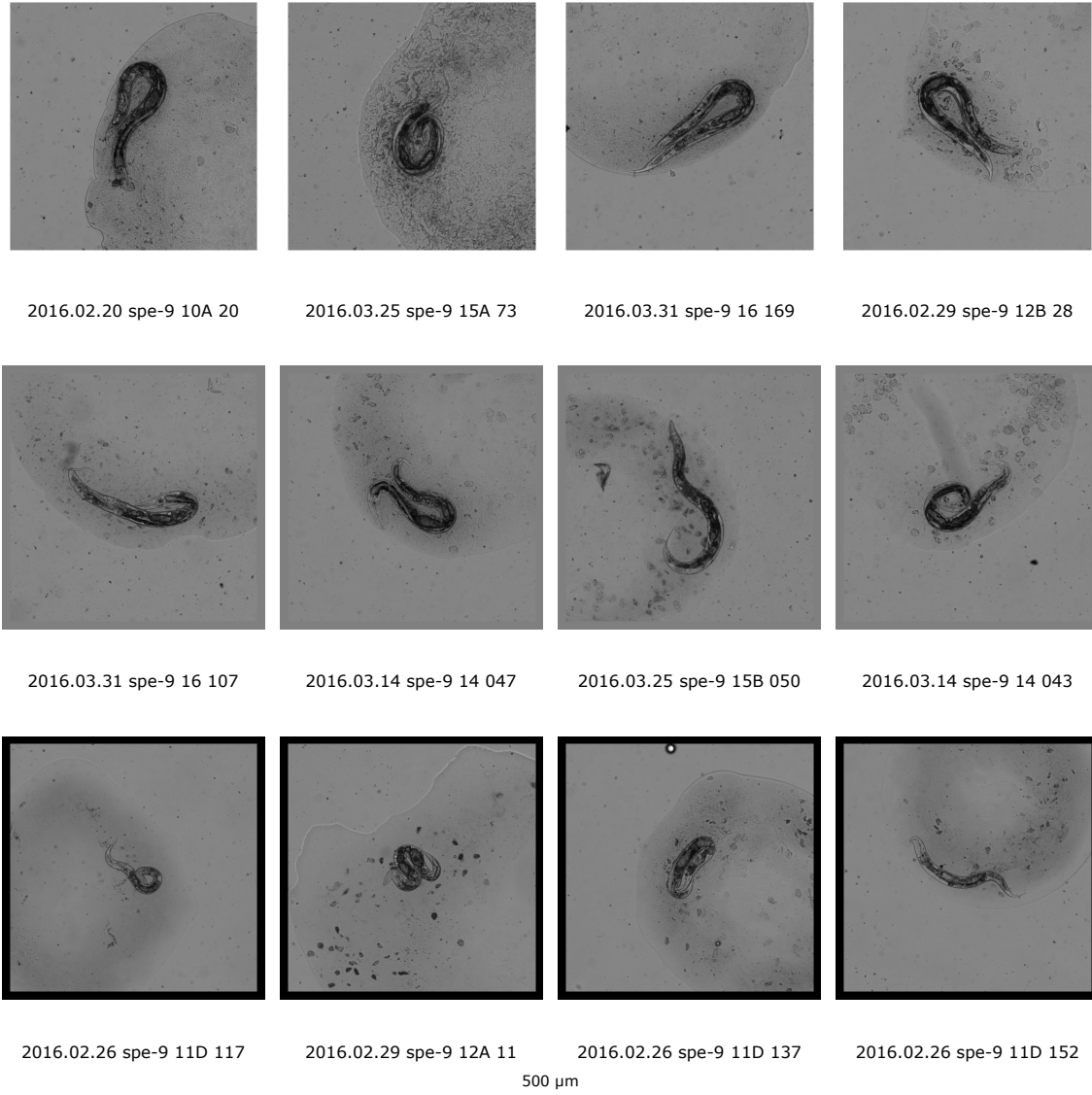


Figure 2.24: Randomly selected sample images of worms in the lower (bottom), middle (middle) and upper (top) quintiles of cross-sectional size at day 8 of adulthood.

Textural Degradation at Day 2.0

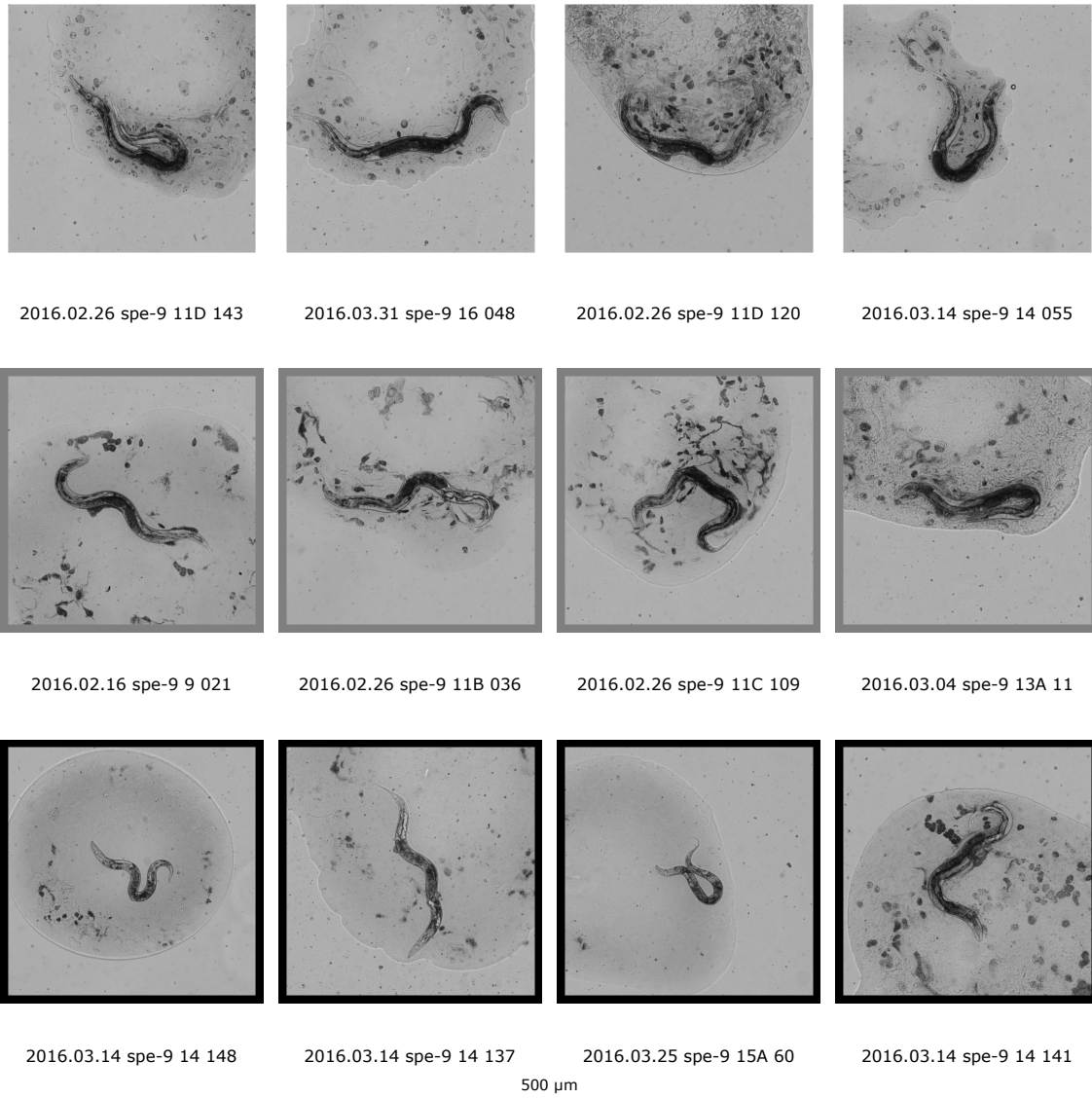


Figure 2.25: Randomly selected sample images of worms in the lower (bottom), middle (middle) and upper (top) quintiles of textural decrepitude at day 2 of adulthood.

Textural Degradation at Day 5.0

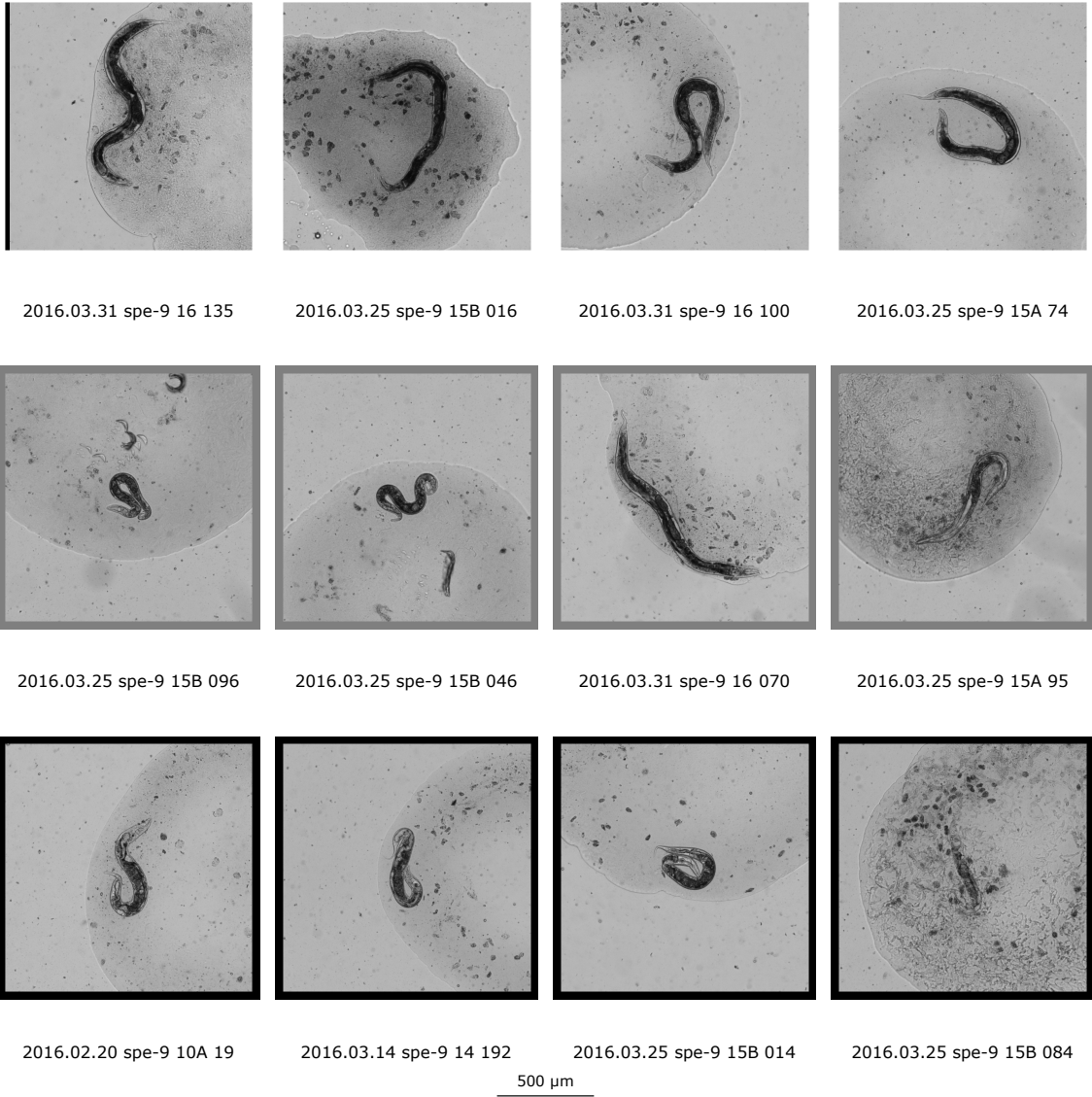


Figure 2.26: Randomly selected sample images of worms in the lower (bottom), middle (middle) and upper (top) quintiles of textural decrepitude at day 5 of adulthood.

Textural Degradation at Day 8.0

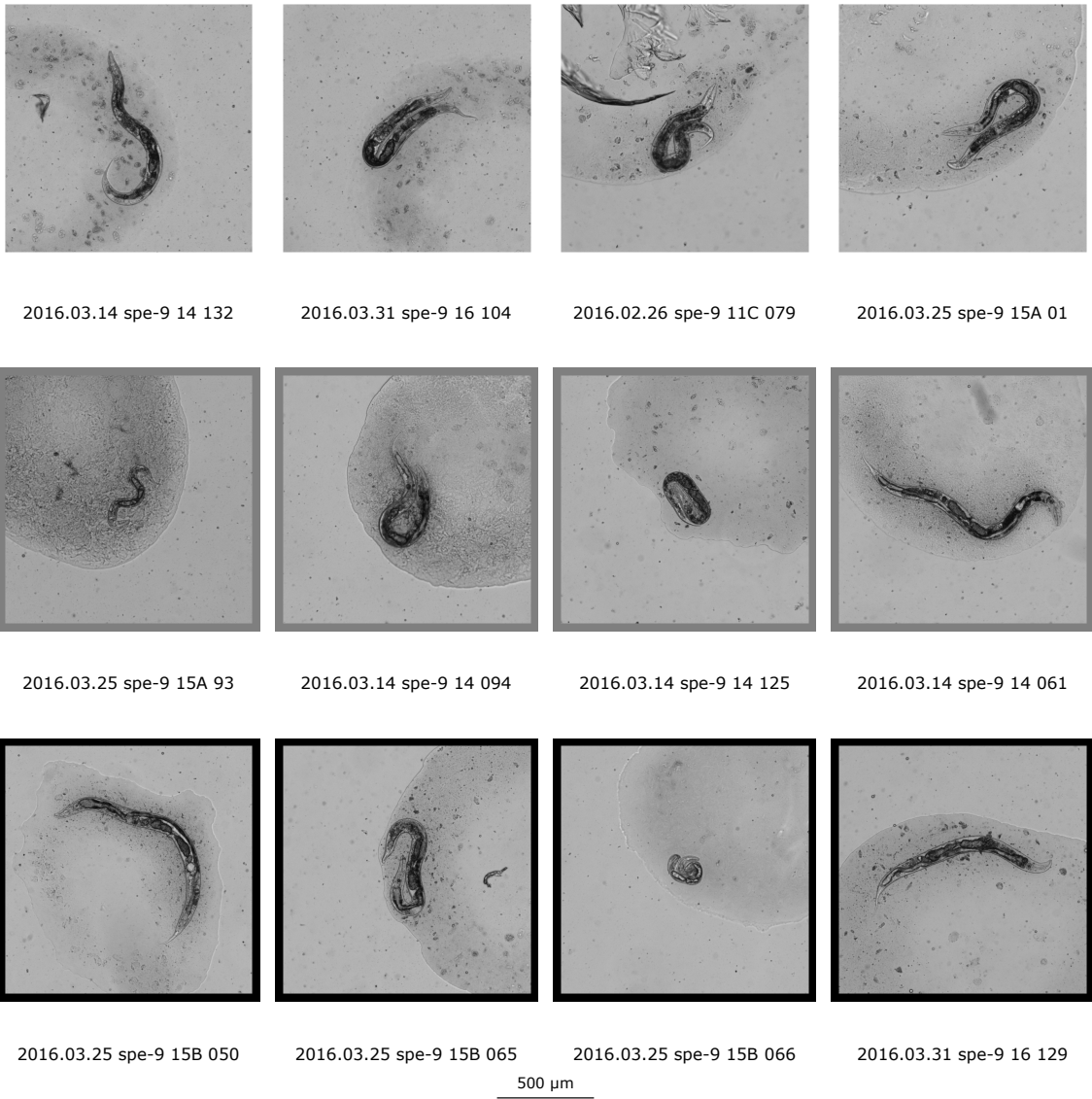


Figure 2.27: Randomly selected sample images of worms in the lower (bottom), middle (middle) and upper (top) quintiles of textural decrepitude at day 8 of adulthood.

Chapter 3

Predicting All-Cause Mortality from Basic Physiology in the Framingham Heart Study

The authors of the following publication [136] are: William B. Zhang and Zachary Pincus.

Abstract

Using longitudinal data from a cohort of 1349 participants in the Framingham Heart Study, we show that as early as 28–38 years of age, almost 10% of variation in future lifespan can be predicted from simple clinical parameters. Specifically, we found diastolic and systolic blood pressure, blood glucose, weight, and body mass index (BMI) to be relevant to lifespan. These and similar parameters have been well characterized as risk factors in the relatively narrow context of cardiovascular disease and mortality in middle to old age. In contrast, we demonstrate here that such measures can be used to predict all-cause mortality from mid-adulthood onward. Further, we find that individual clinical measurements are predictive in different age regimes. Specifically, blood pressure and BMI are predictive of all-cause mortality from ages 35–60, while blood glucose is predictive from ages 57–73. Moreover, we find that several of these parameters are best considered as measures of a rate of “damage accrual”, such that total historical exposure, rather than current measurement values, is the most relevant risk factor (as with pack-years of cigarette smoking). In short, we show that simple physiological measurements have broader lifespan-predictive value than indicated by previous work, and that incorporating

information from multiple time points can significantly increase that predictive capacity. In general, our results apply equally to both men and women, though some differences exist.

3.0 Introduction

Aging is a complex biological process with multiple contributing genetic pathways [16, 25–34], significant variation among even closely related organisms [137], and an ongoing debate about its root causes and origin [12]. At its core, however, aging is simply the statistical phenomenon of an increased probability of death over time. In addition, mortality risk does not increase at equal rates at all ages [18]. Further, aging can vary significantly for different individuals at the same age. As a result, an individual’s chronological age is a limited predictor of their actual mortality risk.

In order to develop improved prognostic capability for mortality, demographers have sought to identify biomarkers of aging, functionally defined as a biological parameter of an organism that either can better predict functional capability or mortality risk than chronological age [57]. This is motivated by an array of valuable applications, including improved actuarial modeling, biological investigations of the mechanisms of aging and therapeutics to slow its progress, and the clinical ability to better target interventions to at-risk patients.

Driven by these goals, researchers in the 1970s and 1980s proposed a large number of candidate biomarkers of aging [58–60]. Though these studies identified several putative biomarkers, many of the published multivariable composite scores were overfit—that is, overly tuned to a very specific dataset. Consequently, these composite scores did not have broad applicability, and later studies failed to validate the original findings [57, 61–64].

As a result, much subsequent work has focused on predicting specific disease processes instead of all-cause mortality [65–67]. Many physiological parameters, such as blood pressure [68] and body mass index (BMI) [69], have been well-characterized as risk factors for cardiovascular disease and other specific morbidities. In general, these studies have focused on middle-aged individuals and have emphasized risk over a limited term, often just 5- or 10-year periods (e.g. [70]). In addition, most of the work on both general biomarkers of aging and specific risk factors has been limited to the analysis of data from single time points.

More recently, Yashin and colleagues have sought to use longitudinal data to gain insight into the

overall aging process and the relationship between physiological change over time and mortality risk (e.g. [71]). In particular, modeling physiological change as a dynamic system allowed mortality risk to be successfully modeled as a function of the difference between an individual's current physiological state and the ideal state for an individual of that age [138,139]. Related analyses classified individuals' likely lifespans according to trajectories of physiological indices [140, 141]. Further, a landmark series of studies of the accumulation of age-related functional deficits in individuals over time identified a "snowball effect" where individuals with physiological deficits are more likely to accumulate further deficits over time, and are exponentially more likely to die [142, 143]. Taken together, these studies indicate that the trajectory of an individual's physiological state over time provides a rich context for understanding future mortality risk.

We therefore set out to address two very simple questions about lifespan prediction from longitudinal data. First, given an individual's history of physiological measurements (blood pressure, height, weight, and similar), how early in life is there any indication of that individual's ultimate lifespan? A very recent investigation showed that that aging is indeed detectable even in young adults [144]. Specifically, these investigators found that young adults who showed signs of accelerated physiological aging also experienced greater functional impairment. We now ask whether such early-life aging has detectable impacts on eventual survival decades hence.

Second, this work seeks to determine if data from multiple timepoints can be aggregated in any way to provide a clearer estimate of future lifespan? Many of the models presented in previous work (e.g. [138, 139, 142]) use longitudinal data, but estimate mortality risk at a particular time only from measurements made at that time. This effectively assumes that mortality risks are a memory-free Markov process. In this work, we test this assumption and determine whether physiological history is helpful in lifespan prediction.

Our investigation of longer-term biomarkers of longevity was made possible by the continued progression of the Framingham Heart Study (FHS). With its large cohort, consistent longitudinal measurements of basic physiology, and excellent level of follow-up in terms of rate and length, the FHS offers a unique opportunity to investigate the contributions of biomarkers from very young ages, as well as the evolution of biomarker effectiveness throughout the aging process. The FHS population also allows us to focus on a single longitudinal cohort of individuals, avoiding the possible confounding effects of using additional cross-sectional data. In this work, we use the Framingham data to understand

the proportion of variation in all-cause mortality that can be predicted from basic clinical measurements. We study these effects from early-to-mid adulthood, and examine how they evolve as a result of the aging process (Table 3.1).

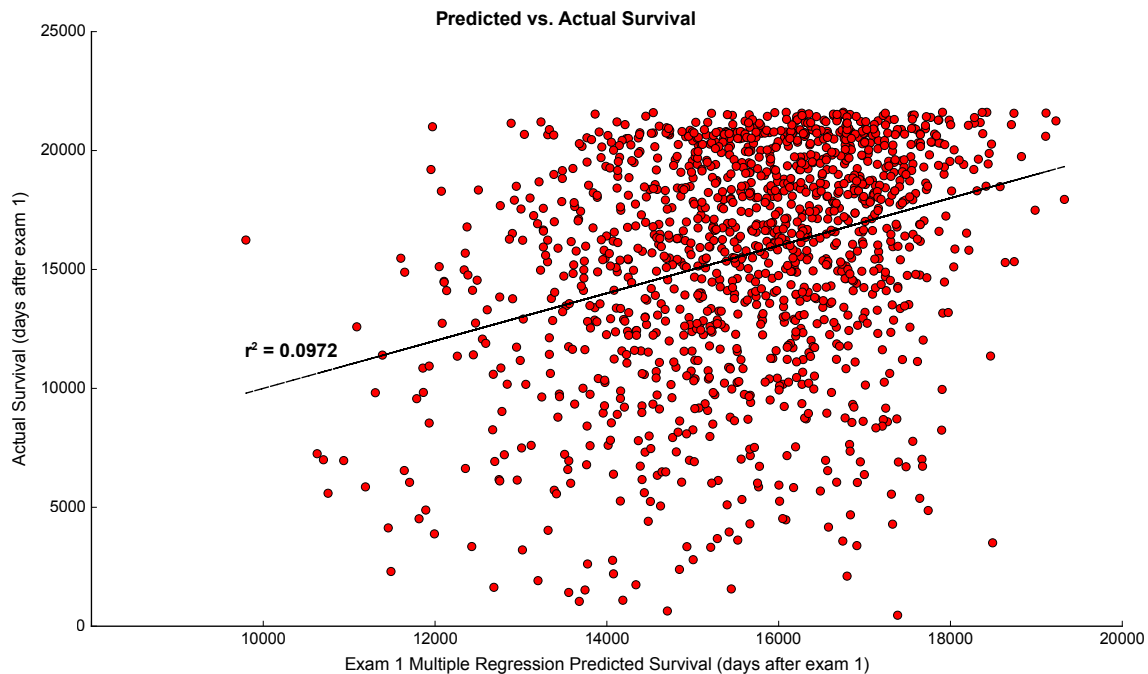
	Living Subcohort Size	Mean Age (Years)	% Males	% Females
Exam 01	1349	34.5 ± 2.2	0.47	0.53
Exam 02	1329	36.6 ± 2.2	0.47	0.53
Exam 03	1311	38.5 ± 2.2	0.47	0.53
Exam 04	1301	40.5 ± 2.2	0.46	0.54
Exam 05	1285	42.5 ± 2.2	0.46	0.54
Exam 06	1270	44.5 ± 2.2	0.46	0.54
Exam 07	1256	46.5 ± 2.2	0.46	0.54
Exam 08	1236	47.9 ± 2.2	0.46	0.54
Exam 09	1216	49.9 ± 2.2	0.46	0.54
Exam 10	1189	52.0 ± 2.2	0.46	0.54
Exam 11	1162	53.8 ± 2.2	0.46	0.54
Exam 12	1136	56.0 ± 2.2	0.46	0.54
Exam 13	1108	58.0 ± 2.2	0.46	0.54
Exam 14	1071	60.0 ± 2.2	0.45	0.55
Exam 15	1031	61.9 ± 2.2	0.45	0.55
Exam 16	987	63.9 ± 2.2	0.44	0.56
Exam 17	956	65.9 ± 2.2	0.44	0.56
Exam 18	893	68.1 ± 2.2	0.43	0.57
Exam 19	836	70.1 ± 2.2	0.42	0.58
Exam 20	789	72.2 ± 2.2	0.41	0.59
Exam 21	724	74.1 ± 2.2	0.39	0.61
Exam 22	646	76.0 ± 2.2	0.39	0.61
Exam 23	580	77.8 ± 2.2	0.37	0.63
Exam 24	488	79.9 ± 2.2	0.36	0.64
Exam 25	455	81.8 ± 2.2	0.35	0.65
Exam 26	376	83.8 ± 2.2	0.32	0.68
Exam 27	301	85.5 ± 2.1	0.31	0.69
Exam 28	236	87.2 ± 2.0	0.32	0.68

Table 3.1: A table of summary statistics about the changing demographics of the surviving cohort over time.

3.1 Results

To understand the mortality-predictive ability of various physiological biomarkers, we began by selecting a well-defined and homogeneous cohort of individuals to analyze. In order to study the effect of biomarkers on mortality risk at a young age and the effects of incorporating past measurements into predictive models, we chose to focus on the youngest individuals in the original cohort of the Framingham Heart Study. The data from these individuals is both the most extensive and begins earliest in life. Moreover, this cohort, aged 28–38 years at the first Framingham exam, shares a birth decade, limiting the opportunity for confounding effects due to cultural and medical changes over time.

Out of the hundreds of measurements made by the Framingham investigators, we chose to focus on basic parameters that were not indicators for any specific pathology and which had a wide dynamic



	Average at Exam 1	Multiple Regression Weight	Single-Variable Correlation (r^2)
Blood Glucose	78.7 ± 15.9 mg/dL	-9.8 days per unit	0.0026
Body Mass Index	24.7 ± 4.12 kg/m ²	-81.1 days per unit	0.0236
Diastolic Blood Pressure	79.9 ± 9.53 mm Hg	-90.3 days per unit	0.0869
Systolic Blood Pressure	126.2 ± 14.07 mm Hg	-43.0 days per unit	0.0814
Height	65.6 ± 3.65 inches	-84.2 days per unit	0.0075
Weight	153.85 ± 30.53 pounds	10.8 days per unit	0.0293
Age	34.5 ± 2.18 Years	n/a	0.0287

Figure 3.1: In early-to-mid adulthood (participants aged 28–38), 9.7% of variation in future lifespan can be predicted from a weighted combination of systolic and diastolic blood pressure, blood glucose, height, weight, and body mass index. (top) Scatter plot of predicted lifespan from clinical measurements and actual future survival. Note that the composite predictor does not simply measure overt pathology, but has a graded response across the full dynamic range of lifespans. (bottom) A table showing summary information for the six components of the composite predictor, along with age for comparison. At the first clinical exam, systolic and diastolic blood pressure are the strongest drivers of predictions of all-cause mortality, as shown by the r^2 for the in the single-variable correlations with future lifespan.

range of variation (e.g. not binary variables such as whether a specific type of cardiac arrhythmia was detected on physical exam). After eliminating parameters that were not consistently measured across the first 28 clinical exams (over 50 years) of the study, we obtained a panel containing weight, height, systolic and diastolic blood pressure, BMI, and blood glucose.

3.1.1 Amount of Mortality Predictable from Physiology

In order to determine the fraction of variability in lifespan that can be predicted from the first exam, we employed multiple linear regression to assign weights to our six selected measurements. This allowed us to combine the six variables into a single composite “risk score” and to assess its relationship

with mortality (measured in days of survival after the first clinical exam). The relationship between predicted lifespan and results is shown in figure 1 (at the first clinical exam, when our cohort of participants is 28-38 years old). Overall, approximately 10% of variation in ultimate lifespan is predictable using a simple linear regression on six basic clinical parameters ($p = 8.52 \times 10^{-32}$).

In this type of analysis, weights for each measured parameter are chosen based on the known survival time of each individual. With sufficiently many parameters, models constructed in this fashion can become “overfit” and not generalize well to future data. In this case we have few parameter weights (seven: six measurements plus a constant offset) compared to the size of the data, and thus the model is unlikely to be overfit. To demonstrate this directly, we estimated the ability of the model to generalize to future data by using 5-fold cross-validation, in which different subsets of the data were used to fit the weights versus evaluate the goodness of that fit. This generated a Pearson r^2 of 0.085, suggesting that these results are indeed not overfit.

Thus, even relatively early in adulthood, a modest but meaningful fraction of future lifespan is already predictable. Further, the lack of sharp demarcations on the scatterplot indicates that this correlation is not driven exclusively by individuals with overt pathologies. Rather, the effect is graded, and is spread over much of the dynamic range that exists for both the clinical measurements and the length of known survival.

Next, we asked how the proportion of predictable mortality from single time-points changes as the cohort ages. Figure 2 (left) shows the correlation between the measured parameters and mortality throughout the aging process, for the subcohort of our original population still alive at each time point, stratified for gender. (Note that the trends in these correlations thus include both the effects of age and of survivorship bias.) The three different traces represent three approaches to constructing a composite “risk score” from the clinical data.

First, we used the weights that were computed to be optimal for predicting lifespan at exam 1, when the mean age of the cohort was 34.5 years (figure 1, bottom). The decrease in the predictive ability of this score over time suggests that the risk factors that are important in early life become less relevant in middle age. To illustrate this more explicitly, we then calculated the set of weights that most optimally predict future lifespan at exam 18, when the mean age was 68.1 years. As expected, the “exam 18” trace is a worse predictor than the “exam 1” trace early on, but is more effective at later time points. We next used regression to determine the optimal weighting of the six parameters at *each* Framingham

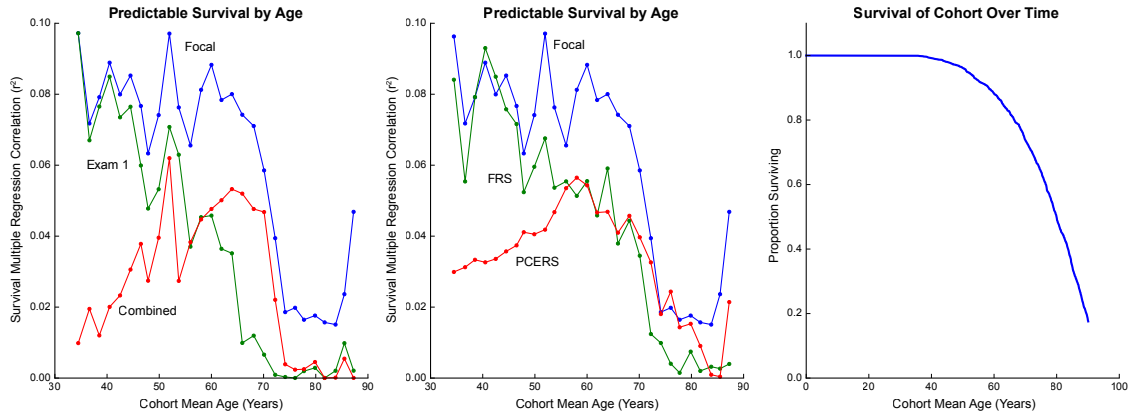


Figure 3.2: (left) The proportion of lifespan predictable from various approaches to constructing composites generally decreases with age. The trace computed by re-calculating the regression weights at each time point independently (“focal”) sets an upper bound on the portion of survival that predictable at each time point. The “exam 1” trace performs well for early exams, but becomes less relevant at more advanced ages. Finally, the “exam 18” trace, created by fitting data from individuals at clinical exam 18, performs worse than the “exam 1” trace at early time points but better at later ones. (center) Our “focal” exam score is compared to the Framingham Heart Score (FHS) and the Pooled Cohort Equation Risk Score (PCERS), two well-known cardiovascular risk scores. Strikingly, the PCERS and FHS seem to behave like the “exam 1” and “combined” traces, respectively. Note that the FHS and PCERS are not subject to the “upper bound” set by the “focal” trace, since they include information from additional variables (such as blood cholesterol and age itself) not used for the “focal” trace calculation. (right) A survival curve for the overall cohort studied, illustrating how the size of the surviving subcohort changes over time.

study exam (the “focal exam”) independently. This provides an upper bound on fraction of lifespan predictable in a linear fashion from these basic measurements over time. (Nonlinear regression models with more free parameters may well be able to predict more about future lifespan; we excluded these from our analysis as a guard against overfitting and multiple hypothesis testing.) Of note is the gradual decline in our ability to predict mortality after roughly age 60. This suggests that the physiological parameters analyzed are able to capture relevant differences between those who die relatively early and those who die later, but not the variation among particularly longer-lived individuals.

To put our findings into the context of previously developed clinical risk scores, figure 2 (center) compares the lifespan-predictive ability of the well-known Framingham Risk Score [145, 146] and Pooled Cohort Score [147] with our “focal exam” estimates. These clinical scores were designed specifically to assess cardiovascular risk in a 5–10 year timeframe, using some of the parameters we examined as well as smoking status, blood cholesterol, and age. Despite this narrow focus, however, both scores are able to predict a significant proportion of variation in all-cause mortality over 50+ years of follow-up. Indeed, their predictive value remains valid even at the earliest clinical exam, when the average age of participants is 34.5 years. This demonstrates a surprising robustness of the lifespan-predictive

signal in these data: even risk scores such as these, which were not specifically tuned to the task, are effective biomarkers of aging.

Next, figure 3 illustrates how the individual measurements' (from figure 1) correlations with future lifespan change over time. As expected, the predictive ability of most of the parameters under investigation declines as the overall predictable mortality (measured by the focal exam trace from figure 2) declines. This trend is most strongly illustrated by the three blood pressure variables, systolic, diastolic and pulse pressure, which are highly predictive of lifespan from ages 35–60 and increasingly less predictive thereafter. On the other hand, blood glucose is a striking exception. Up to age 70, as all other significant predictors' correlations are declining, the correlation of blood glucose with all-cause mortality rises consistently, achieving its highest values from the ages of 57–73. Overall, it appears that blood pressure and BMI are predictive of all-cause mortality early in life (ages 35–60, with pulse pressure interestingly being a stronger predictor in late life than systolic and diastolic blood pressure), while blood glucose is more meaningful in middle age (ages 57–73). This reinforces the evidence from figure 2 that the mortality-predictive ability of our clinical variables changes during different phases of life.

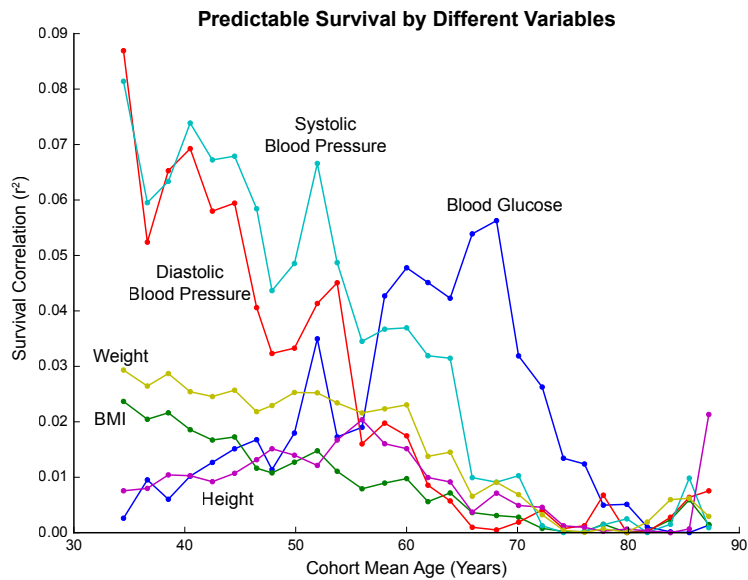


Figure 3.3: The individual variables' ability to predict survival changes over time. Blood pressure, BMI, and weight are predictive of mortality primarily from ages 35–60 and while blood glucose is most predictive from ages 57–73. Also, note that BMI, all three measures of blood pressure, and weight all decrease in predictivity as the cohort ages, but blood glucose's ability to predict survival increases in middle age before declining again.

3.1.2 Incorporating Physiological History into Mortality Prediction

As the Framingham data provide measurements of the same physiological parameters at different ages for each individual, we next investigated whether and how trends in these measures over time are predictive of future lifespan (figure 4). The simplest possibility is that a particular measurement directly reflects the current state of health of an individual at that moment (central panel in figure 4). In this case, the previous values of that measurement are redundant/irrelevant. Alternately, there may be cases where the precise value of a clinical measurement itself is not particularly important for prognosis, but its rate of change with time is more reflective of future health (illustrated by the slope of the tangent line in the left panel in figure 4). For example, progressive increases in the size of a skin blemish could indicate a malignancy, while the actual size of the blemish itself may be less relevant. Finally, other clinical measures may directly capture rates of change of health, such that the relevant information for prognosis is the cumulative change over time (the integrated “area under the curve”, illustrated by the shaded region in the right panel in figure 4). One clear example is an individual’s risk from their history of smoking. In that case, there is significant evidence that one’s smoking “rate” (packs per day) is in some sense a rate of decline of health, and that the true risk is best predicted by total accumulated underlying damage (typically reported as “pack-years” of smoking), rather than the current smoking rate.

To see which of these possibilities best fits the observed data, we computed “rates of change” (i.e. differentiated) and “cumulative” (i.e. integrated) versions of our variables and analyzed their correlations with mortality. We first attempted several formulations of “rates of change”: taking the difference between successive exams; reducing noise by finding the slope of a line fitted to three exam time points rather than two; and smoothing the data by averaging multiple adjacent exams before obtaining pointwise rates of change as above. We found that no “rate of change” formulation was predictive of mortality (data not shown).

We next focused on the accumulation hypothesis, in which integrating past values for a given measurement might yield improved predictive ability. To explore the idea of accumulated risk, we constructed variables analogous to pack-years for smoking by simply summing past measurements, weighed to account for the uneven timing of the Framingham exams. If, as hypothesized, a particular variable represents a “rate of change” of health, then its accumulated history will be more predictive

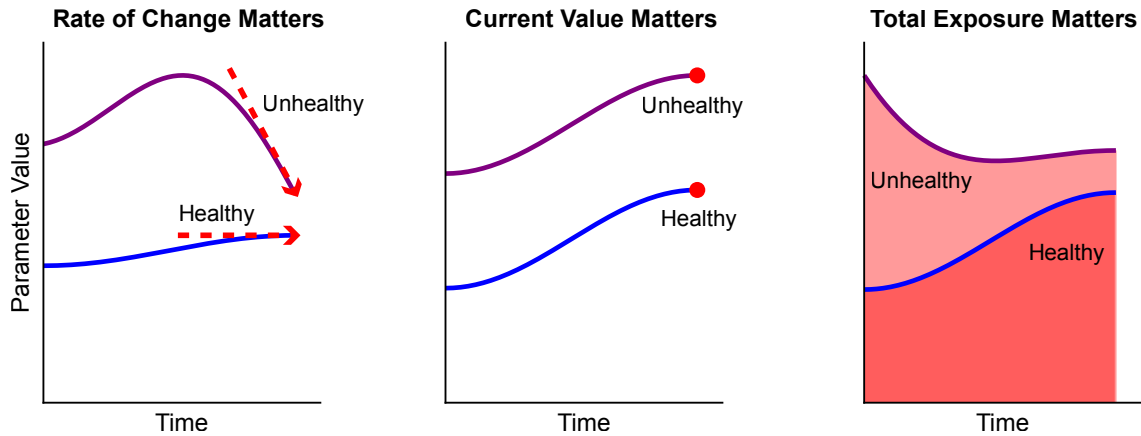


Figure 3.4: Hypotheses for the relationship between health (risk of mortality) and trends in physiological measurements. The potential scenarios considered are: (left) the derivative (“rate of change”) of a measurement is the most relevant quantity for predicting mortality; (center) the current value of the measured parameter is most predictive of mortality; (right) the integral (“accumulated exposure”) is most predictive of mortality. In each panel, a blue line represents a “healthy” time course, while a purple line represents a more “unhealthy” time course at higher risk for mortality. In the left panel, the precise values of the measurements over time are not important, but their stability over time is. Thus, a trajectory in the midst of a sharp decline may be a risk factor, while a more stable trajectory is lower-risk. The middle panel illustrates the case in which a parameter value directly relates to underlying risk, so the current value of that parameter is most useful as a quantitative risk factor. Finally, the right panel shows the case when an individual’s accumulated exposure is the relevant risk factor. Here, the total historical exposure (area under the curve) is more predictive of mortality than the measure’s current value or rate of change; as such, in this example the trajectory with the larger shaded area underneath is the more at-risk.

of mortality than its current single-time value. Continuing the example of smoking, an individual’s accumulated pack-years of smoking should have a stronger correlation with survival than their current smoking rate. Further, looking at intermediate amounts of history should yield intermediate levels of predictive capacity. For example, if we obtain individuals’ smoking history for only the previous 5 years, that variable’s correlation with mortality should be greater than the correlation from the single-time measurement, but less than the correlation obtained for their full lifetime history of smoking. If, on the other hand, integrating the most recent 5 years or so of history improves predictive abilities but earlier historical data adds nothing, this may suggest that the “integrated recent history” may simply be a de-noised estimate of the current physiological state. While such denoising may be clinically useful, it is not good evidence that the risk factor truly is cumulative.

For this analysis, we begin with the single-time correlation at a particular exam (the “focal exam”), then trace the mortality-predictive abilities of individual clinical parameters as progressively more years of history are incorporated (figure 5). In this figure, each successive point in the line includes history from one additional Framingham study exam. As more history is incorporated (by summing variable-years), some variables’ correlation with survival increases consistently and roughly linearly,

suggesting that these variables are indeed cumulative. Figure 5 shows these traces with exams 16 and 20 as the focal exams. (These exams were conducted when the participants were 59–69 and 67–77 years old, respectively.) For focal exam 16, diastolic blood pressure exhibits a consistent increase in mortality-prediction with each additional unit of history for both men and women. In contrast, for focal exam 20, diastolic blood pressure does not seem to accumulate predictivity from history, while blood glucose does. We have also excluded the effects of hypertension treatment in figures 5 and 6. This caused the size of the observed effects to decrease marginally without creating any substantial differences from the same analysis of data uncontrolled for hypertension treatment (data not shown). We believe that this steady increase in mortality-predictive capacity with additional historical data is the hallmark of a variable that affects health through cumulative exposure. The switch in which variables predict future risk at different ages between exams 16 and 20 is consistent with our earlier analysis, and much other work [148] demonstrating the dramatic change in risk factors with age (figure 3).

To further examine these trends, we focused on diastolic blood pressure, BMI, and blood glucose, which appear to be cumulative when considered from the perspective of exams 16 and 20. For each variable, figure 6 shows the utility of additional years of history when starting from a range of focal exams, rather than just exams 16 and 20. In particular, BMI seems to increase in mortality-predictive capacity as more history is incorporated, regardless of the clinical exam from which we begin the analysis. In contrast, diastolic blood pressure appears to stop showing signs of cumulative risk after clinical exam 17, which corresponds to an average age of 65.9 years. Blood glucose, however, seems to behave as an accumulating variable for all exams after clinical exam 13, which corresponds to an average age of 58.0 years. Again, this extends our result from earlier: Not only do blood glucose and blood pressure seem to be important for mortality-risk prediction at different age regimes (ages 35–60 and 57–73, respectively), their predictive capability within their regimes is cumulative (ages 35–65, and 58–87, respectively). That is, blood glucose and blood pressure appear to primarily predict mortality through accumulated lifetime exposure.

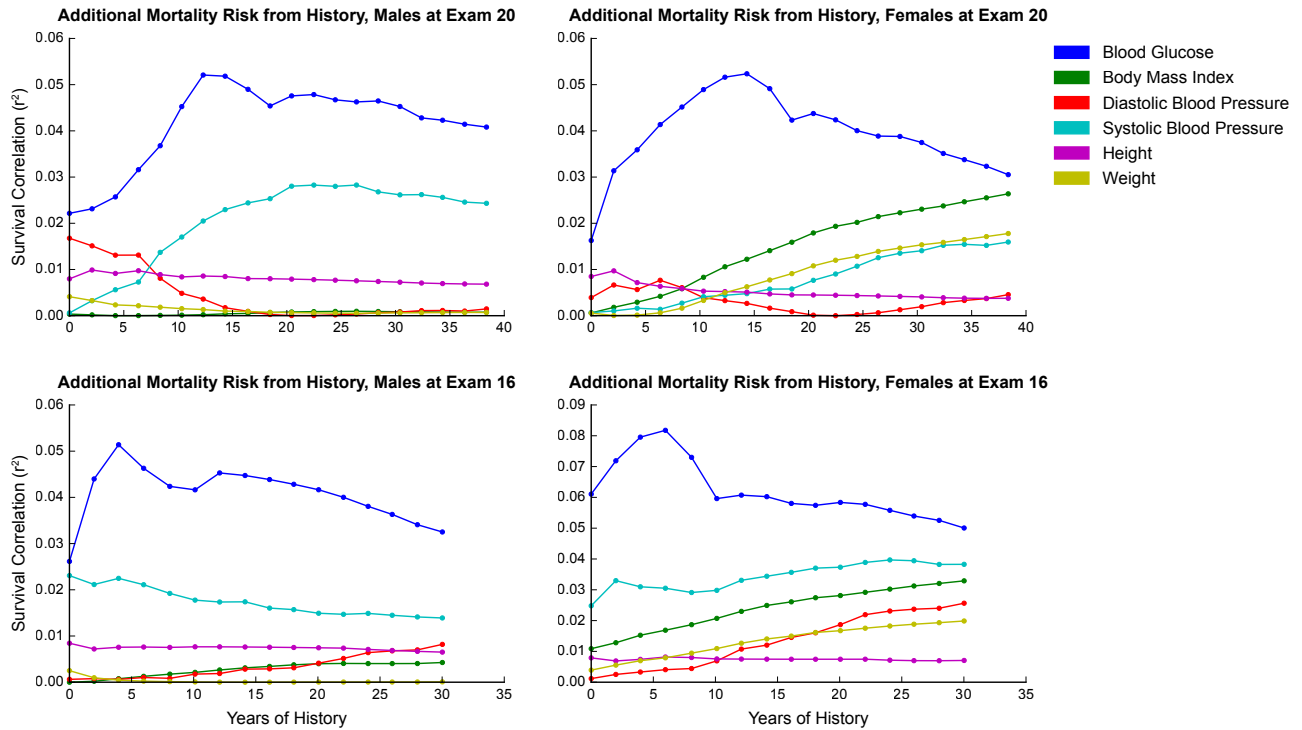


Figure 3.5: A plot of how the mortality-predictive ability of single variables changes as more history is incorporated into an accumulated risk score at “focal exams” 16 and 20. Accumulating variables are identified by a steady increase in mortality-prediction with each additional unit of history. At exam 16, diastolic blood pressure exhibits a consistent increase in mortality-prediction with each additional unit of history for both men and women, though the effect is smaller in size for men. In contrast, at exam 20, blood glucose accumulates predictivity with additional history for approximately 15 years, corresponding to ages 57–73. BMI, on the other hand, behaves as an accumulating variable for women at focal exams 16 and 20, but is relatively unresponsive of mortality for men at these exams.

3.2 Discussion

We surveyed the amount of variation in all-cause mortality that could be predicted from physiology at early-to-mid adulthood, finding a modest but non-trivial effect: 9.7% of variation in mortality at ages 28–38 can be predicted using the common physiological measurements of height, weight, body mass index, blood glucose level, and systolic and diastolic blood pressure. In addition, we have shown that our results are generally valid for both men and women. Though there are several quantitative differences in the magnitudes of effects and their precise timing, our overarching conclusions apply to both genders.

Further, the amount of predictable mortality generally decreases as a cohort ages and the least healthy individuals die off. This result is consistent with survivorship bias: as the unhealthy individuals die off, the surviving cohort becomes more homogeneous. As a result, the surviving cohort will have

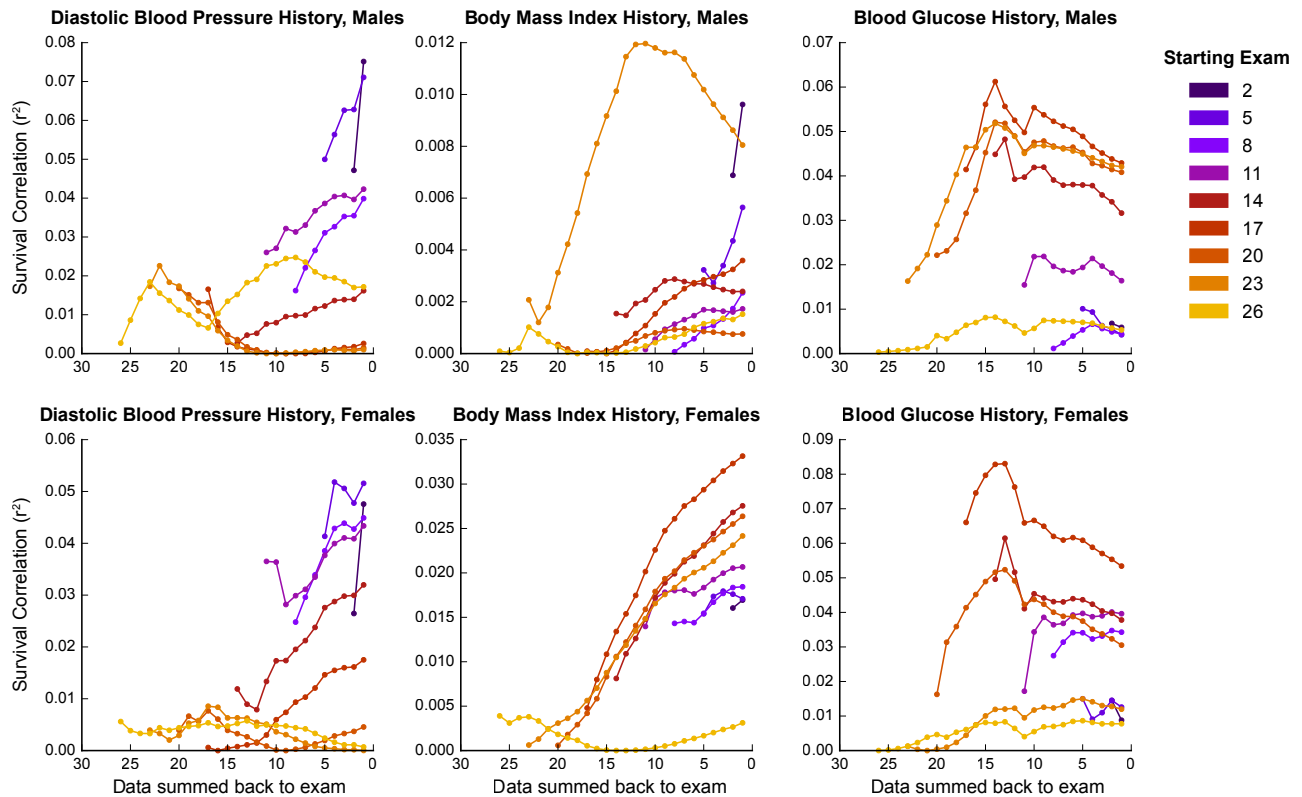


Figure 3.6: The accumulation of predictivity using additional years of history, starting at different exams. Each single time trace shown here is analogous to a single time trace in figure 5. Each panel illustrates how additional years of historical data improve risk prediction for a different physiological variable. Unlike figure 5, which presents these results from exams 16 and 20, here a range of “focal exams” are shown. Each trace represents the change in mortality predictivity as additional years of history are incorporated into the mortality prediction from a given starting point (“focal exam”). For example, the yellow traces show how the predictive ability of a given measure at exam 26 can be increased by adding additional historical data. Each particular point on a yellow trace then represents the gain in predictive ability when data area (as illustrated in the right panel of figure 4) is added from exam 26 back to that particular point in time. As in figure 5, the hallmark of an accumulating variable is a steady increase of predictivity with the incorporation of additional history. Note that BMI seems to accumulate predictivity as more history is incorporated, regardless of the focal exam from which the analysis is begun. In contrast, diastolic blood pressure and blood glucose only accumulate predictivity in limited regimes. Diastolic blood pressure and blood glucose accumulate risk from exams 1–14 and 13–20, respectively, which correspond to average ages of 35–60 and 57–73 years.

less predictable variation in survival; that is, a greater proportion of the variation will be random and not predictable.

Specifically, figure 3 shows that the ability of blood pressure (diastolic, systolic, and pulse pressure), BMI, and weight to predict variation in survival is high in early-to-mid adulthood, and gradually decreases up to roughly age 60. Although there is some fluctuation in this trend, likely the result of measurement noise, the overall direction for most variables is clear. Blood glucose’s predictivity presents an interesting exception. While essentially all other variables are decreasing in predictive capacity (up to age 60), blood glucose’s predictive ability seems to sharply increase from age 57, peaking

around the age of 70. The fact that blood pressure, BMI, and weight are predictive of mortality primarily from ages 35–60 and while blood glucose is most predictive from ages 57–73 suggests a fundamental difference between their contributions to all-cause mortality.

In parallel, figure 6 demonstrates that harm mediated by hypertension and obesity accumulates from ages 35–65, while mortality risk from blood glucose accumulates from ages 58–87. In conjunction with the results from figure 3 discussed above, these results suggest certain “critical periods” [149] for damage accumulation and mortality predictivity. These “critical periods” vary between different physiological parameters, but seem to represent times of damage accumulation and high mortality predictivity for each parameter. Again, all-cause mortality risk before age 70 seems is best predicted using blood pressure and BMI, while mortality during the age regime from age 60 and through age 80 is associated with blood glucose. While the confounding effects of changing societal habits over the years need to be taken into account, this type of analysis promises to yield important insights into the evolution of health and accumulated mortality risk over the course of the aging process.

The simplistic explanation for these observed “critical periods” is that the changing predictive ability of blood glucose and other measurements is entirely due to the aging process: in general, perhaps blood pressure becomes a less important predictor with increasing age while the predictive value of blood glucose increases. This interpretation, however, is confounded by the changing life habits of the American population over recent history. Shifts in diet and lifestyle have steadily increased the contribution of diabetes mellitus to morbidity and mortality over the past half-century, and advances in hypertension treatment have altered the physiological interpretation of blood pressure measurements. Disentangling these effects calls for additional analysis of both the Framingham data as well as other cohorts.

In addition to surveying mortality predictivity in the single-time point context, we investigated trends in variables over time. Rates of change for height, weight, body mass index, blood glucose level, and systolic and diastolic blood pressure were utterly unproductive of future mortality, despite several different approaches to estimating these rates of change. However, in many cases the measured variables’ accumulated history yielded substantially higher correlations in comparison to the single-time point context.

Specifically, the ability of diastolic blood pressure and BMI to predict all-cause mortality risk increases steadily and roughly linearly as more historical information is included for individuals below

the age of 67. For blood glucose, this effect is observed most prominently from the age 58 onward. In conjunction with our result that indicates that blood glucose is mortality-predictive at later ages than blood pressure and BMI, these "accumulating regimes" indicate that these variables' effects on mortality are cumulative.

This is consistent with the current understanding of the harms mediated by obesity, high blood glucose, and high blood pressure. While the precise mechanisms by which high blood pressure is pathological are still a subject of active research, the consensus so far is that the hemodynamic forces of hypertension initiate a signal which is transduced by endothelial cells, initiating various pathways involving ion channels, growth factors, extracellular matrix interactions, and various other molecular components [150]. The end result of these effects is generally a combination of vascular remodeling—blood vessels becoming less pliable, weaker, narrower—and specific organ damage, commonly in kidneys. Overall, it is generally agreed that the harmful effects of hypertension occur gradually over time. Similar lines of evidence suggest that pathologies from high blood glucose and obesity occur gradually as well [151].

Thus, it is not merely having high blood pressure, high blood glucose, or being overweight that instantaneously puts one at risk for the various associated pathologies. Rather, it is the sustained level of increased stress on one's organ systems that causes a gradual accumulation of damage. This suggests that many current preventative medicine guidelines, which focus on cardiovascular risk factors in older patients, may be failing to fully capture the lasting dangers of an unhealthy lifestyle, especially for younger individuals. In addition, while the concept of additional risk from sustained lifetime exposure may be intuitively understood by physicians, this study quantitatively highlights the magnitude of the effect, and suggests a straightforward way to estimate risk from accumulated exposure: simply summing historical physiological measurements. Further, some recent work on functional impairment during the aging process, as measured by frailty indices [152, 153], may be evidence of downstream effects of accumulated physiological damage.

With the advent of electronic medical records and ever-increasing computing power, it is becoming commonplace to have access to patients' previous physiological measurements. By exploiting longitudinal information in novel ways, we have shown that the predictive capacity of many well-studied risk factors can be greatly increased. Further, these statistical improvements can also drive new biomedical insights and provide avenues for testing those hypotheses. Much previous work has demonstrated

the utility of physiological history for understanding the processes that drive aging and the relationship between disease risk and specific physiological measurements [138–140]. Our results add to this understanding by demonstrating clearly that early-life physiology informs late-life survival, and that cumulative historical exposure can be a useful variable to track in addition to the present state of an individual’s physiology. Incorporating early-life data (where available) and recent history into existing quantitative models may further improve our understanding of how and why mortality risk increases with aging.

3.3 Experimental Procedures

3.3.1 Data Collection

The design of the Framingham Heart Study has been previously described [154, 155]. For our present study, subjects in the original cohort who were ages 28 to 38 at the first examination (1948–1953, 1451/5079 subjects) were eligible. We excluded participants that were lost to follow-up (defined by lacking both a known date of death and having no recorded data from clinical exam 28) and those who were missing sufficient data for any of the six physiological measures we studied (systolic blood pressure, diastolic blood pressure, blood glucose, height, weight, body mass index). After applying our criteria, 91 individuals were excluded on the basis of incomplete follow-up and 10 individuals were excluded on the basis of insufficient data. We then manually removed a single outlier individual, who had a systolic blood pressure of 250 mm Hg at the first clinical exam (an extraordinarily pathological reading, approximately 8.8 standard deviations from the mean) and died approximately 3 months later. We thus obtained a cohort of 1349 participants who remained eligible for this study. In Table 3.2, we see that the differences between our chosen cohort and individuals excluded for lack of follow-up or insufficient data are minimal, and are unlikely to cause significant bias in our results. By selecting a birth decade cohort, we hope to minimize the confounding effects of age, since all participants in our study are similar in age.

3.3.2 Statistics

Statistics (Pearson correlation coefficient, multiple regression weights, partial correlations) were computed using the Python programming language and associated packages.

	Living Subcohort Size	Mean Age (Years)	% Males	% Females
Exam 01	1349	34.5 ± 2.2	0.47	0.53
Exam 02	1329	36.6 ± 2.2	0.47	0.53
Exam 03	1311	38.5 ± 2.2	0.47	0.53
Exam 04	1301	40.5 ± 2.2	0.46	0.54
Exam 05	1285	42.5 ± 2.2	0.46	0.54
Exam 06	1270	44.5 ± 2.2	0.46	0.54
Exam 07	1256	46.5 ± 2.2	0.46	0.54
Exam 08	1236	47.9 ± 2.2	0.46	0.54
Exam 09	1216	49.9 ± 2.2	0.46	0.54
Exam 10	1189	52.0 ± 2.2	0.46	0.54
Exam 11	1162	53.8 ± 2.2	0.46	0.54
Exam 12	1136	56.0 ± 2.2	0.46	0.54
Exam 13	1108	58.0 ± 2.2	0.46	0.54
Exam 14	1071	60.0 ± 2.2	0.45	0.55
Exam 15	1031	61.9 ± 2.2	0.45	0.55
Exam 16	987	63.9 ± 2.2	0.44	0.56
Exam 17	956	65.9 ± 2.2	0.44	0.56
Exam 18	893	68.1 ± 2.2	0.43	0.57
Exam 19	836	70.1 ± 2.2	0.42	0.58
Exam 20	789	72.2 ± 2.2	0.41	0.59
Exam 21	724	74.1 ± 2.2	0.39	0.61
Exam 22	646	76.0 ± 2.2	0.39	0.61
Exam 23	580	77.8 ± 2.2	0.37	0.63
Exam 24	488	79.9 ± 2.2	0.36	0.64
Exam 25	455	81.8 ± 2.2	0.35	0.65
Exam 26	376	83.8 ± 2.2	0.32	0.68
Exam 27	301	85.5 ± 2.1	0.31	0.69
Exam 28	236	87.2 ± 2.0	0.32	0.68

Table 3.2: Comparison of the selected vs. excluded Framingham Heart Study (FHS) participants. All parameter mean values are within a single standard deviation, suggesting that our exclusion criteria did not introduce any obvious bias. The only statistically significant differences (at a $p = 0.05$ level) between included and excluded cohorts are in BMI and weight. However, even for BMI and weight, the excluded individuals' mean values are still within a standard deviation of those of the included cohort. Further, relatively few individuals were excluded in relation to those who remained in the cohort, so we believe the risk of bias from our exclusion criteria to be minimal.

3.3.3 Construction of Clinical Risk Scores

It should be noted that although we made every effort to reconstruct the Framingham and Pooled Cohort Equations risk scores as completely as possible, the smoking and high-density lipoprotein cholesterol terms had to be excluded due to the lack of consistent longitudinal measurement in the Framingham Heart Study. For example, early blood cholesterol measurements did not distinguish between high-, low-, and very low-density lipoproteins. The data from smoking questionnaires also varied among clinical exams, and was difficult to interpret consistently for all longitudinal time points.

3.3.4 Blood Pressure Treatment

To minimize the confounding effects of blood pressure treatment in figures 5 and 6, we adjusted individuals' blood pressure measurements to reflect our best estimates of their untreated blood pressure.

We achieved this by adding the average effect of blood pressure treatment to all individuals. Our results computed with controlled blood pressure were not substantially different from those from the same analysis on uncontrolled blood pressure (data not shown).

3.3.5 Pulse Pressure

Pulse pressure, a derived variable defined as the difference between an individual's systolic and diastolic blood pressures, was included as a seventh variable in our analysis from figure 3 onward. We excluded pulse pressure from figures 1 and 2, which employed multiple linear regression, because it is linearly dependent on systolic and diastolic blood pressure and would not have made any meaningful contribution to the derived composite variable.

3.3.6 Exam Weighting in History Accumulation

To adjust for unequal timing of clinical exams, we assumed that at any given point in time, each patient has the same measurement as the closest clinical exam. For example, if a patient has a measured systolic blood pressure (in mm Hg) of 120 in 1960, 130 in 1966, and 140 in 1976, our analysis would use this adjustment to assign blood pressures of 120 for 1960–1963, 130 for 1964–1971, and 140 for 1972–1976. Further, to avoid artificially diminishing the impact of the first and last available time points, we pad the first and last exams with half of the average inter-exam period. In the given example, we would actually assign blood pressures of 120 for 1956–1963, 130 for 1964–1971, and 140 for 1972–1980.

3.4 Acknowledgements

We would like to thank Drs. Mike Province and Sharon Cresci for helpful discussions.

3.5 Funding

ZP and WZ are supported by NIH grant R00 AG042487 and Longer Life Foundation grant 2015-008. WZ is additionally supported by NIH grant T32 GM07200.

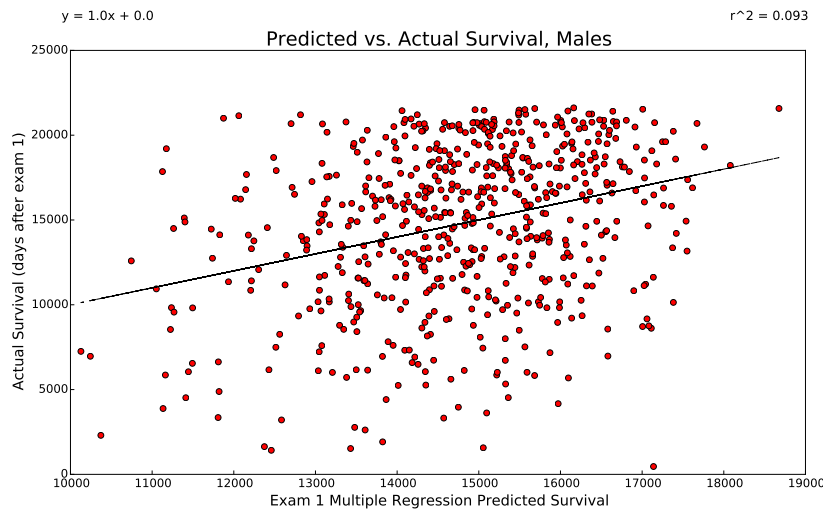
3.6 Conflict of interest

None declared.

3.7 Author contributions

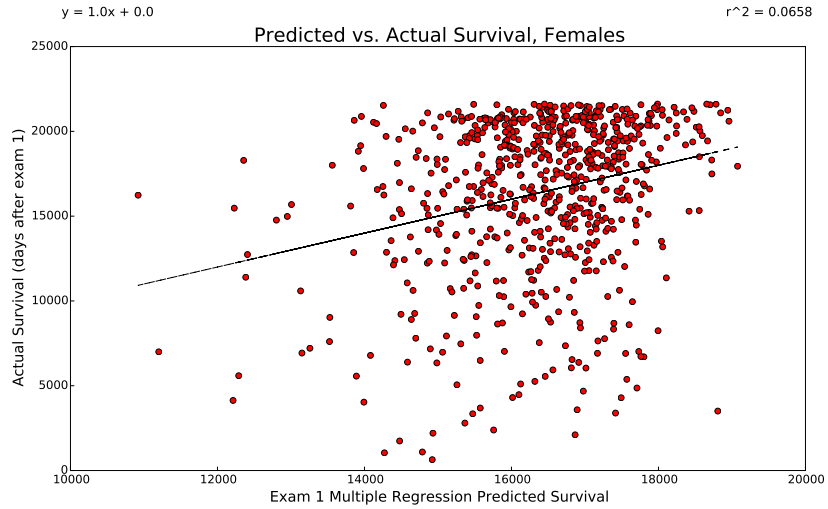
WZ and ZP designed the experiments. WZ carried out the analysis, and WZ and ZP wrote the manuscript.

3.8 Supplementary Information



	Average at Exam 01	Multiple Regression Weight	Single-Variable Correlation r^2
Blood Glucose	79.1 ± 18.65 mg/dL	-11.2 days per unit	0.0029
Body Mass Index	25.6 ± 3.71 kg/m ²	-394.0 days per unit	0.0126
Diastolic Blood Pressure	82.7 ± 9.77 mm Hg	-94.9 days per unit	0.0792
Systolic Blood Pressure	131.1 ± 14.04 mm Hg	-41.9 days per unit	0.0671
Height	68.4 ± 2.74 inches	-225.0 days per unit	0.0060
Weight	172.58 ± 26.24 pounds	65.44 days per unit	0.0038
Age	34.5 ± 2.16 years	nan	0.0247

Figure 3.7: For men in early-to-mid adulthood (participants aged 28–38), 9.3% of variation in future lifespan can be predicted from a weighted combination of systolic and diastolic blood pressure, blood glucose, height, weight, and body mass index. This is marginally less than the predictable portion of variation for men and women combined. This indicates that our composite predictor is to some extent capturing male-female differences in physiology and their effect on lifespan.



	Average at Exam 01	Multiple Regression Weight	Single-Variable Correlation r^2
Blood Glucose	78.3 ± 12.86 mg/dL	-9.2 days per unit	0.0020
Body Mass Index	23.8 ± 4.28 kg/m ²	239.4 days per unit	0.0167
Diastolic Blood Pressure	77.4 ± 8.56 mm Hg	-77.5 days per unit	0.0580
Systolic Blood Pressure	121.9 ± 12.59 mm Hg	-39.9 days per unit	0.0546
Height	63.1 ± 2.34 inches	241.9 days per unit	0.0007
Weight	137.34 ± 23.78 pounds	-48.48 days per unit	0.0141
Age	34.5 ± 2.19 years	nan	0.0338

Figure 3.8: For women in early-to-mid adulthood (participants aged 28–38), 6.6% of variation in future lifespan can be predicted from a weighted combination of systolic and diastolic blood pressure, blood glucose, height, weight, and body mass index. This is less than the predictable portion of variation for men and women combined. This indicates that our composite predictor is to some extent capturing male-female differences in physiology and their effect on lifespan. Another possible contributing factor is that more women remain alive at the latest clinical exam, so follow-up is less complete for women than for men.

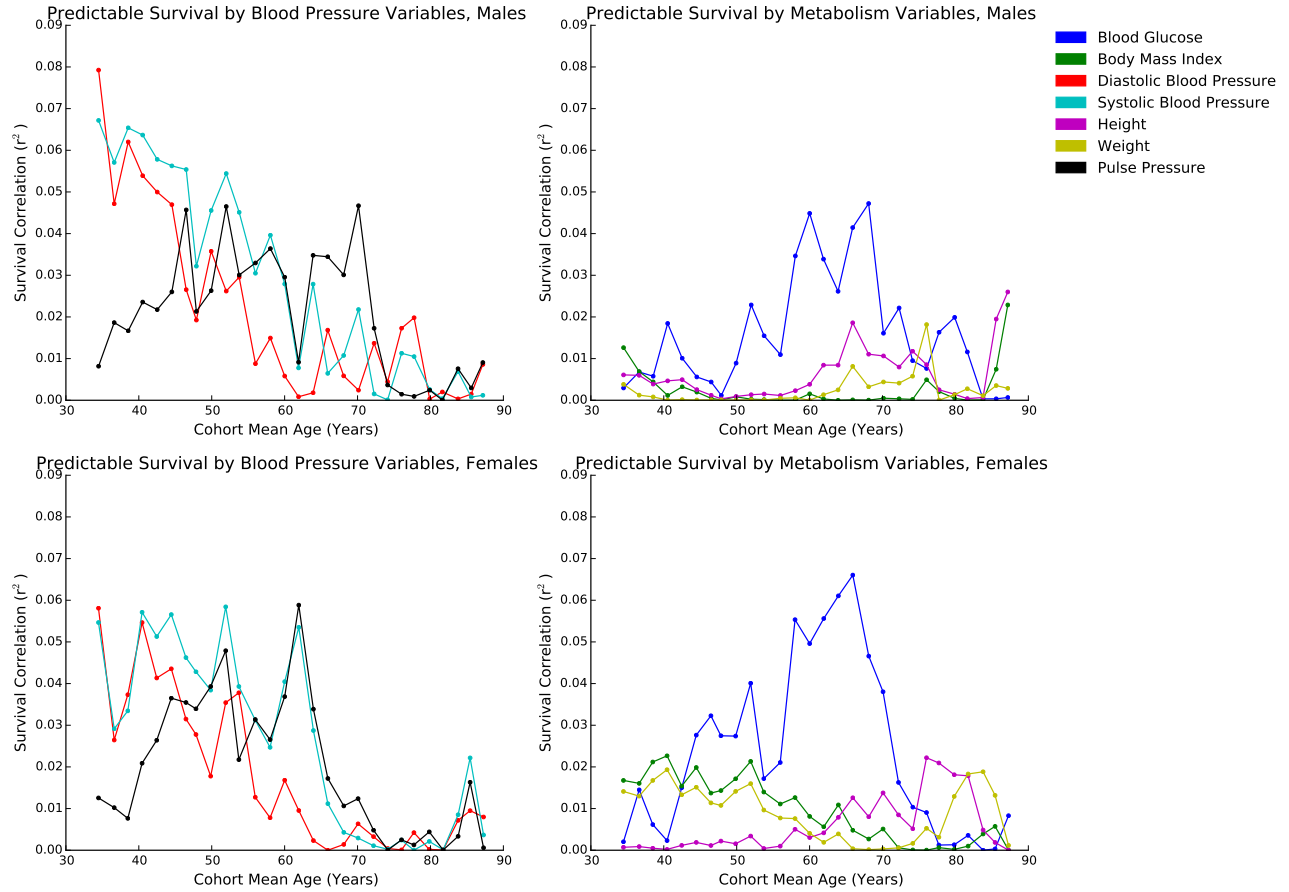


Figure 3.9: The individual variables' ability to predict survival in a single-time point context, stratified by gender. We see that the overall patterns of mortality-predictivity are very similar for women and men, though relatively minor differences in the magnitude of predictable mortality and the timing of longitudinal trends exist. As in figure 3 in the main text, blood pressure, BMI, and weight are predictive of mortality primarily from ages 35-60 and while blood glucose is most predictive from ages 57-73.

Bibliography

- [1] Gerald J Gruman. A history of ideas about the prolongation of life: the evolution of longevity hypotheses to 1800. *Transactions of the American Philosophical Society*, pages 1–102, 1966.
- [2] Luis H Toledo-Pereyra and Marjean M Toledo. A critical study of Lister’s work on antiseptic surgery. *The American Journal of Surgery*, 131(6):736–744, 1976.
- [3] Gregory L Armstrong, Laura A Conn, and Robert W Pinner. Trends in infectious disease mortality in the united states during the 20th century. *Jama*, 281(1):61–66, 1999.
- [4] Steven I Hajdu. A note from history: landmarks in history of cancer, part 1. *Cancer*, 117(5):1097–1102, 2011.
- [5] Steven I Hajdu. A note from history: landmarks in history of cancer, part 2. *Cancer*, 117(12):2811–2820, 2011.
- [6] Steven I Hajdu. A note from history: landmarks in history of cancer, part 3. *Cancer*, 118(4):1155–1168, 2012.
- [7] Steven I Hajdu. A note from history: landmarks in history of cancer, part 4. *Cancer*, 118(20):4914–4928, 2012.
- [8] Steven I. Hajdu and Farbod Darvishian. A note from history: Landmarks in history of cancer, part 5. *Cancer*, 119(8):1450–1466, 2013.
- [9] Steven I Hajdu and Manjunath Vadmal. A note from history: Landmarks in history of cancer, part 6. *Cancer*, 119(23):4058–4082, 2013.
- [10] Steven I Hajdu, Manjunath Vadmal, and Ping Tang. A note from history: Landmarks in history of cancer, part 7. *Cancer*, 2015.

-
- [11] Brian J Druker, François Guilhot, Stephen G O'Brien, Insa Gathmann, Hagop Kantarjian, Norbert Gattermann, Michael WN Deininger, Richard T Silver, John M Goldman, Richard M Stone, et al. Five-year follow-up of patients receiving imatinib for chronic myeloid leukemia. *New England Journal of Medicine*, 355(23):2408–2417, 2006.
- [12] Thomas BL Kirkwood. Understanding the odd science of aging. *Cell*, 120(4):437–447, 2005.
- [13] Cynthia Kenyon. The plasticity of aging: insights from long-lived mutants. *Cell*, 120(4):449–460, 2005.
- [14] Kaare Christensen, Thomas E Johnson, and James W Vaupel. The quest for genetic determinants of human longevity: challenges and insights. *Nature Reviews Genetics*, 7(6):436–448, 2006.
- [15] David B Friedman and Thomas E Johnson. A mutation in the age-1 gene in *caenorhabditis elegans* lengthens life and reduces hermaphrodite fertility. *Genetics*, 118(1):75–86, 1988.
- [16] Cynthia Kenyon, Jean Chang, Erin Gensch, Adam Rudner, and Ramon Tabtiang. A *c. elegans* mutant that lives twice as long as wild type. *Nature*, 366(6454):461–464, 1993.
- [17] Benjamin Gompertz. On the nature of the function expressive of the law of human mortality, and on a new mode of determining the value of life contingencies. *Philosophical transactions of the Royal Society of London*, pages 513–583, 1825.
- [18] James W Vaupel, James R Carey, Kaare Christensen, Thomas E Johnson, Anatoli I Yashin, Niels V Holm, Ivan A Iachine, Väinö Kannisto, Aziz A Khazaeli, Pablo Liedo, et al. Biodemographic trajectories of longevity. *Science*, 280(5365):855–860, 1998.
- [19] August Weismann, Edward Bagnall Poulton, Selmar Schönland, and Arthur Everett Shipley. *Essays upon heredity and kindred biological problems*, volume 1. Clarendon press, 1891.
- [20] Peter Brian Medawar. *An unsolved problem of biology*. H. K. Lewis, 1952.
- [21] George C. Williams. Pleiotropy, natural selection, and the evolution of senescence. *Evolution*, 11(4):pp. 398–411, 1957.
- [22] Tom B Kirkwood. Evolution of ageing. *Nature*, 270(5635):301–304, 1977.

-
- [23] Armand M Leroi, Andrzej Bartke, Giovanna De Benedictis, Claudio Franceschi, Anton Gartner, Eleftherios Gonos, Martin E Feder, Toomas Kivisild, Sylvia Lee, Nesrin Kartal-Özer, et al. What evidence is there for the existence of individual genes with antagonistic pleiotropic effects? *Mechanisms of ageing and development*, 126(3):421–429, 2005.
- [24] Aristotle. *Metaphysics*. The Internet Classics Archive, 350BCE.
- [25] Bernard Lakowski and Siegfried Hekimi. Determination of life-span in *caenorhabditis elegans* by four clock genes. *science*, 272(5264):1010–1013, 1996.
- [26] S Felkai, JJ Ewbank, J Lemieux, J-C Labbé, GG Brown, and S Hekimi. Clk-1 controls respiration, behavior and aging in the nematode *caenorhabditis elegans*. *The EMBO journal*, 18(7):1783–1792, 1999.
- [27] Popi Syntichaki, Kostoula Troulinaki, and Nektarios Tavernarakis. eif4e function in somatic cells modulates ageing in *caenorhabditis elegans*. *Nature*, 445(7130):922–926, 2007.
- [28] Kally Z Pan, Julia E Palter, Aric N Rogers, Anders Olsen, Di Chen, Gordon J Lithgow, and Pankaj Kapahi. Inhibition of mrna translation extends lifespan in *caenorhabditis elegans*. *Aging cell*, 6(1):111–119, 2007.
- [29] Malene Hansen, Stefan Taubert, Douglas Crawford, Nataliya Libina, Seung-Jae Lee, and Cynthia Kenyon. Lifespan extension by conditions that inhibit translation in *caenorhabditis elegans*. *Aging cell*, 6(1):95–110, 2007.
- [30] Kathryn L Lunetta, Ralph B D’Agostino, David Karasik, Emelia J Benjamin, Chao-Yu Guo, Raju Govindaraju, Douglas P Kiel, Margaret Kelly-Hayes, Joseph M Massaro, Michael J Pencina, et al. Genetic correlates of longevity and selected age-related phenotypes: a genome-wide association study in the framingham study. *BMC medical genetics*, 8(Suppl 1):S13, 2007.
- [31] Yang Li, Wen-Jing Wang, Huiqing Cao, Jiehua Lu, Chong Wu, Fang-Yuan Hu, Jian Guo, Ling Zhao, Fan Yang, Yi-Xin Zhang, et al. Genetic association of foxo1a and foxo3a with longevity trait in han chinese populations. *Human molecular genetics*, 18(24):4897–4904, 2009.
- [32] Bradley J Willcox, Timothy A Donlon, Qimei He, Randi Chen, John S Grove, Katsuhiko Yano, Kamal H Masaki, D Craig Willcox, Beatriz Rodriguez, and J David Curb. Foxo3a genotype

-
- is strongly associated with human longevity. *Proceedings of the National Academy of Sciences*, 105(37):13987–13992, 2008.
- [33] Shin-ichiro Imai and Leonard Guarente. Nad⁺ and sirtuins in aging and disease. *Trends in cell biology*, 24(8):464–471, 2014.
- [34] Akiko Satoh and Shin-ichiro Imai. Systemic regulation of mammalian ageing and longevity by brain sirtuins. *Nature communications*, 5, 2014.
- [35] Leonard Hayflick and Paul S Moorhead. The serial cultivation of human diploid cell strains. *Experimental cell research*, 25(3):585–621, 1961.
- [36] Leonard Hayflick. The limited in vitro lifetime of human diploid cell strains. *Experimental cell research*, 37(3):614–636, 1965.
- [37] H Cherif, JL Tarry, SE Ozanne, and CN Hales. Ageing and telomeres: A study into organ-and gender-specific telomere shortening. *Nucleic Acids Research*, 31(5):1576–1583, 2003.
- [38] Kyu Sang Joeng, Eun Joo Song, Kong-Joo Lee, and Junho Lee. Long lifespan in worms with long telomeric dna. *Nature genetics*, 36(6):607–611, 2004.
- [39] Richard M Cawthon, Ken R Smith, Elizabeth O’Brien, Anna Sivatchenko, and Richard A Kerber. Association between telomere length in blood and mortality in people aged 60 years or older. *The Lancet*, 361(9355):393–395, 2003.
- [40] María A Blasco, Han-Woong Lee, M Prakash Hande, Enrique Samper, Peter M Lansdorp, Ronald A DePinho, and Carol W Greider. Telomere shortening and tumor formation by mouse cells lacking telomerase rna. *Cell*, 91(1):25–34, 1997.
- [41] Carmen M Martin-Ruiz, Jacobijn Gussekloo, Diana Heemst, Thomas Zglinicki, and Rudi GJ Westendorp. Telomere length in white blood cells is not associated with morbidity or mortality in the oldest old: a population-based study. *Aging cell*, 4(6):287–290, 2005.
- [42] Claus Bischoff, Hans Christian Petersen, Jesper Graakjaer, Karen Andersen-Ranberg, James W Vaupel, Vilhelm A Bohr, Steen Kølvrå, and Kaare Christensen. No association between telomere length and survival among the elderly and oldest old. *Epidemiology*, 17(2):190–194, 2006.

-
- [43] Marc Tatar, Andrzej Bartke, and Adam Antebi. The endocrine regulation of aging by insulin-like signals. *Science*, 299(5611):1346–1351, 2003.
- [44] Leonard Guarente and Cynthia Kenyon. Genetic pathways that regulate ageing in model organisms. *Nature*, 408(6809):255–262, 2000.
- [45] CMw McCay, Mary F Crowell, and LA Maynard. The effect of retarded growth upon the length of life span and upon the ultimate body size. *J nutr*, 10(1):63–79, 1935.
- [46] Ricki J Colman, Rozalyn M Anderson, Sterling C Johnson, Erik K Kastman, Kristopher J Kosmatka, T Mark Beasley, David B Allison, Christina Cruzen, Heather A Simmons, Joseph W Kemnitz, et al. Caloric restriction delays disease onset and mortality in rhesus monkeys. *Science*, 325(5937):201–204, 2009.
- [47] Julie A Mattison, George S Roth, T Mark Beasley, Edward M Tilmont, April M Handy, Richard L Herbert, Dan L Longo, David B Allison, Jennifer E Young, Mark Bryant, et al. Impact of caloric restriction on health and survival in rhesus monkeys from the nia study. *Nature*, 2012.
- [48] Ricki J Colman, T Mark Beasley, Joseph W Kemnitz, Sterling C Johnson, Richard Weindruch, and Rozalyn M Anderson. Caloric restriction reduces age-related and all-cause mortality in rhesus monkeys. *Nature communications*, 5, 2014.
- [49] Kenneth B Beckman and Bruce N Ames. The free radical theory of aging matures. *Physiological reviews*, 78(2):547–581, 1998.
- [50] S Jay Olshansky. On the biodemography of aging: a review essay, 1998.
- [51] Thomas BL Kirkwood. Deciphering death: a commentary on gompertz (1825)‘on the nature of the function expressive of the law of human mortality, and on a new mode of determining the value of life contingencies’. *Philosophical Transactions of the Royal Society of London B: Biological Sciences*, 370(1666):20140379, 2015.
- [52] David L Wilson. The analysis of survival (mortality) data: fitting gompertz, weibull, and logistic functions. *Mechanisms of ageing and development*, 74(1):15–33, 1994.

-
- [53] William Matthew Makeham. On the law of mortality and the construction of annuity tables. *The Assurance Magazine, and Journal of the Institute of Actuaries*, pages 301–310, 1860.
- [54] William Matthew Makeham. On the law of mortality. *Journal of the Institute of Actuaries (1866)*, pages 325–358, 1867.
- [55] Leonid A Gavrilov and Natalia S Gavrilova. The reliability theory of aging and longevity. *Journal of theoretical Biology*, 213(4):527–545, 2001.
- [56] James W Vaupel. Biodemography of human ageing. *Nature*, 464(7288):536–542, 2010.
- [57] George T Baker and Richard L Sprott. Biomarkers of aging. *Experimental gerontology*, 23(4-5):223–239, 1988.
- [58] GT Baker. Identical age-dependent patterns of enzyme changes in dipteran insects. *Exp. Gerontol.*, 10:231, 1975.
- [59] Frederic C Ludwig and Mary E Smoke. The measurement of biological age. *Experimental aging research*, 6(6):497–522, 1980.
- [60] Donald K Ingram and Mark A Reynolds. Assessing the predictive validity of psychomotor tests as measures of biological age in mice. *Experimental aging research*, 12(3):155–162, 1986.
- [61] Paul T. Costa and Robert R. McCrae. Measures and markers of biological aging: 'a great clamoring... of fleeting significance'. *Archives of Gerontology and Geriatrics*, 7(3):211–214, September 1988.
- [62] Ward Dean and Robert F. Morgan. In defense of the concept of biological aging measurement—current status. *Archives of Gerontology and Geriatrics*, 7(3):191–210, September 1988.
- [63] Donald K. Ingram. Key questions in developing biomarkers of aging. *Experimental Gerontology*, 23(4–5):429–434, 1988.
- [64] David L. Wilson. Aging hypothesis, aging markers and the concept of biological age. *Experimental gerontology*, 23(4):435–438, 1988.

-
- [65] Ramachandran S Vasam, Martin G Larson, Eric P Leip, Jane C Evans, Christopher J O'Donnell, William B Kannel, and Daniel Levy. Impact of high-normal blood pressure on the risk of cardiovascular disease. *New England Journal of Medicine*, 345(18):1291–1297, 2001.
- [66] Nancy R Cook, Jerome Cohen, Patricia R Hebert, James O Taylor, and Charles H Hennekens. Implications of small reductions in diastolic blood pressure for primary prevention. *Archives of Internal Medicine*, 155(7):701–709, 1995.
- [67] Howard D Sesso, Nancy R Cook, Julie E Buring, JoAnn E Manson, and J Michael Gaziano. Alcohol consumption and the risk of hypertension in women and men. *Hypertension*, 51(4):1080–1087, 2008.
- [68] William B Kannel. Blood pressure as a cardiovascular risk factor: prevention and treatment. *Jama*, 275(20):1571–1576, 1996.
- [69] Robert H Eckel, Ronald M Krauss, et al. American heart association call to action: obesity as a major risk factor for coronary heart disease. *Circulation*, 97(21):2099–2100, 1998.
- [70] Gerd Assmann, Paul Cullen, and Helmut Schulte. Simple scoring scheme for calculating the risk of acute coronary events based on the 10-year follow-up of the prospective cardiovascular münster (procam) study. *Circulation*, 105(3):310–315, 2002.
- [71] Anatoliy I Yashin, Konstantin G Arbeev, Deqing Wu, Liubov S Arbeeva, Alexander Kulminski, Igor Akushevich, Irina Culminkaya, Eric Stallard, and Svetlana V Ukraintseva. How lifespan associated genes modulate aging changes: lessons from analysis of longitudinal data. *Frontiers in genetics*, 4, 2013.
- [72] William B. Zhang, Drew Sinha, William E. Pittman, Erik Hvatum, Nicholas Stroustrup, and Zachary Pincus. The physiological basis of variation in longevity within an isogenic population. *Cell Systems*, Accepted, 2016.
- [73] Cynthia J Kenyon. The genetics of ageing. *Nature*, 464(7288):504–512, 2010.
- [74] Martin Gögele, Cristian Pattaro, Christian Fuchsberger, Cosetta Minelli, Peter P Pramstaller, and Matthias Wjst. Heritability analysis of life span in a semi-isolated population followed across

-
- four centuries reveals the presence of pleiotropy between life span and reproduction. *The Journals of Gerontology Series A: Biological Sciences and Medical Sciences*, 66(1):26–37, 2011.
- [75] Jenni E Pettay, Loeske EB Kruuk, Jukka Jokela, and Virpi Lummaa. Heritability and genetic constraints of life-history trait evolution in preindustrial humans. *Proceedings of the National Academy of Sciences of the United States of America*, 102(8):2838–2843, 2005.
- [76] Anne Maria Herskind, Matthew McGue, Niels V Holm, Thorkild IA Sørensen, Bent Harvald, and James W Vaupel. The heritability of human longevity: a population-based study of 2872 danish twin pairs born 1870–1900. *Human genetics*, 97(3):319–323, 1996.
- [77] Thomas BL Kirkwood, Martin Feder, Caleb E Finch, Claudio Franceschi, Amiela Globerson, Christian Peter Klingenberg, Kelly LaMarco, Stig Omholt, and Rudi GJ Westendorp. What accounts for the wide variation in life span of genetically identical organisms reared in a constant environment? *Mechanisms of ageing and development*, 126(3):439–443, 2005.
- [78] Nicholas Stroustrup, Winston E Anthony, Zachary M Nash, Vivek Gowda, Adam Gomez, Isaac F López-Moyado, Javier Apfeld, and Walter Fontana. The temporal scaling of caenorhabditis elegans ageing. *Nature*, 2016.
- [79] Zachary Pincus, Thalyana Smith-Vikos, and Frank J Slack. MicroRNA predictors of longevity in caenorhabditis elegans. *PLoS Genet*, 7(9):e1002306, 2011.
- [80] Tamara R Golden, Alan Hubbard, Caroline Dando, Michael A Herren, and Simon Melov. Age-related behaviors have distinct transcriptional profiles in caenorhabditis elegans. *Aging cell*, 7(6):850–865, 2008.
- [81] Adolfo Sánchez-Blanco and Stuart K Kim. Variable pathogenicity determines individual lifespan in caenorhabditis elegans. *PLoS Genet*, 7(4):e1002047, 2011.
- [82] Charles F Glenn, David K Chow, Lawrence David, Carol A Cooke, Minaxi S Gami, Wendy B Iser, Keaton B Hanselman, Ilya G Goldberg, and Catherine A Wolkow. Behavioral deficits during early stages of aging in caenorhabditis elegans result from locomotory deficits possibly linked to muscle frailty. *The Journals of Gerontology Series A: Biological Sciences and Medical Sciences*, 59(12):1251–1260, 2004.

-
- [83] David K Chow, Charles F Glenn, Josiah L Johnston, Ilya G Goldberg, and Catherine A Wolkow. Sarcopenia in the *caenorhabditis elegans* pharynx correlates with muscle contraction rate over lifespan. *Experimental gerontology*, 41(3):252–260, 2006.
- [84] D Mark Eckley, Salim Rahimi, Sandra Mantilla, Nikita V Orlov, Christopher E Coletta, Mark A Wilson, Wendy B Iser, John D Delaney, Yongqing Zhang, William Wood III, et al. Molecular characterization of the transition to mid-life in *caenorhabditis elegans*. *Age*, 35(3):689–703, 2013.
- [85] Michael R Klass. Aging in the nematode *caenorhabditis elegans*: major biological and environmental factors influencing life span. *Mechanisms of ageing and development*, 6:413–429, 1977.
- [86] Ryuji Hosono, Yoshiko Sato, Shin-Ichi Aizawa, and Youji Mitsui. Age-dependent changes in mobility and separation of the nematode *caenorhabditis elegans*. *Experimental gerontology*, 15(4):285–289, 1980.
- [87] Laura A Herndon, Peter J Schmeissner, Justyna M Dudaronek, Paula A Brown, Kristin M Listner, Yuko Sakano, Marie C Paupard, David H Hall, and Monica Driscoll. Stochastic and genetic factors influence tissue-specific decline in ageing *c. elegans*. *Nature*, 419(6909):808–814, 2002.
- [88] Cheng Huang, Chengjie Xiong, and Kerry Kornfeld. Measurements of age-related changes of physiological processes that predict lifespan of *caenorhabditis elegans*. *Proceedings of the National Academy of Sciences of the United States of America*, 101(21):8084–8089, 2004.
- [89] Matthew S Gill, Anders Olsen, James N Sampayo, and Gordon J Lithgow. An automated high-throughput assay for survival of the nematode *caenorhabditis elegans*. *Free Radical Biology and Medicine*, 35(6):558–565, 2003.
- [90] Maren Hertweck and Ralf Baumeister. Automated assays to study longevity in *c. elegans*. *Mechanisms of ageing and development*, 126(1):139–145, 2005.
- [91] Nicholas Stroustrup, Bryne E Ulmschneider, Zachary M Nash, Isaac F López-Moyado, Javier Apfeld, and Walter Fontana. The *caenorhabditis elegans* lifespan machine. *Nature methods*, 10(7):665–670, 2013.
- [92] Zachary Pincus and Frank J Slack. Developmental biomarkers of aging in *caenorhabditis elegans*. *Developmental Dynamics*, 239(5):1306–1314, 2010.

-
- [93] Josiah Johnston, Wendy B Iser, David K Chow, Ilya G Goldberg, and Catherine A Wolkow. Quantitative image analysis reveals distinct structural transitions during aging in *caenorhabditis elegans* tissues. *PLoS One*, 3(7):e2821, 2008.
- [94] George V Clokey and Lewis A Jacobson. The autofluorescent “lipofuscin granules” in the intestinal cells of *caenorhabditis elegans* are secondary lysosomes. *Mechanisms of ageing and development*, 35(1):79–94, 1986.
- [95] Beate Gerstbrein, Georgios Stamatias, Nikiforos Kollias, and Monica Driscoll. In vivo spectrofluorimetry reveals endogenous biomarkers that report healthspan and dietary restriction in *caenorhabditis elegans*. *Aging cell*, 4(3):127–137, 2005.
- [96] Greg J Hermann, Lena K Schroeder, Caroline A Hieb, Aaron M Kershner, Beverley M Rabbitts, Paul Fonarev, Barth D Grant, and James R Priess. Genetic analysis of lysosomal trafficking in *caenorhabditis elegans*. *Molecular biology of the cell*, 16(7):3273–3288, 2005.
- [97] Zachary Pincus, Travis C Mazer, and Frank J Slack. Autofluorescence as a measure of senescence in *c. elegans*: look to red, not blue or green. *Aging*, 8(4), 2016.
- [98] S Elizabeth Hulme, Sergey S Shevkoplyas, Alison P McGuigan, Javier Apfeld, Walter Fontana, and George M Whitesides. Lifespan-on-a-chip: microfluidic chambers for performing lifelong observation of *c. elegans*. *Lab on a Chip*, 10(5):589–597, 2010.
- [99] Christopher L Pickett, Nicholas Dietrich, Junfang Chen, Chengjie Xiong, and Kerry Kornfeld. Mated progeny production is a biomarker of aging in *caenorhabditis elegans*. *G3: Genes/Genomes/Genetics*, 3(12):2219–2232, 2013.
- [100] L Byerly, RC Cassada, and RL Russell. The life cycle of the nematode *caenorhabditis elegans*: I. wild-type growth and reproduction. *Developmental biology*, 51(1):23–33, 1976.
- [101] Thomas J Fabian and Thomas E Johnson. Production of age-synchronous mass cultures of *caenorhabditis elegans*. *Journal of gerontology*, 49(4):B145–B156, 1994.
- [102] James F Fries. Aging, natural death, and the compression of morbidity. *New England journal of medicine*, 303(3):130–135, 1980.

-
- [103] Gary A Borkan and Arthur H Norris. Assessment of biological age using a profile of physical parameters. *Journal of Gerontology*, 35(2):177–184, 1980.
- [104] Linda P Fried, Catherine M Tangen, Jeremy Walston, Anne B Newman, Calvin Hirsch, John Gottdiener, Teresa Seeman, Russell Tracy, Willem J Kop, Gregory Burke, et al. Frailty in older adults evidence for a phenotype. *The Journals of Gerontology Series A: Biological Sciences and Medical Sciences*, 56(3):M146–M157, 2001.
- [105] Ruth E Hubbard. Sex differences in frailty. In *Frailty in Aging*, volume 41, pages 41–53. Karger Publishers, 2015.
- [106] Shane L Rea, Deqing Wu, James R Cypser, James W Vaupel, and Thomas E Johnson. A stress-sensitive reporter predicts longevity in isogenic populations of *caenorhabditis elegans*. *Nature genetics*, 37(8):894–898, 2005.
- [107] H Montgomery. Cardiac reserve: linking physiology and genetics. *Intensive Care Med*, 26(S 137):144, 2000.
- [108] EM Ghezzi and JA Ship. Aging and secretory reserve capacity of major salivary glands. *Journal of dental research*, 82(10):844–848, 2003.
- [109] Bruce S McEwen. Interacting mediators of allostasis and allostatic load: towards an understanding of resilience in aging. *Metabolism*, 52:10–16, 2003.
- [110] Ankita Bansal, Lihua J Zhu, Kelvin Yen, and Heidi A Tissenbaum. Uncoupling lifespan and healthspan in *caenorhabditis elegans* longevity mutants. *Proceedings of the National Academy of Sciences*, 112(3):E277–E286, 2015.
- [111] Jeong-Hoon Hahm, Sunhee Kim, Race DiLoreto, Cheng Shi, Seung-Jae V Lee, Coleen T Murphy, and Hong Gil Nam. *C. elegans* maximum velocity correlates with healthspan and is maintained in worms with an insulin receptor mutation. *Nature communications*, 6, 2015.
- [112] Simon Melov. Geroscience approaches to increase healthspan and slow aging. *F1000Research*, 5, 2016.

-
- [113] Paola Sebastiani, Fangui Sun, Stacy Lynn Andersen, Joseph Lee, Mary Kaye Wojczynski, Jason L Sanders, Anatoliy I Yashin, Anne B Newman, and Thomas T Perls. Families enriched for exceptional longevity also have increased health-span: findings from the long life family study. *Frontiers in public health*, 1:38, 2013.
- [114] Arlene S Ash, Aimee R Kroll-Desrosiers, David C Hoaglin, Kaare Christensen, Hua Fang, and Thomas T Perls. Are members of long-lived families healthier than their equally long-lived peers? evidence from the long life family study. *The Journals of Gerontology Series A: Biological Sciences and Medical Sciences*, 70(8):971–976, 2015.
- [115] Khadija Ismail, Lisa Nussbaum, Paola Sebastiani, Stacy Andersen, Thomas Perls, Nir Barzilai, and Sofiya Milman. Compression of morbidity is observed across cohorts with exceptional longevity. *Journal of the American Geriatrics Society*, 2016.
- [116] Danan Gu, Matthew E Dupre, Jessica Sautter, Haiyan Zhu, Yuzhi Liu, and Zeng Yi. Frailty and mortality among chinese at advanced ages. *The Journals of Gerontology Series B: Psychological Sciences and Social Sciences*, page gbn009, 2009.
- [117] Bernd Rechel, Emily Grundy, Jean-Marie Robine, Jonathan Cylus, Johan P Mackenbach, Cecile Knai, and Martin McKee. Ageing in the european union. *The Lancet*, 381(9874):1312–1322, 2013.
- [118] Vicki A Freedman, Douglas A Wolf, and Brenda C Spillman. Disability-free life expectancy over 30 years: A growing female disadvantage in the us population. *American Journal of Public Health*, (0):e1–e7, 2016.
- [119] Jerome P Kassirer. The principles of clinical decision making: an introduction to decision analysis. *The Yale journal of biology and medicine*, 49(2):149, 1976.
- [120] Milton C Weinstein and William B Stason. Foundations of cost-effectiveness analysis for health and medical practices. *New England journal of medicine*, 296(13):716–721, 1977.
- [121] Anna Lee, Gavin M Joynt, Anthony MH Ho, Sheri Keitz, Thomas McGinn, Peter C Wyer, EBM Teaching Scripts Working Group, et al. Tips for teachers of evidence-based medicine:

-
- making sense of decision analysis using a decision tree. *Journal of general internal medicine*, 24(5):642–648, 2009.
- [122] Rebeca Garcia-Valles, Mari Carmen Gomez-Cabrera, Leocadio Rodriguez-Mañas, Francisco J Garcia-Garcia, Ana Diaz, Inma Noguera, Gloria Olaso-Gonzalez, and Jose Viña. Life-long spontaneous exercise does not prolong lifespan but improves health span in mice. *Longevity & healthspan*, 2(1):1, 2013.
- [123] Andrew Singson, Kristina B Mercer, and Steven W L’Hernault. The *c. elegans* *spe-9* gene encodes a sperm transmembrane protein that contains *egf*-like repeats and is required for fertilization. *Cell*, 93(1):71–79, 1998.
- [124] Edward N Anderson, Mark E Corkins, Jia-Cheng Li, Komudi Singh, Sadé Parsons, Tim M Tucey, Altar Sorkaç, Huiyan Huang, Maria Dimitriadi, David A Sinclair, et al. *C. elegans* lifespan extension by osmotic stress requires *fudr*, base excision repair, *foxo*, and sirtuins. *Mechanisms of ageing and development*, 154:30–42, 2016.
- [125] Sydney Brenner. The genetics of *caenorhabditis elegans*. *Genetics*, 77(1):71–94, 1974.
- [126] Lawrence Firestone, Kitty Cook, Kevin Culp, Neil Talsania, and Kendall Preston. Comparison of autofocus methods for automated microscopy. *Cytometry*, 12(3):195–206, 1991.
- [127] John F Brenner, Brock S Dew, J Brian Horton, Thomas King, Peter W Neurath, and William D Selles. An automated microscope for cytologic research a preliminary evaluation. *Journal of Histochemistry & Cytochemistry*, 24(1):100–111, 1976.
- [128] Stacey L Edwards, Nicole K Charlie, Marie C Milfort, Brandon S Brown, Christen N Gravlin, Jamie E Knecht, and Kenneth G Miller. A novel molecular solution for ultraviolet light detection in *caenorhabditis elegans*. *PLoS Biol*, 6(8):e198, 2008.
- [129] Massimo Piccardi. Background subtraction techniques: a review. In *Systems, man and cybernetics, 2004 IEEE international conference on*, volume 4, pages 3099–3104. IEEE, 2004.
- [130] John Canny. A computational approach to edge detection. *Pattern Analysis and Machine Intelligence, IEEE Transactions on*, (6):679–698, 1986.

-
- [131] Corinna Cortes and Vladimir Vapnik. Support-vector networks. *Machine learning*, 20(3):273–297, 1995.
- [132] Ao-Lin Hsu, Zhaoyang Feng, Meng-Yin Hsieh, and XZ Shawn Xu. Identification by machine vision of the rate of motor activity decline as a lifespan predictor in *c. elegans*. *Neurobiology of aging*, 30(9):1498–1503, 2009.
- [133] Cassandra Coburn, Erik Allman, Parag Mahanti, Alexandre Benedetto, Filipe Cabreiro, Zachary Pincus, Filip Matthijssens, Caroline Araiz, Abraham Mandel, Manolis Vlachos, et al. Anthranilate fluorescence marks a calcium-propagated necrotic wave that promotes organismal death in *c. elegans*. *PLoS Biol*, 11(7):e1001613, 2013.
- [134] Lior Shamir, Catherine A Wolkow, and Ilya G Goldberg. Quantitative measurement of aging using image texture entropy. *Bioinformatics*, 25(23):3060–3063, 2009.
- [135] Abraham Savitzky and Marcel JE Golay. Smoothing and differentiation of data by simplified least squares procedures. *Analytical chemistry*, 36(8):1627–1639, 1964.
- [136] William B Zhang and Zachary Pincus. Predicting all-cause mortality from basic physiology in the framingham heart study. *Aging cell*, 15(1):39–48, 2016.
- [137] Owen R Jones, Alexander Scheuerlein, Roberto Salguero-Gómez, Carlo Giovanni Camarda, Ralf Schaible, Brenda B Casper, Johan P Dahlgren, Johan Ehrlén, María B García, Eric S Menges, et al. Diversity of ageing across the tree of life. *Nature*, 505(7482):169–173, 2014.
- [138] Konstantin G Arbeev, Svetlana V Ukraintseva, Igor Akushevich, Alexander M Kulminski, Liubov S Arbeeva, Lucy Akushevich, Irina V Culminkaya, and Anatoliy I Yashin. Age trajectories of physiological indices in relation to healthy life course. *Mechanisms of ageing and development*, 132(3):93–102, 2011.
- [139] Anatoli I Yashin, Konstantin G Arbeev, Igor Akushevich, Aliaksandr Kulminski, Lucy Akushevich, and Svetlana V Ukraintseva. Stochastic model for analysis of longitudinal data on aging and mortality. *Mathematical biosciences*, 208(2):538–551, 2007.

-
- [140] Anatoli I Yashin, Igor V Akushevich, Konstantin G Arbeev, Lucy Akushevich, Svetlana V Ukraintseva, and Aliaksandr Kulminski. Insights on aging and exceptional longevity from longitudinal data: novel findings from the framingham heart study. *Age*, 28(4):363–374, 2006.
- [141] Anatoli I Yashin, Konstantin G Arbeev, Igor Akushevich, Svetlana V Ukraintseva, Alexander Kulminski, Liubov S Arbeeva, and Irina Culminskaya. Exceptional survivors have lower age trajectories of blood glucose: lessons from longitudinal data. *Biogerontology*, 11(3):257–265, 2010.
- [142] Arnold Mitnitski, Le Bao, and Kenneth Rockwood. Going from bad to worse: a stochastic model of transitions in deficit accumulation, in relation to mortality. *Mechanisms of ageing and development*, 127(5):490–493, 2006.
- [143] Arnold Mitnitski, Xiaowei Song, Ingmar Skoog, Gerald A Broe, Jafna L Cox, Eva Grunfeld, and Kenneth Rockwood. Relative fitness and frailty of elderly men and women in developed countries and their relationship with mortality. *Journal of the American Geriatrics Society*, 53(12):2184–2189, 2005.
- [144] Daniel W Belsky, Avshalom Caspi, Renate Houts, Harvey J Cohen, David L Corcoran, Andrea Danese, HonaLee Harrington, Salomon Israel, Morgan E Levine, Jonathan D Schaefer, et al. Quantification of biological aging in young adults. *Proceedings of the National Academy of Sciences*, 112(30):E4104–E4110, 2015.
- [145] Peter WF Wilson, Ralph B D’Agostino, Daniel Levy, Albert M Belanger, Halit Silbershatz, and William B Kannel. Prediction of coronary heart disease using risk factor categories. *Circulation*, 97(18):1837–1847, 1998.
- [146] Donald M Lloyd-Jones, Peter WF Wilson, Martin G Larson, Alexa Beiser, Eric P Leip, Ralph B D’Agostino, and Daniel Levy. Framingham risk score and prediction of lifetime risk for coronary heart disease. *The American journal of cardiology*, 94(1):20–24, 2004.
- [147] David C Goff, Donald M Lloyd-Jones, Glen Bennett, CJ O’Donnell, S Coady, and J Robinson. 2013 acc/aha guideline on the assessment of cardiovascular risk. *J Am Coll Cardiol*, 2014.

-
- [148] Cecilia Albala, M Yanez, Enzo Devoto, Cecilia Sostin, Loreto Zeballos, and JL Santos. Obesity as a protective factor for postmenopausal osteoporosis. *International journal of obesity and related metabolic disorders: journal of the International Association for the Study of Obesity*, 20(11):1027–1032, 1996.
- [149] William H Dietz. Critical periods in childhood for the development of obesity. *The American journal of clinical nutrition*, 59(5):955–959, 1994.
- [150] Friedrich C Luft, Eero Mervaala, Dominik N Müller, Volkmar Gross, Folke Schmidt, Joon Keun Park, Christian Schmitz, Andrea Lippoldt, Volker Breu, Ralph Dechend, et al. Hypertension-induced end-organ damage a new transgenic approach to an old problem. *Hypertension*, 33(1):212–218, 1999.
- [151] Steven E Kahn, Rebecca L Hull, and Kristina M Utzschneider. Mechanisms linking obesity to insulin resistance and type 2 diabetes. *Nature*, 444(7121):840–846, 2006.
- [152] Alexander Kulminski, Svetlana V Ukraintseva, Igor Akushevich, Konstantin G Arbeev, Kenneth Land, and Anatoli I Yashin. Accelerated accumulation of health deficits as a characteristic of aging. *Experimental gerontology*, 42(10):963–970, 2007.
- [153] Arnold Mitnitski, Xiaowei Song, and Kenneth Rockwood. Assessing biological aging: the origin of deficit accumulation. *Biogerontology*, 14(6):709–717, 2013.
- [154] William B Kannel, Manning Feinleib, Patricia M McNamara, Robert J Garrison, and William P Castelli. An investigation of coronary heart disease in families the Framingham offspring study. *American journal of epidemiology*, 110(3):281–290, 1979.
- [155] R Collins, R Peto, S MacMahon, J Godwin, N Qizilbash, P Hebert, KA Eberlein, JO Taylor, CH Hennekens, and NH Fiebach. Blood pressure, stroke, and coronary heart disease: part 2, short-term reductions in blood pressure: overview of randomised drug trials in their epidemiological context. *The Lancet*, 335(8693):827–838, 1990.

Do not go gentle into that good night,
Old age should burn and rave at close of day;
Rage, rage against the dying of the light.

Though wise men at their end know dark is right,
Because their words had forked no lightning they
Do not go gentle into that good night.

Good men, the last wave by, crying how bright
Their frail deeds might have danced in a green bay,
Rage, rage against the dying of the light.

Wild men who caught and sang the sun in flight,
And learn, too late, they grieved it on its way,
Do not go gentle into that good night.

Grave men, near death, who see with blinding sight
Blind eyes could blaze like meteors and be gay,
Rage, rage against the dying of the light.

And you, my father, there on the sad height,
Curse, bless, me now with your fierce tears, I pray.
Do not go gentle into that good night.
Rage, rage against the dying of the light.

—Dylan Thomas, *Do not go gentle into that good night*